

Rational design, synthesis, characterization and application of phenylenevinylene and fluorene derivatives as novel MALDI matrices

Juan Sebastian Ramírez Pradilla  
Chemist, Master in Science

Thesis presented to qualify for a doctorate degree in chemistry

Advisor  
Marianny Yajaira Combariza Montañez  
Ph D in chemistry

Co-advisor  
Cristian Blanco-Tirado  
Ph D in chemistry

Universidad Industrial de Santander

Facultad de Ciencias

Escuela de Química

Doctorado en Química

Bucaramanga

2019

“Tanaka showed first that it could be done, that large proteins could be ionized, analyzed, and detected using any kind of laser desorption” “The success of Tanaka’s engineering team also reminded the rest of us that ionizing proteins was not sufficient. It was also necessary to customize the rest of the instrument, especially the detector.”

*Catherine Fenselau*

### **Acknowledgments**

To my advisors, Yajaira and Cristian to help me during the last four years of knowledge and personal growing.

My gratitude to all my family, my grandma Jeanette, my brother Tomas, my mom Bertha and my dad Arcesio.

My special gratitude to my second family which host myself at home during the Ph D, my uncle Luis Enrique, my aunt Yaneth, and my cousins Alejandro & Andres.

My friends, Juan Diego, Rafael David, Mauricio Cerón, Marisol, Marilyn, Mauro, Luis Carlos, Deisy, to be part of my self-growing.

## Table of Contents

1. Matrix Assisted Laser Desorption Ionization: an overview on principles.....	20
1.1. Cluster Mechanism.....	22
1.2. The Coupled Physical and Chemical Dynamics Mechanism .....	24
1.3. Primary Ionization.....	25
1.4. Secondary Ionization.....	27
1.5. Factors influencing the matrix's performance and analyte signals in ET-MALDI: the clues behind finding the right matrix .....	30
References.....	34
2. Electron transfer ionization of nanoparticles, polymers, porphyrins and fullerenes using synthetically-tunable $\alpha$ -cyano-phenylenevinylenes as UV MALDI-MS matrices.....	38
2.1. Abstract .....	38
2.2. Introduction .....	39
2.3. Results and Discussion.....	43
2.3.1. $\alpha$ -CNPVs synthesis and characterization.....	43
2.3.2. Vacuum stability $\alpha$ -CNPV-CH <sub>3</sub> and $\alpha$ -CNPV-OCH <sub>3</sub> derivatives.....	50
2.3.3. Analysis of polyaromatic hydrocarbons, porphyrins, phtalocyanines and solar cell sensitizers using $\alpha$ -CNPV-CH <sub>3</sub> , $\alpha$ -CNPV-OCH <sub>3</sub> as ET matrices.....	52
2.3.4. ET-MALDI applications to complex mixture analysis using $\alpha$ -CNPV-CH <sub>3</sub> as matrix: ..	55
2.3.4.1. Direct identification of biomarkers (nickel and vanadyl porphyrins) in crude oils.....	55

2.3.4.2. Polymer analysis.....	57
2.3.4.3. ET-MALDI analysis of labile materials using $\alpha$ -CNPV-CH <sub>3</sub> as matrix: Gold Nanoparticles. ....	60
2.3.4.4. Fullerene derivatives.....	62
2.4. Conclusions .....	64
References.....	66
3. Tunable Fluorene-based light-harvesting materials as MALDI MS matrices for macrocyclic ligands and metal complexes analysis via Electron-Transfer Ionization.....	79
3.1. Abstract .....	79
3.2. Introduction .....	79
3.3. Experimental Section .....	83
3.3.1. UV-vis spectroscopy measurements and Ionization Energy measurement.....	83
3.3.2. LDI and UV-MALDI sample preparation.....	84
3.3.3. Mass Spectrometry .....	84
3.4. Results and Discussions .....	85
3.4.1. Fluorene derivatives as Electron transfer in MALDI-MS.....	90
3.5. Conclusions .....	97
References.....	98
4. Electron Transfer in MALDI-FTICR-MS: a non-chromatographic approach for the targeted analysis of Nickel and Vanadyl Porphyrins in complex mixtures.....	105
4.1. Abstract .....	105
4.2. Introduction .....	106
4.3. Experimental Section .....	110
4.3.1. Materials.....	110
4.3.2. Sample preparation.....	110

4.3.3. Mass spectrometry.....	111
4.3.4. Data processing .....	111
4.4. Results and Discussion.....	112
4.4.1. ET-MALDI, LDI, and APPI analysis:.....	112
4.4.2. Nickel and Vanadyl porphyrin molecular formula assignments .....	116
4.4.3. Porphyrin Diversity .....	119
4.5. Conclusions .....	120
References.....	122
5. A comprehensive Petroporphyrin Identification in Crude Oils Using Highly Selective Electron Transfer Reactions in MALDI-FTICR MS .....	128
5.1. Abstract .....	128
5.2. Introduction .....	129
5.3. Experimental Section .....	135
5.3.1. Materials.....	135
5.3.2. Mass spectrometry.....	136
5.4. Results and Discussion.....	137
5.4.1. Direct analysis of an ACN extract via ET-MALDI-FTICR.....	137
5.4.2. HPTLC-ET-MALDI-FTICR .....	143
5.4.3. Observation of new oxygenated vanadyl porphyrins .....	147
5.5. Conclusion.....	149
References.....	150

### List of figures

Figure 1 Desorption event simulation by molecular dynamics at different times. (upper) molecules being desorbed from sample surface (middle) intermediate surface nucleation (lower) expansion of cold clusters. ....	23
Figure 2 Lucky ion formation within cluster mechanism, proposed by Michael Karas. ....	24
Figure 3 Desorption event simulation by molecular dynamics at different times. (upper) molecules being desorbed from sample surface (middle) intermediate surface nucleation (lower) expansion of cold clusters. ....	25
Figure 4 Two-step ionization mechanism proposed by Richard Knochenmuss. ....	27
Figure 5 Radar chart in arbitrary units for most relevant matrix's properties to be considered during ET experiments. ....	33
Figure 6 A) Synthetic approach to $\alpha$ -CNPV derivatives. B) Radar chart for the correlation between each synthesized $\alpha$ -CNPVs and their physicochemical properties: molar extinction coefficients at 355 nm, experimental IP values by UPS, molecular ion $[M+\bullet]$ abundance a.....	44
Figure 7 LDI MS spectra for the $\alpha$ -CNPV derivatives $\alpha$ -CNPV-H, $\alpha$ -CNPV-Cl, $\alpha$ -CNPV-CH <sub>3</sub> , $\alpha$ -CNPV-OCH <sub>3</sub> , $\alpha$ -CNPV-N(CH <sub>3</sub> ) <sub>2</sub> , $\alpha$ -CNPV-NPh <sub>2</sub> and DCTB using 0.819 $\mu$ J of laser output and 2.5 pmol of each compound on target. ....	49

Figure 8 Changes on $[M]^+$ S/N ratios for cobalt porphyrin as a function of residence time in the ion source using $\alpha$ -CNPV-CH <sub>3</sub> , $\alpha$ -CNPV-OCH <sub>3</sub> and DCTB as matrices. 1.25 pmol of analyte on target .....	51
Figure 9 MALDI spectra of polyaromatic hydrocarbons 1-6, porphyrins and phtalocyanines 7-15 and triphenylamine pigments 16-20. 1.25 pmol of each analyte on target and laser energy of 0.89 $\mu$ J per pulse .....	54
Figure 10 ET-MALDI-TOF spectra showing selective ionization, when using $\alpha$ -CNPV-CH <sub>3</sub> as matrix, of nickel and vanadyl porphyrins present in a heavy American crude-oil. ....	57
Figure 11 ET-MALDI-TOF mass spectra of 3-hexylpolythiophene using $\alpha$ -CNPV-CH <sub>3</sub> and DCTB as matrices, at 1.24 $\mu$ J per pulse of laser energy and 1:1000 matrix to analyte ratio.....	59
Figure 12 ET-MALDI-TOF-(+) spectrum in reflectron (left) and linear modes (right) of thiolated gold nanoparticles using $\alpha$ -CNPV-CH <sub>3</sub> and DCTB as matrices. ....	61
Figure 13 Analysis of fullerene derivatives by electron transfer ionization using $\alpha$ -CNPV-CH <sub>3</sub> , TPB and DCTB as MALDI matrices.....	63
Figure 14 LDI-MS spectra of all fluorene derivatives in comparisson with standar matrix DCTB, 5 pmol on target and 1.24 $\mu$ J per pulse. (middle) UV-Vis absorption screening of fluorene derivatives; inset dot line refers to 355 nm (Nd:YAG photon wavelenght). ....	87
Figure 15 (TOP) Diffuse reflection (DR) spectra for all FL derivatives and standard matrix DCTB taken in BaSO <sub>4</sub> . (BOTTON) Kubelka-Munk transformation for FL derivatives. Insets correspond to a linear fit and the cut on x-axis denotes the E <sub>g</sub> of each derivative. ....	88
Figure 16 Ion appearance curve for FL derivatives and DCTB.....	90

Figure 17 (left) ET-MALDI spectra for the ionization of cobalt porphyrin (CoPp) using Fl-CN, Fl-CH <sub>3</sub> , Fl-OCH <sub>3</sub> and DCTB as matrices. (right) ion appearance curves following the analyte radical cation signal [CoPp] <sup>+•</sup> and [M] <sup>+•</sup> ranging the laser energy from 0.34 to 2.16 $\mu$ J per pulse. ....	92
Figure 18 (left) Limit of detection for the ionization of CoPp using Fl-CN, Fl-CH <sub>3</sub> , Fl-OCH <sub>3</sub> and DCTB. (right) vacuum stability of Fl-CN, Fl-CH <sub>3</sub> , Fl-OCH <sub>3</sub> and DCTB during a long time experiment following the [CoPp] <sup>+•</sup> signal. ....	93
Figure 19 LDI and MALDI spectra using the Fl-CN and Fl-CH <sub>3</sub> of a mixture of ten porphyrins at 1.24 $\mu$ J per pulse and 1000:1 matrix to analyte molar ratio. ....	97
Figure 20 Ionization potential values for N <sub>1</sub> , S <sub>1</sub> , O <sub>1</sub> , N <sub>4</sub> VO, N <sub>4</sub> Ni core extracted from NIST. Inset at 8.42 eV corresponds to $\alpha$ -CNPV-CH <sub>3</sub> 's ionization potential. ....	110
Figure 21 Extract E6 APPI, LDI and ET-MALDI spectra in positive ion mode.....	114
Figure 22 Heteroatom class distribution in E6 for APPI(+), LDI(+) and ET-MALDI(+). ....	115
Figure 23 DBE vs Carbon Number plots for most abundant species in extract E6, using APPI, LDI and ET-MALDI. ....	117
Figure 24 Mass scale expanded-scale spectrum (m/z 513 – 518) of extract E6 using ET-MALDI(+). Insets show the isotopic fine structure determination, <sup>13</sup> C, <sup>15</sup> N and <sup>60</sup> Ni contribution corroborate the molecular formula assignments. ....	118
Figure 25 (TOP) Double Bond Equivalent (DBE) vs Number of Carbon plots for Vanadyl and Nickel porphyrins observed in extract E <sub>6</sub> . (BOTTON) Proposed structures for Vanadyl and Nickel porphyrins founded in extract E <sub>6</sub> . ....	120
Figure 26 Geochemical transformations of chlorophylls. Diagenesis involves phytol loss, decarboxylation, aromatization, metalation and heteroatom insertion; catagenesis involves thermal induced transalkylation and degradation.(Filby & Berkel, 1987).....	130

Figure 27 ET-MALDI FTICR spectra resulting from the direct analysis of the L-L ACN extract (A) and the HPTLC band (corresponding to porphyrins) (B) from a Middle-Eastern crude oil sample. ....	139
Figure 28 Expanded scale mass spectrum of the ACN extract containing Ni and V porphyrins. Insets correspond to isotopologue assignment for Nickel porphyrin DBE 18 $C_{30}H_{30}N_4Ni$ . ....	141
Figure 29 Isoabundance color-map plots corresponding to all porphyrin families found in the ACN and the HPTLC fractions. ....	142
Figure 30 Expanded scale ET-MALDI mass spectra for the ACN extract and the HPTLC fraction. ....	146
Figure 31 Significant increase in S/N ratios in the simultaneous identification of $N_4OV$ , $N_4VOS$ and $N_4VO_2$ porphyrins by ET-MALDI experiments. ....	147
Figure 32 HPTLC purification combined with high sensitivity ET-MALDI experiments, provided a significant increasing on signal-to-noise ratio corresponding to novel $N_4VO_2$ at DBE 17 porphyrins. ....	148

**List of Tables**

Table 1 Mass accuracy and signal-to-noise ratio for porphyrins and phtalocyanines ..... 96

Table 2. Relevant MS contributions to porphyrin identification ..... 132

## Resumen

**Título:** Diseño racional, síntesis, caracterización y aplicación de derivados de fenilvinileno y fluoreno como nuevas matrices MALDI

**Autor:** Juan Sebastian Ramírez Pradilla, M Sc \*

**Palabras Clave:** MALDI, matriz, fluoreno, fenilvinileno, transferencia electrónica

La espectrometría de masas por desorción laser asistida por una matriz “MALDI”, ha cumplido un papel fundamental en el análisis de macromoléculas, compuestos lábiles, moléculas de bajo peso molecular, fracciones de crudo, entre otras. Los procesos de ionización en espectrometría de masas MALDI requieren la formación de iones de la matriz la cual debe tener buena absorción de luz ultravioleta, solubilidad, cristalización homogénea y estabilidad química. Los compuestos que se emplean actualmente presentan deficiencia en los procesos de ionización, baja estabilidad química y un mal desempeño analítico gracias a la formación de agregados y productos de descomposición. Todos estos problemas se deben a que no existe un proceso racional de diseño de nuevos compuestos aptos para ser empleados como matrices MALDI. Durante las últimas dos décadas el uso de fenilvinileno y fluoreno como bloques de construcción, ha permitido la obtención de diversos materiales con aplicaciones en celdas fotovoltaicas, pantallas OLED, etc., debido a su alta conjugación, bajo costo y propiedades optoelectrónicas modulables. Este proyecto de investigación se basa en el diseño racional de derivados estructurales de fenilvinileno y fluoreno como parte de un sistema de síntesis racional soportado en cálculos teóricos que ayudarán a predecir propiedades fisicoquímicas de las moléculas las cuales serán sintetizadas y caracterizadas para su posterior aplicación como matrices MALDI. La propuesta de investigación a desarrollar se encuentra en el marco del Proyecto financiado por COLCIENCIAS convocatoria 712: “Ionización por transferencia electrónica en MALDI-MS: derivados ciano de fenilvinileno y fluoreno como matrices para el análisis de compuestos lábiles, optoelectrónicos y polímeros”

---

\*Tesis para optar el título de doctor en Química

\*\*Facultad de ciencias. Escuela de Química. Doctorado en Química. Directora: Marianny Yajaira Combariza, Ph. D. Codirector: Cristian Blanco-Tirado, Ph. D.

### Abstract

**Title:** Rational design, synthesis and applications of phenylenevinylene and fluorene derivatives as novel MALDI matrices

**Author:** Juan Sebastian Ramírez Pradilla, M Sc

**Keywords:** MALDI, matrix, fluorene, phenylenevinylene, electron transfer

Matrix-assisted laser desorption ionization mass spectrometry "MALDI", has played a fundamental role in the analysis of macromolecules, labile compounds, low molecular weight molecules, crude fractions, among others. The ionization processes in MALDI mass spectrometry require the formation of matrix ions which must have good ultraviolet light absorption, solubility, homogeneous crystallization and chemical stability. The compounds that are currently used have a deficiency in the ionization processes, low chemical stability and poor analytical performance thanks to the formation of aggregates and decomposition products. All these problems are due to the fact that there is no rational process for the design of new compounds suitable for use as MALDI matrices. During the last two decades, the use of phenylenevinylene and fluorene as building blocks has allowed obtaining different materials with applications in photovoltaic cells, OLED screens, etc., due to its high conjugation, low cost and optoelectronic tunable properties. This research project is based on the rational design of structural derivatives of phenylenevinylene and fluorene as part of a rational synthesis system supported by theoretical calculations that will help predict the physicochemical properties of the molecules which will be synthesized and characterized for subsequent application as matrices MALDI. The research proposal to be developed is within the framework of the Project funded by COLCIENCIAS call 712: " Ionización por transferencia electrónica en MALDI-MS: derivados ciano de fenilenvinileno y fluoreno como matrices para el análisis de compuestos lábiles, optoelectrónicos y polímeros "

---

\*Thesis as partial requirement for doctoral degree

\*\*Faculty of Science. School of Chemistry. Doctorate in Chemistry. Advisor: Marianny Yajaira Combariza, Ph. D. Co-advisor: Cristian Blanco-Tirado, Ph. D.

## Introduction

The accelerated growth of human race demands innovation and discovering of novel materials with applications in medicine, renewable energies, nanoscience, food, cosmetics and technology in addition with enlarging the knowledge about sources of life consumption materials like fossil fuels, agronomy soils, and sea environments. In recent years, the field of analytical chemistry has become progressively the most important tool which explain the physical and chemical transformation of the matter and phenomena related with the environmental behavior and earth life. In general, analytical sciences can extract in high confidence, valuable quantitative and qualitative information spanning from small systems to entire planets.

Since the introduction of first mass spectrograph by J.J. Thomson in 1899, mass spectrometry born as an essential tool to ionize, separate and characterize elements and compounds by their mass-to-charge ratio. Nowadays, several instruments varying the ion sources and analyzers are indispensable for current analysis in biochemistry, material science, organic chemistry, medicine, pharmacy, and fuel industry. However, despite the significant growth in the field of mass spectrometry, the physicochemical phenomena involved during the experiments are still a mystery and subject of daily study.

In 1989, Michael Karas and Franz Hillenkamp introduced the matrix-assisted laser desorption ionization, a robust and rapid method for the analysis of proteins and peptides, not possible to analyze to date; typically, analysis in MALDI-MS involves the use of an organic compound with

specific physicochemical properties as a matrix which lead the desorption/ablation and ionization step. This contribution opened a new window for macromolecule analysis by mass spectrometry, considered the Achilles' heel during century XX. Actually, a large number of macromolecules, including polymers can be analyzed using MALDI-MS, however, there is a wide range of molecules that cannot be analyzed due to particular limitations such as chemical stability, solubility, and absence of ionizable groups, demanding new developments in ionization fundamentals.

In MALDI-MS, two mechanisms dominate the ionization step; first, the well-studied proton/cation transfer from the analyte to matrix or matrix to analyte depending upon the desired ions and second, the secondary electron-transfer (ET) reactions from neutral analytes to primary ions of the matrix. Essentially, proton/cation transfer reactions yield  $[A+H]^+/[A+M]^+$  or  $[A-H]^-$  where M equals to  $Na^+$ ,  $K^+$ ,  $Ag^+$ ,  $NH_4^+$ , among others, contrarily to charge-transfer reactions which mostly yield radical species such as  $[M]^{+\bullet}$  and  $[M]^{-\bullet}$ . Surprisingly, the secondary electron-transfer reactions in MALDI-MS have been less studied than proton/cation transfer due to the complex mechanism involved during the desorption/ionization and the lack of suitable matrices. One of the advantages of secondary ET reactions in MALDI-MS is related with the ability to ionize compounds with the absence of polar groups, high-labile analytes, macromolecules and electronic polymers, that are not easily affordable using current ion sources like electrospray (ESI), electron impact (EI), atmospheric pressure photoionization (APPI) and fast atom bombardment (FAB). ET experiments are commonly held in the absence of acidic/basic media, salts, and using non-protic solvents such as dichloromethane, tetrahydrofuran, and 1,4-dioxane, which majorly prevent decomposition, reactivity and allow the analysis of intact molecules.

Nowadays, the development of MALDI matrices is focused on the design of novel compounds which effectively promotes the ionization of peptides, proteins, saccharides, metabolites and lipids. Currently used matrices such as  $\alpha$ -CHCA, DHB, dithranol, sinapinic acid, 3,4,5-trihydroxyacetophenone, HABA and 1,5-DAN enlarge the number of application in bioscience, biochemistry, and medicine. Contrarily, the design and synthesis of electron transfer matrices for MALDI-MS is still lack due to the uncomprehending ionization mechanism, the physicochemical properties whose influence the desorption/ionization process and the absence of proved applications which decrease the scientific interest.

Since the electron transfer reactions in MALDI-MS depends strongly on matrix's physicochemical properties and a better understanding on ionization mechanism, the introduction of novel compounds with well-established characteristics in order to expand the scope of the technique is desired. Along these lines, the rational design of novel electron transfer matrices within the thermodynamic framework during the secondary charge-transfer ionization in MALDI mass spectrometry is used to explain better the ET phenomena and introduce new applications on the analysis of high-labile organic compounds, polymers, nanoparticles, pigments, and crude-oil components. Chapter 1 introduce the readers into the Matrix Assisted Laser Desorption Ionization phenomena, offering a close view on secondary ionization process by electron transfer reactions. A comprehensive timeline discussion on a proposed mechanism is presented. Chapter 2 introduce the rational design of novel phenylenevinylene matrices, their spectroscopic characterization and ionization behavior within a thermodynamic framework. It is given a detailed analysis of analytical descriptors in order to select the best ET matrix from a total of six synthesized compounds for further applications in the analysis of nanoparticles, fullerenes, polymers, and biomarkers.

A detailed view on experimental conditions; since the desorption/ionization of such compounds depends strongly on the matrix to analyte ratios, deposition on target and instrument conditions, are shown. The  $\alpha$ -CNPV-CH<sub>3</sub> matrix efficiently promotes the ionization of electronic polymers like polythiophene, commercial polystyrene and thiolated nanoparticles, compounds of great importance in material science.

Chapter 3 present the design and synthesis of novel fluorene derivatives as new matrices for the analysis of macrocyclic metal organic complexes (porphyrins and phthalocyanines). Their application for petroporphyrin analysis is shown. Finally, Chapter 4 and 5 highlights the applications of electron transfer reactions in MALDI-MS for petroleomics, not reported yet in literature. ET experiments on crude-oil fractions using the  $\alpha$ -CHPV-CH<sub>3</sub> matrix enable a selective ionization of low ionization potential species occurring in fossil fuels. The experimental evidence suggests that targeted analysis of Nickel and Vanadyl porphyrins, currently associated with crude-oil lithology, kerogen formation, and origins, can be achieved after a rational design of ET experiments without extensive purification process, discussing the experimental and ionization insights when compared with current ion sources like APPI and LDI.

## 1. Matrix Assisted Laser Desorption Ionization: an overview on principles

Through the history of mass spectrometry, the discovery and evolution of ion sources and analyzers have expanded the number of applications, actually, mass spectrometry is an indispensable tool for daily analysis in biochemistry,(Vitale et al., 2015)(Mattras et al., 2002)(Reid, Brewer, & Clarke, 2004)(Satterlee et al., 2008) medicine,(Lightning et al., 2000)(Ouertatani-Sakouhi et al., 2009)(Murai, Murakami, Ito, & Miyoshi, 2015)(Calvo et al., 2012) materials science,(Liu, Loewe, & McCullough, 1999)(Dass, 2009)(De Winter et al., 2011) fuel industry,(Giraldo-Dávila, Chacón-Patiño, Ramirez-Pradilla, Blanco-Tirado, & Combariza, 2018) research, and academics. In general terms, mass spectrometry is in the purview of analytical chemistry, like other relevant techniques such as NMR, HPLC, x-ray diffraction and spectroscopy. In early years, mass spectrometry experiments were focused on obtaining valuable information about the isotopic composition of elements, and was not until the second world war, the beginning of molecule analysis for medical and fuel purposes.

In the fifties, the contributions of McLafferty, Biemann, and Djerassi for structure elucidation looking onto fragmentation patterns for small organic molecules, opened the mind of many scientists who despised the power of MS. During '60s to '80s, the analysis of macromolecules was considered the Achilles' heel due to the lack of techniques capable to turn on the gas phase, molecular elephants like proteins, nucleic acids or polymers. One of the critical impediments relied on how to volatilize and ionize these chemically sensitive molecules skipping the gas-phase collisions with reactive species, in order to prevent the decomposition or fragmentation during the

experiments. Some attempts were carried out using fast atom bombardment (FAB), plasma desorption and thermospray ionization, however, none of them were successfully done for big proteins in addition with the required amounts of each sample (milligram scale). Later on, at the end of the eighties, the simultaneous introduction of electrospray (ESI) by John Fenn and matrix-assisted laser desorption ionization (MALDI) by Franz Hillenkamp and Michael Karas for the analysis of peptides and proteins was considered the first stone to build the macromolecule-analysis world. (Karas & Hillenkamp, 1988)

Actually, electrospray ionization is considered one of the most important ion sources. As a soft ionization technique, the analysis of high labile biomolecules, ionization of large proteins by adding several charges and its ability to be coupled to HPLC instruments, makes ESI the preferred technique for many scientists. Nevertheless, several compounds with the absence of polar groups like polyaromatic compounds, fullerenes, dendrimers, electronic polymers, dyes, and non-polar polymers cannot be easily ionized by ESI, demanding novel alternatives for their analysis. Consequently, MALDI-MS emerged as a suitable technique for the analysis of titled compounds, with large differences with ESI; low amounts of sample, high sensitivity, contaminants allowance among others. One of the greatest advantages of MALDI-MS, relies in the ability to modulate the experiment conditions and sample preparation to address the ionization of analytes yielding species like **(1)**  $[A+H]^+$ , **(2)**  $[A+M]^+$ , **(3)**  $[A-H]^-$ , **(4)**  $[A]^{+\bullet}$  and **(5)**  $[A]^{-\bullet}$ , depending upon the solvent, additives and instrument conditions. As mentioned above, the ionization mechanism in MALDI goes under two general pathways; the proton/cation transfer reactions from the matrix to analytes or vice versa (ions **1**, **2** and **3**) and charge-transfer reactions involving valence electrons (ions **4** and **5**).

### 1.1. Cluster Mechanism

Almost one decade after the introduction of MALDI, the number of reports increased as a result of the potential applications on many fields, however, scientists not induced a vital discussion about ionization mechanism, leaving all aspects on sample preparation and instrument conditions. The MALDI mechanism is summarized under the “one-laser-shot-one-mass-spectrum” concept, and its difficulty relies on the speed of all events, commonly at nano/pico/femtosecond scale; consequently measurements at given level is still a challenge, especially for events involving solid ablation/desorption. The first postulate about MALDI ionization mechanism treated the events separately; ablation process, plume evolution and ion detection, however, the inability to understand the energetics of each process separately, motivated several researchers to go deeper into the MALDI ionization fundamentals, considering it as a whole process. In 2003, Michael Karas and Ralf Krüger, (Karas & Krüger, 2003) introduced the cluster mechanism, which briefly explained the process as an emission of clusters containing analytes ions into a larger crystal of the matrix. One of the crucial events in cluster mechanism is the desorption process, in figure 1, a time-scale snapshots obtained after molecular dynamics calculations revealed that cold/hot clusters and single molecules can be ejected after laser irradiation as a dense gas-phase, known as MALDI plume; the desorption step depends on the cross section of molecules, volatility, the presence of solvents within the solid solution, applied voltages, angle of laser irradiance, laser fluence and photon energy (considering IR and UV sources). Hot cluster can be considered as tiny and short-live aggregate of sample’s components containing enough energy to vaporizes during the evolution of MALDI plume, in contrast, the cold cluster does not contain enough energy to vaporizes itself and cannot be resolved over the  $m/z$ , causing the chemical noise during the experiments.

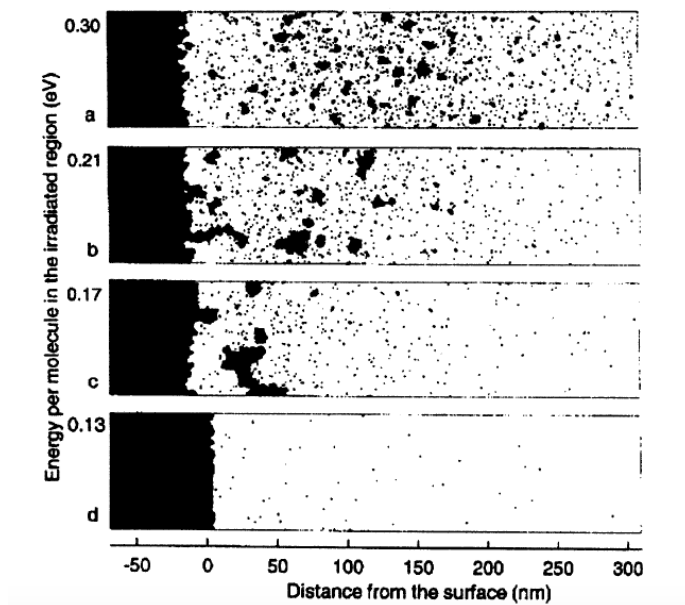


**Figure 1** Desorption event simulation by molecular dynamics at different times. (upper) molecules being desorbed from sample surface (middle) intermediate surface nucleation (lower) expansion of cold clusters.

Once the clusters are ejected from target surface, the ionization step can be considered as an ESI-like process, the preformed ions occurring into the crystals are released to the analyzer after disintegration of large aggregates (matrix evaporation) mediated by internal energy and expansion into the gas-phase, then, lucky single charged ions reach the analyzer. Consequently, detected species came from charge reduction and recombination process, depending upon the counter ions, figure 2. The main factors influencing this event are pH, presence of salts, matrix and analyte characteristics like basicity and solubility. Karas and Krüger established the lucky survival ion for cluster mechanism being the analyte's basicity the crucial factor during the ionization (peptides and proteins showing high basicity, were used during the experiments), therefore, photoionization of clusters was not largely considered, even, with having observed signals corresponding to radical cations in the resulting spectra. One of the flaws of the cluster mechanism is the scarce explanation

about the efficient formation of radical cation/anion during the MALDI experiments, especially, when low-basicity analytes or samples with the absence of proton/cations are used, hence, Karas mentioned that photoionization of surrounded matrix molecules in clusters can be possible and cannot be neglected for further considerations.

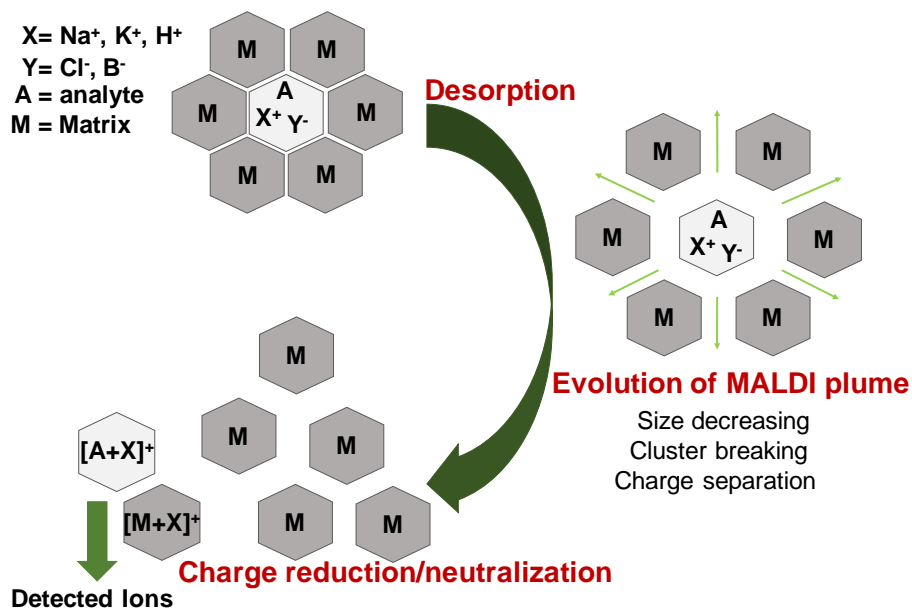


**Figure 2** Lucky ion formation within cluster mechanism, proposed by Michael Karas.

## 1.2. The Coupled Physical and Chemical Dynamics Mechanism

During early days of MALDI-MS, the observation of radical ions during the experiments meant a novel approach for the ionization and analysis of non-polar, labile and aromatic compounds of great relevance in material science.<sup>15,16</sup> Until the end of the '90s the ionization mechanism explaining the formation of radical ions remained understood and the lack of experimental evidence inspired several scientists to perform controlled experiments, disclosing the thermodynamic and kinetic aspects during the desorption and ionization events. In 1998, Richard

Knochenmuss and Renato Zenobi, introduced by the first time the concept of MALDI mechanism as separate events based on photoionization; firstly, the primary ionization of matrix step followed by the secondary gas-phase reactions to ionize the analytes occurring into the matrix clusters. Consequently, during the early days of MALDI the most forthright explanation for detected radical ions after laser irradiation, desorption and ionization was the single molecule multiphoton ionization ( $M + n(h\nu) \rightarrow M^{+\bullet} + e^{-}$ ).

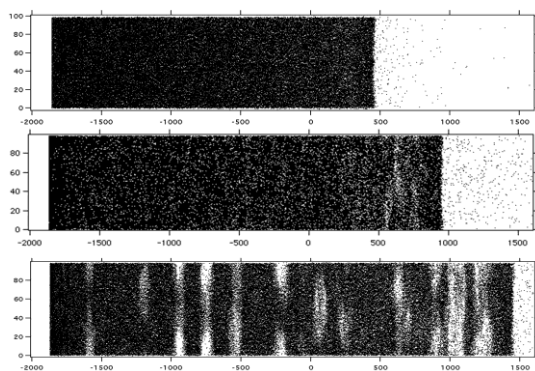


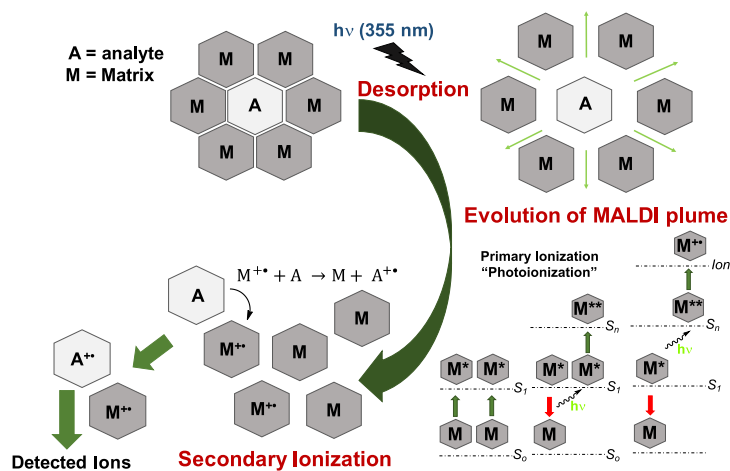
**Figure 3** Desorption event simulation by molecular dynamics at different times. (upper) molecules being desorbed from sample surface (middle) intermediate surface nucleation (lower) expansion of cold clusters.

### 1.3. Primary Ionization

The first approach was based on previous Karas' statement; matrix's radical cations/anions can be enrolled during the desorption/ionization since these ions in the gas-phase exhibit a high reactivity against protons, cations or counterions. Nevertheless, the single molecule multiphoton ionization depends directly on matrix's ionization potential, which commonly exhibits values over 8.0 eV for matrices like DHB or  $\alpha$ -CHCA and more important, the emitted photon's energy, which commonly spans from 3.67 eV ( $N_2$  laser) to 3.50 eV (Nd:YAG laser) doesn't has the enough

energy to reach the ionized state in a multiphoton process. Having considered that matrix molecules can efficiently absorb photons from laser, Knochenmuss in the same work proposed that energy pooling during the evolution of MALDI plume can occur and need to be conceivable; it is worthy of mention that ionization potential is considerably reduced when molecules are stacked, for example, DHB almost decreases its ionization potential by 0.2 eV when is clustered in the solid phase. The Knochenmuss' postulation involves an intermediate excited state whose interaction with other species results in the ionization of matrices (Figure 3). Energy pooling is plausible since the packaging of the matrix's molecules in the cluster ensures their interaction; the ionization event may occur by 3 steps, first the hopping of matrix molecules from basal state  $S_0$  to excited state ( $S_1$ ) by photon-molecule absorption, second the energy pooling by  $S_1 \rightarrow S_0 + hv$  decay, which excites a neighboring matrix in the excited state ( $S_1$ ) to a double excited state ( $S_n$ ), and third, an additional decay of one matrix in the excited state ( $S_1$ ) providing the enough energy to one matrix in the  $S_n$  state to reach the ionized state ( $S_{ion}$ ), as illustrated in the figure 3. Previous reports about solid state fluorescence measurements, (Richard Knochenmuss, 2006) proved that luminescence for commonly used matrices is quenched probably by coalescence of excitons, suggesting that annihilation process is possible, in addition, the threshold energy for matrices with given interplanar distances increases or decreases as a result of the distance between molecules. These observations supported the Knochenmuss statement and established the UV-absorption in solid state, vapor pressure, two-photon absorption properties, molecular packaging, matrix's and cluster's ionization potential as a crucial factor for primary ionization. In consequence, Knochenmuss in 2016 introduced a summarized mechanism entitled as CPCD (Coupled Physical and Chemical Dynamics) which bracketed the photophysical, kinetic and thermodynamic aspects of primary and secondary ionization step in a whole comprehended phenomenon which explains

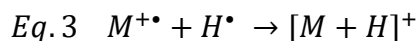
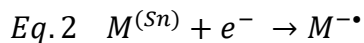
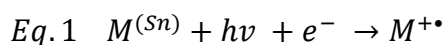
better the observed signals during MALDI experiments. Along this dissertation, the CPCD mechanism is adopted as the main ionization mechanism based on the rationale background which explains better the observation of radical species during MALDI experiments.

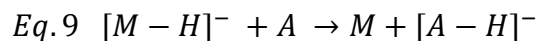
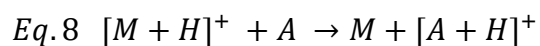
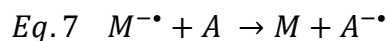
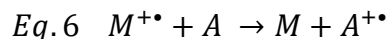
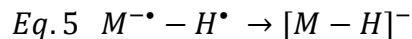
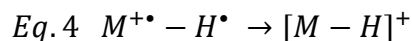


**Figure 4** Two-step ionization mechanism proposed by Richard Knochenmuss.

#### 1.4. Secondary Ionization

Contrarily to cluster mechanism in which detected ions came from preformed species (protonated or cationated form), the CPCD established the secondary ion-molecule reactions during the evolution of MALDI plume as the analyte ion source, however, this kind of ionization is a more complex event to understand and several thermodynamic aspects need to be considered. Equations 1-7 shows the ionization pathways proposed by Zenobi and Knochenmuss in 1998, based on the observed ions during controlled experiments:

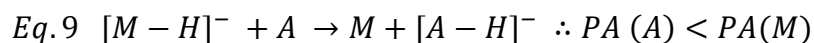
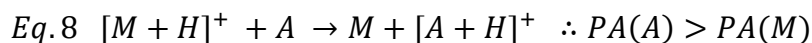




In general, secondary ionization is determined by the yield of primary ions, as far, the photoionization of matrices (equations 1-2) represent the key step of the process. Once the radicals are formed, the reactivity against added species, remaining solvent or humidity, address the secondary ionization yielding as a result  $[M+H]^+$ ,  $[M-H]^{-}$ , and, in some cases,  $[M+X]^+$  ( $X=Na, K, Ag,$  etc) ions, depending upon the functional groups, polarity and proton/cation affinity (Equations 3-5). It is widely known that excited-state basicity/acidity is dramatically affected when compared with basal state values, aftereffects, the preformed matrix's ions react with analyte neutrals, equations 6-7 under two accepted process: the matrix to analyte charge transfer reactions, involving the electrons occurring into HOMO/LUMO orbitals and proton/cation transfer ionization from matrix to analyte or vice versa, as discussed above.

In MALDI-MS, the ionization by proton/cation transfer is the largest observed phenomena in the “omics” area; metabolomics, proteomics and lipidomics.(Jaskolla, Lehmann, & Karas, 2008)(Stübiger & Belgacem, 2007)(Aboulmagd et al., 2017)(Kaya et al., 2017) Because samples came from biological systems, these molecules exhibit high proton affinities by the presence of carbonyls/amino/hydroxyl groups or carboxylic acid units. During the evolution of MALDI plume,

proton/cation transfer takes place and physicochemical properties such as proton affinities, drive the kinetic and thermodynamic aspects, then, equations 8 and 9 can be rewritten as;



Proton affinities play a crucial role, since the reaction is thermodynamically favored if the proton affinity (PA) of analytes is larger than the matrix's PA, in positive ion mode, contrarily to negative ion mode in which ions with high acidity and low proton affinity can be efficiently ionized as  $[A-H]^-$ , and matrix's preformed ions act as basic species. Summarizing, the analyte and matrix's physicochemical properties to be considered in proton/cation transfer reactions are, in order of priority, proton affinity, UV absorption, solubility, and ionization potentials.

On the other hand, secondary electron transfer (ET) reactions, of great importance for the development of current work, represent a more complex mechanism to understand. Here, the electrons occurring into valence orbitals are transferred from neutral analytes to matrix's primary ions or vice versa, accordingly to equations 6 and 7. Here, knowing the electronic structure of analytes and matrix is crucial for understand the ionization. In 1998, McCarley and Limbach, (McCarley, McCarley, & Limbach, 1998) reported by the first time the concept of electron transfer ionization in MALDI-MS, then, in 1999, reported a rational design of experiments disclosing the thermodynamic aspects during the ionization of non-polar compounds in positive ion mode MALDI experiments. As discussed in the chapters below, the electron transfer reactions between primary ions of the matrix and neutral analytes are thermodynamically favored if the  $\Delta IP$

( $\Delta IP = \text{Ionization Potential (analyte)} - \text{Ionization Potential (matrix)}$ ), yielding as a result, the radical cation corresponding to the analyte. In negative ion mode, electron affinity is the crucial factor; ( $\Delta EA = \text{Electron Affinity (analyte)} - \text{Electron Affinity (matrix)}$ ) and the reaction is thermodynamically favored when the analyte's electron affinity is larger than matrix's value. In 2006, Vasil'ev et al. (Vasil'ev et al., 2006) reported the electron transfer reactivity within the thermodynamic framework for ET reactions using non-polar analytes with defined physicochemical properties and DCTB matrix. They demonstrated the high influence of electron affinities and ionization potentials during the ET-MALDI experiments. These findings opened a new window for the analysis of non-polar compounds and the development of novel matrices for ET ionization. Henceforth, to simplify the discussion, the proton/cation transfer will be excluded, focusing on the electron transfer reactions, the main objective of this dissertation.

### **1.5. Factors influencing the matrix's performance and analyte signals in ET-MALDI: the clues behind finding the right matrix**

As summarized in the previous session, the matrix's performance in MALDI-MS relies in several physicochemical and chemical properties, in addition, the matrix's properties, sample preparation, and instrument conditions dramatically affect the analyte signals, being necessary to comprehend the behind of observed results for further discussions in chapters 1, 2 and 3. As discussed above, the mechanistic aspects of MALDI, treated the process as a two-step event; primary and secondary ionization. Going beyond the CPCD model, (R. Knochenmuss, 2016) physicochemical and chemical properties like UV absorption, fluorescence, conjugation, ionization potential, electron affinity, gas-phase reactivity, crystallization, and solubility need to

be considered during the experimentation. Commonly, manufacturers of MALDI instruments incorporate a tripled Nd:YAG solid state-laser emitting UV photons at 355 nm with a specific energy of 3.5 eV. From a simplified point of view, MALDI can be treated as a UV process in which electrons on the valence orbitals (HOMO) are involved (as shown in figure 4). From a given energy and laser fluence, the ion yields of matrices differing on UV absorption properties can significantly vary; we previously demonstrated that phenylenevinylene derivatives with donor substituents and high  $\epsilon_{\lambda=355}$  values showed higher ion yields and low energy threshold in contrast with phenylenevinylenes containing acceptor groups and low  $\epsilon_{\lambda=355}$  values, when subjected to LDI experiments at the same laser output energy.(Castellanos-García et al., 2017) In consequence, a matrix with low UV absorption properties results in hard threshold energy and low yield of primary ions, then, the signal of the analyte is drastically affected.

During the evolution of MALDI plume, the interaction between matrix molecules also affects the yield of primary ions; a good crystallization in which the aromatic rings of the matrix are in a distance  $<4\text{\AA}$ , may help during the energy pooling, in addition, the fluorescence properties are important since low values of radiative quantum yields " $\phi_f$ " ensures that emitted photons stay within the cluster, driving the matrix molecules to the excited/ionized state. In previous reports, solid state fluorescence experiments,(Richard Knochenmuss, 2004) using DHB matrix, revealed that emitted photons rarely overcome the half of absorbed ones and exhibits a typical non-radiative process. Interestingly, packaging of DHB molecules also revealed a significant decreasing on ionization potential from 8.05 to 7.93 eV. Considering an ideal event in which primary ions are formed in high yields, there are other critical factors affecting the signal of analytes. Since analyte molecules need to be occluded into the matrix crystal, the solubility of sample components in a

common solvent is desired. For non-polar matrices like anthracene, 9,10-diphenylanthracene or DCTB, solvents like tetrahydrofuran, dichloromethane, 1,4-dioxane, and ether are commonly used,(Ulmer, Mattay, Torres-Garcia, & Luftmann, 2000)(Nazim Boutaghou & Cole, 2012) instead of DHB,  $\alpha$ -CHCA or sinapinic acid which are solubilized in polar and protic solvents like water, acetonitrile, methanol and ethanol, in the presence of acidic media. In the hypothetical case of low solubility, exclusion of analytes from crystal matrix is commonly observed affecting the ion yields. Additionally, the solvent determines the crystal size, then, large and compact crystals are hard to ionize, whereas well distributed tinny crystals on MALDI target can be efficiently desorbed/ionized during the experiments. In MALDI-MS, electron transfer ionization is used for the analysis of non-polar and high-labile compounds. Sample preparation for ET experiments reduces the use of acidic/basic media or protic solvents in order to prevent the chemical decomposition or reactivity in the gas-phase. In addition, common matrices for ET ionization, 9-nitroanthracene,(Juhasz & Costello, 1993) DCTB,(Ulmer et al., 2000)(Wyatt, Stein, & Brenton, 2006) anthracene, 9,10-diphenylanthracene,(Nazim Boutaghou & Cole, 2012) terthiophene, and tetraphenyl-1,3-butadiene are highly soluble in non-polar solvents, which are likely chosen to reduce the matrix-solvent reaction ensuring the formation of intact radical species. These matrices have been used for the analysis of high labile analytes based on fullerene, chlorophylls, porphyrins, polymers, and pigments with good results, however, the lack on performance related with a poor rational design gives limited physicochemical properties and dramatically affects the final results during the experiments. Under controlled conditions and the same matrix-to-analyte ratio, the signal of analyte after ET ionization is conditioned to the thermodynamics of the ET reaction; for a hypothetic analyte ionization potential value of 7.4 eV, the  $\Delta IP$  using DCTB (8.54 eV), 9-nitroanthracene (7.8 eV) and 9,10-diphenylanthracene (7.5 eV) is -1.04, -0.3 and -0.1 eV

respectively, thus, the analyte signal for DCTB using is expected to show the highest abundance. Consequently, matrices with ionization potentials between 8.0 and 9.0 eV are desired. The radar chart shown in figure 5, summarizes the optimal matrix's physicochemical properties to be considered during the election of compounds; as mentioned above, a higher ionization potential ensures the ionization of a wide range of analytes, a good primary ion formation as a consequence of higher UV absorption and low energy threshold and solubility/crystallization in a common solvent used for analytes.

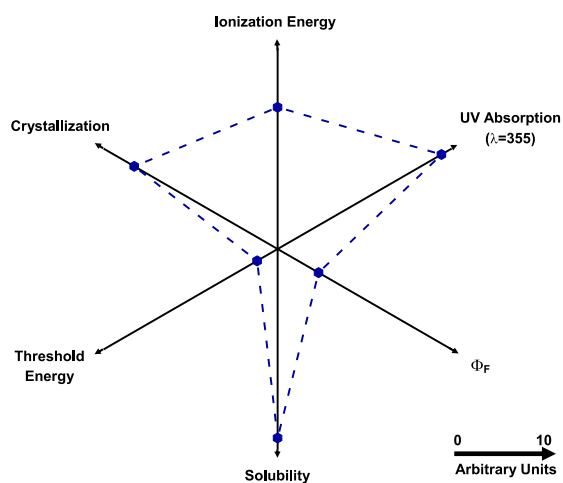


**Figure 5** Radar chart in arbitrary units for most relevant matrix's properties to be considered during ET experiments.

Along the chapters 2 and 3, the correlation between physicochemical properties of rationally designed matrices, their performance in LDI-MS and the analytical behavior for their use as MALDI matrices are shown. This manuscript focuses on the study of analytical descriptors obtained after extensive MS experiments in MALDI-TOF and MALDI-FTICR using the fluorene and  $\alpha$ -cyanophenylenevinylene matrices for the ionization of organic materials, nanoparticles, crude-oil biomarkers.

## References

- Aboulmagd, S., Esteban-Fernández, D., Moreno-Gordaliza, E., Neumann, B., El-Khatib, A. H., Lázaro, A., ... Linscheid, M. W. (2017). Dual Internal Standards with Metals and Molecules for MALDI Imaging of Kidney Lipids. *Analytical Chemistry*, 89(23), 12727–12734.
- Calvo, E., Barasoain, I., Matesanz, R., Pera, B., Camafeita, E., Pineda, O., ... Díaz, J. F. (2012). Cyclostreptin Derivatives Specifically Target Cellular Tubulin and Further Map the Paclitaxel Site. *Biochemistry*, 51(1), 329–341.
- Castellanos-García, L. J., Agudelo, B. C., Rosales, H. F., Cely, M., Ochoa-Puentes, C., Blanco-Tirado, C., ... Combariza, M. Y. (2017). Oligo p-Phenylenevinylene Derivatives as Electron Transfer Matrices for UV-MALDI. *Journal of The American Society for Mass Spectrometry*.
- Dass, A. (2009). Mass spectrometric identification of Au<sub>68</sub>(SR)<sub>34</sub> molecular gold nanoclusters with 34-electron shell closing. *Journal of the American Chemical Society*, 131(33), 11666–11667.
- De Winter, J., Deshayes, G., Boon, F., Coulembier, O., Dubois, P., & Gerbaux, P. (2011). MALDI-ToF analysis of polythiophene: Use of trans-2-[3-(4-t-butyl-phenyl)-2-methyl-2-propenyldene]malononitrile - DCTB - as matrix. *Journal of Mass Spectrometry : JMS*, 46, 237–246.
- Giraldo-Dávila, D., Chacón-Patiño, M. L., Ramirez-Pradilla, J. S., Blanco-Tirado, C., & Combariza, M. Y. (2018). Selective ionization by electron-transfer MALDI-MS of vanadyl porphyrins from crude oils. *Fuel*, 226(March), 103–111.
- Jaskolla, T. W., Lehmann, W.-D., & Karas, M. (2008). 4-Chloro-alpha-cyanocinnamic acid is an

- advanced, rationally designed MALDI matrix. *Proceedings of the National Academy of Sciences of the United States of America*, 105(34), 12200–12205.
- Juhasz, P., & Costello, C. E. (1993). Generation of large radical ions from oligometalloenes by matrix-assisted laser desorption ionization. *Rapid Communications in Mass Spectrometry*, 7(5), 343–351.
- Karas, M., & Hillenkamp, F. (1988). Laser desorption ionization of proteins with molecular masses exceeding 10,000 daltons. *Analytical Chemistry*, 60(20), 2299–2301.
- Karas, M., & Krüger, R. (2003). Ion Formation in MALDI: The Cluster Ionization Mechanism. *Chemical Reviews*, 103(2), 427–440.
- Kaya, I., Michno, W., Brinet, D., Iacone, Y., Zanni, G., Blennow, K., ... Hanrieder, J. (2017). Histology-Compatible MALDI Mass Spectrometry Based Imaging of Neuronal Lipids for Subsequent Immunofluorescent Staining. *Analytical Chemistry*, 89(8), 4685–4694.
- Knochenmuss, R. (2016). *The Coupled Chemical and Physical Dynamics Model of MALDI. Annual Review of Analytical Chemistry* (Vol. 9).
- Knochenmuss, Richard. (2004). Photoionization pathways and free electrons in UV-MALDI. *Analytical Chemistry*, 76(11), 3179–3184.
- Knochenmuss, Richard. (2006). Ion formation mechanisms in UV-MALDI. *Analyst*, 131(9), 966–986.
- Lightning, L. K., Jones, J. P., Friedberg, T., Pritchard, M. P., Shou, M., Rushmore, T. H., & Trager, W. F. (2000). Mechanism-Based Inactivation of Cytochrome P450 3A4 by L-754,394. *Biochemistry*, 39(15), 4276–4287.
- Liu, J., Loewe, R. S., & McCullough, R. D. (1999). Employing MALDI-MS on Poly(alkylthiophenes): Analysis of Molecular Weights, Molecular Weight Distributions,

- End-Group Structures, and End-Group Modifications. *Macromolecules*, 32(18), 5777–5785.
- Mattras, H., Aliau, S., Richard, E., Bonnafous, J.-C., Jouin, P., & Borgna, J.-L. (2002). Identification by MALDI-TOF Mass Spectrometry of 17 $\alpha$ -Bromoacetamidopropylestradiol Covalent Attachment Sites on Estrogen Receptor  $\alpha$ . *Biochemistry*, 41(52), 15713–15727.
- McCarley, T. D., McCarley, R. L., & Limbach, P. A. (1998). Electron-transfer ionization in matrix-assisted laser desorption/ionization mass spectrometry. *Analytical Chemistry*, 70(20), 4376–4379.
- Murai, M., Murakami, S., Ito, T., & Miyoshi, H. (2015). Amilorides Bind to the Quinone Binding Pocket of Bovine Mitochondrial Complex I. *Biochemistry*, 54(17), 2739–2746.
- Nazim Boutaghou, M., & Cole, R. B. (2012). 9, 10-Diphenylanthracene as a matrix for MALDI-MS electron transfer secondary reactions. *Journal of Mass Spectrometry*, 47(8), 995–1003.
- Ouertatani-Sakouhi, H., El-Turk, F., Fauvet, B., Roger, T., Le Roy, D., Karpinar, D. P., ... Lashuel, H. A. (2009). A New Class of Isothiocyanate-Based Irreversible Inhibitors of Macrophage Migration Inhibitory Factor. *Biochemistry*, 48(41), 9858–9870.
- Reid, C. W., Brewer, D., & Clarke, A. J. (2004). Substrate Binding Affinity of *Pseudomonas aeruginosa* Membrane-Bound Lytic Transglycosylase B by Hydrogen–Deuterium Exchange MALDI MS. *Biochemistry*, 43(35), 11275–11282.
- Satterlee, J. D., Suquet, C., Bidwai, A. K., Erman, J. E., Schwall, L., & Jimenez, R. (2008). Mass Instability in Isolated Recombinant FixL Heme Domains of *Bradyrhizobium japonicum*. *Biochemistry*, 47(6), 1540–1553.
- Stübiger, G., & Belgacem, O. (2007). Analysis of Lipids Using 2,4,6-Trihydroxyacetophenone as a Matrix for MALDI Mass Spectrometry. *Analytical Chemistry*, 79(8), 3206–3213.
- Ulmer, L., Mattay, J., Torres-Garcia, H. G., & Luftmann, H. (2000). Letter: The use of 2-[(2E)-3-

(4-tert-butylphenyl)-2-methylprop-2-enylidene] malononitrile as a matrix for matrix-assisted laser desorption/ionization mass spectrometry. *European Journal of Mass Spectrometry*, 6(1), 49–52.

- Vasil'ev, Y. V, Khvostenko, O. G., Streletskii, A. V, Boltalina, O. V, Kotsiris, S. G., & Drewello, T. (2006). Electron transfer reactivity in matrix-assisted laser desorption/ionization (MALDI): ionization energy, electron affinity and performance of the DCTB matrix within the thermochemical framework. *The Journal of Physical Chemistry A*, 110(18), 5967–5972.
- Vitale, R., Angelini, R., Lobasso, S., Capitanio, G., Ludwig, B., & Corcelli, A. (2015). MALDI-TOF MS Lipid Profiles of Cytochrome c Oxidases: Cardiolipin Is Not an Essential Component of the *Paracoccus denitrificans* Oxidase. *Biochemistry*, 54(4), 1144–1150.
- Wyatt, M. F., Stein, B. K., & Brenton, A. G. (2006). Characterization of Various Analytes Using Matrix-Assisted Laser Desorption/Ionization Time-of-Flight Mass Spectrometry and 2-[(2E)-3-(4-tert-Butylphenyl)-2-methylprop-2-enylidene] malononitrile Matrix. *Analytical Chemistry*, 78(1), 199–206.

## **2. Electron transfer ionization of nanoparticles, polymers, porphyrins and fullerenes using synthetically-tunable $\alpha$ -cyano-phenylenevinylenes as UV MALDI-MS matrices**

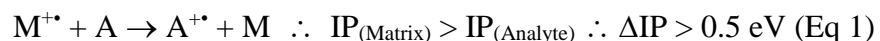
### **2.1. Abstract**

Electron transfer (ET) ionization in MALDI is widely used for the analysis of functional materials which are labile, unstable and reactive in nature. However, conventional ET matrices (e.g. DCTB) still lack in performance due to cluster formation, reactivity with analytes and vacuum instability. In this contribution we report the use of  $\alpha$ -cyano-phenylenevinylene derivatives as UV-MALDI matrices for the analysis, by ET ionization, of nanoparticles, polymers, porphyrins and fullerenes. The synthetic versatility of the phenylenevinylene (PV) core allowed us to modulate physicochemical properties, fundamental for efficient formation of primary ions in the gas phase under MALDI conditions, such as planarity, ionization potentials, molar absorptivity and laser thresholds. For instance, introduction of -CN groups in vinyl positions of the PV core induced structural disruption in planarity in the new  $\alpha$ -CNPV derivatives, shifting their maximum molar absorptivity to UV wavelengths, and increasing their ionization energy values above 8.0 eV. UV MALDI-relevant photophysical properties in solution and solid state are reported ( $\lambda_{\text{max}}$  and  $\epsilon_{355\text{nm}}$ ). LDI spectra of  $\alpha$ -CNPVs exhibit predominantly signals due to  $M^{+}$  and  $[M+H]^{+}$  species, while the standard matrix DCTB show peaks associated with clusters and non-desirable products. The MS performance of six  $\alpha$ -CNPV derivatives was assessed for the ionization of a standard compound, with  $\alpha$ -CNPV-CH<sub>3</sub> and  $\alpha$ -CNPV-OCH<sub>3</sub> exhibiting better analytical figures of merit than those of a standard matrix (DCTB). These new matrices display high vacuum stability (79%) for up to 240

minutes of residence in the ionization source, in contrast with DCTB with 13%. Vacuum stability is vital, particularly for applications such as high-throughput analysis and imaging MS. In addition, when a mixture of twenty analytes (PAHs, porphyrins and triphenylamine dyes) ranging from  $m/z$  300 to 1700 was analyzed via ET MALDI, we observe analyte coverage of 90% with the  $\alpha$ -CNPV-CH<sub>3</sub> derivative, while DCTB afforded only 70%. Finally,  $\alpha$ -CNPV-CH<sub>3</sub> was tested, and compared with DCTB, as ET-MALDI matrix for petroporphyrins, conjugated polymers, gold nanoparticles, and fullerene derivatives analysis, outperforming in most cases the standard matrix.

## 2.2. Introduction

In MALDI-MS the electron transfer (ET) process in positive ion mode, involves a transfer of an electron from a low ionization potential (IP) neutral molecule (A:analyte) to an already ionized high IP molecule (M:matrix) to yield an analyte molecular ion (A<sup>+</sup>), according to the following mechanism:(McCarley, McCarley, & Limbach, 1998)



This versatile gas-phase reaction is used to charge molecules of fundamental importance in material science, that otherwise would not be amenable to mass spectrometric analysis, such as non-volatile molecules,(Wyatt, Stein, & Brenton, 2006) conjugated polymers,(De Winter et al., 2011) non-polar hydrocarbons,(McCarley et al., 1998) nanoparticles,(Chaki, Negishi, Tsunoyama, Shichibu, & Tsukuda, 2008) fullerene derivatives and dyes.(Ulmer, Mattay, Torres-Garcia, & Luftmann, 2000)(Castellanos-García et al., 2017) However, a widespread analytical use of ET

processes in MALDI strongly depends on the availability of adequate matrices to effectively promote the bimolecular ET reaction. Since the first reports on ET-MALDI in the 90s, (Juhász & Costello, 1993) the development of suitable matrices for this process has been timid to say the least. Systematic searches for new organic compounds as MALDI matrices are rare in literature, and most efforts are isolated, analyte-dependent and amount to a really small group of compounds including 9-nitroanthracene (9-NA), (Juhász & Costello, 1993) trans-2-[3-(4-tert-butylphenyl)-2-methyl-2-propenylidene] malononitrile (DCTB), (Ulmer et al., 2000) 1,9-diphenylanthracene (1,9-DPA), (Nazim Boutaghou & Cole, 2012) terthiophene (TER) and 1,5-diaminonaphthalene (1,5-DAN), (Calvano, Ventura, Cataldi, & Palmisano, 2015) 9,10-DPA is an efficient ET MALDI matrix for analysis of compounds like retinol, fullerenes and chlorophyll-a; however, a low IP value (7.25 eV) restricts its use to the analysis of compounds with IPs below 7.0 eV. (Nazim Boutaghou & Cole, 2012) A similar issue is observed with oligomers such as terthiophene (TER, IP= 7.5 eV), used by Suzuki and co-workers for the analysis of chlorophyll derivatives. More recently Calvano, *et al.* reported the use of 1,5-diaminonaphthalene (1,5-DAN, IP 6.74 eV), a traditional matrix for in source decay ISD, for the electron transfer ionization of bacteriochlorophylls from cyanobacteria. (Calvano et al., 2017) The 1,5-DAN outperformed DCTB and TER, in terms of sensitivity, due perhaps to high yields of primary ions ( $M^{+\bullet}$  and  $M^{\bullet}$ ) which favor chlorophylls (IP 6.0-6.3 eV) secondary ion formation. The DCTB, perhaps the most successful ET-MALDI matrix to date, was put forward by Ulmer, *et al.* for the analysis of fullerene derivatives. (Ulmer et al., 2000) This compound has advantages such as good solubility, high IP (8.54 eV) and good UV molar absorptivity making it a good matrix for the analysis of fullerenes, (Kotsiris et al., 2006) polymers, (Macha & Limbach, 2002) conjugated polymers, (Chendo et al., 2015) and conjugated organic compounds. (Wyatt et al., 2006) However,

DCTB still lacks in performance as ET MALDI matrix due to several issues related to cluster formation in the low-mass region, reactivity with analytes, chemical decomposition and vacuum instability, among others.(Wyatt et al., 2006)(Lou, de Waal, van Dongen, Vekemans, & Meijer, 2010)

In organic material science, highly conjugated structures based on oligo-*p*-phenylenevinylenes (*p*-PV) exhibit outstanding performance as OLEDs,(Moorthy, Venkatakrishnan, Natarajan, Lin, & Chow, 2010)(Jandke, Strohrriegl, Gmeiner, Brütting, & Schwoerer, 1999) sensitizers,(J.-J. Li, Chen, Yu, Cheng, & Liu, 2018)(Ding et al., 2018) bioimage dopants,(Chen et al., 2018)(Feng, Wang, & Ju, 2018) non-linear optic materials,(Camposeo, Del Carro, Persano, & Pisignano, 2012) two-photon absorption compounds,(Chung et al., 2005)(Scotognella et al., 2011)(Fang et al., 2010) and organic solar cell light harvesters.(Ameri, Khoram, Min, & Brabec, 2013)(Vandenbergh et al., 2011)(Masuda et al., 2010)(Mikroyannidis, Kabanakis, Suresh, & Sharma, 2011) The photophysical properties of PV, and similar compounds such as fluorenes, prompted us to systematically study the feasibility of using these organic materials as ET MALDI matrices in mass spectrometry. In an exploratory report we reported the successful use of *p*-PV,(Castellanos-García et al., 2017) with electron-donor and electron withdrawing groups on the peripheral phenyl rings, as ET MALDI matrices for the ionization of porphyrins, phthalocyanines and polyaromatics. The position of the substituents on the PV core dramatically influenced the derivatives photophysical and mass spectrometric performance. In this first approach we singled out the *p*-CNPV derivative, from eight different structures tested, as promising ET-MALDI matrix due to its analytical performance. For instance, when compared with DCTB, *p*-CNPV increased the S/N for standard analytes from 3 up to 500 times. However, despite its interesting properties

as ET-MALDI matrix, the *p*-CNPV derivative has some structurally-related disadvantages such as low IP (7.96 eV) -which restricts the molecule's use for ET ionization of a wider range of analytes- and low solubility in MALDI-suitable solvents which dramatically affects crystallization and sample distribution homogeneity.

Continuing with our quest for developing broad-spectrum ET MALDI matrices, here we report the development of six new phenylenevinylene derivatives with -CN groups on the vinyl bridges ( $\alpha$ -CNPVs) and a variety of EDG (-CH<sub>3</sub>, OCH<sub>3</sub>, N(CH<sub>3</sub>)<sub>2</sub>, N(Ph)<sub>2</sub>) and EWG (-Cl) on the peripheral *p*-positions, following the rational design concept introduced by Jaskolla and co-workers.(Jaskolla, Lehmann, & Karas, 2008) When compared with the previously reported *p*-CNPV, introduction of -CN groups in vinyl positions induced structural disruption in planarity in the new  $\alpha$ -CNPV derivatives, shifting their maximum molar absorptivity to lower wavelengths, and increasing their ionization energy values above 8.0 eV. In addition, the presence of electron donor groups (EDG) causes a red shift in the UV absorption maxima increasing molar absorptivity of the derivatives due to changes in the HOMO energy and electron enrichment over the  $\pi$ -backbone. Meanwhile, electron-withdrawing groups (EWG) exhibit a blue-shift in the UV absorption maxima and significant decrease in the molar extinction coefficient. EWG and EDG substituents can, respectively, increase (>8.2) or decrease (<8.2) theoretical ionization potentials (IP). UV MALDI-relevant photophysical properties in solution and solid state are reported ( $\lambda_{\max}$  and  $\epsilon_{355\text{nm}}$ ) as well as the  $\alpha$ -CNPVs analytical performance as ET-MALDI matrices for the analysis of a wide range of functional materials such as dyes, polyaromatics, fullerenes, porphyrinic compounds, gold nanoparticles and electronic polymers. We always compared the  $\alpha$ -CNPV's performance with the standard DCTB.

## 2.3. Results and Discussion

**2.3.1.  $\alpha$ -CNPVs synthesis and characterization.** Figure 6A shows a straightforward and synthetically elegant route to  $\alpha$ -CNPV derivatives ( $\alpha$ -CNPV-H,  $\alpha$ -CNPV-Cl,  $\alpha$ -CNPV-CH<sub>3</sub>,  $\alpha$ -CNPV-OCH<sub>3</sub>,  $\alpha$ -CNPV-N(CH<sub>3</sub>)<sub>2</sub> and  $\alpha$ -CNPV-NPh<sub>2</sub>) using the classic Knoevenagel reaction in basic media. This versatile approach easily allows the introduction of EWG and EDG substituents on the para positions of  $\alpha$ -CNPV, through the aldehyde precursor, which not only allows modulation of solid-phase absorption properties (causing red or blue shifts respectively) but also physicochemical properties such as ionization potential (IP) and solubility. Supporting information (Scheme S1) contains detailed description of  $\alpha$ -CNPV synthesis. From our previous work we know that *p*-CNPVs efficiently aggregate in solid and liquid phases, forming  $\pi$  stacking structures with low interplanar distances ( $< 8 \text{ \AA}$ ) that favor exciton formation in solid phase and increase the ability to incorporate conjugated analytes such as polyaromatics, dyes and porphyrins.(Castellanos-García et al., 2017)(Wang, Collison, & Rothberg, 2001)(Cornil, Heeger, & Bredas, 1997)(R. Knochenmuss, 2016) However, aggregation proneness in *p*-CNPV results in decreased solubility in common electron-transfer MALDI solvents such as THF, ACN, toluene and DCM. Introduction of -CN groups onto the vinyl bridges of the PV core (Figure 6A), instead of the *p* position of the phenylene ring, improved  $\alpha$ -CNPV solubility and altered their structure by breaking planarity. This latter effect also resulted in increased IPs for  $\alpha$ -CNPVs while also induced a blue shift in the solid state and two-photon absorption properties of the derivatives.(Yoo et al., 2003)(Xu, Xie, Zhang, Shen, & Ma, 2016)(Chung et al., 2005)(Pond et al., 2002) The two photon absorption, a phenomenon related with nonlinear optics, is a characteristic property of organic materials associated with the ability to absorb two photons from different sources (laser or

a neighbor-emitted photon) to reach an excited state ( $S_n$ ) non linearly, as reported by Bubeck and co-workers.(Bubeck et al., 1989) It is well-know that introducing a high electron affinity cyano group on a vinyl bridge in PVs enhance the effective two photon absorption cross section of the molecule turning it into a donor-acceptor push pull system (D-A- $\pi$ -A-D).(Yoo et al., 2003):(Pond et al., 2002)

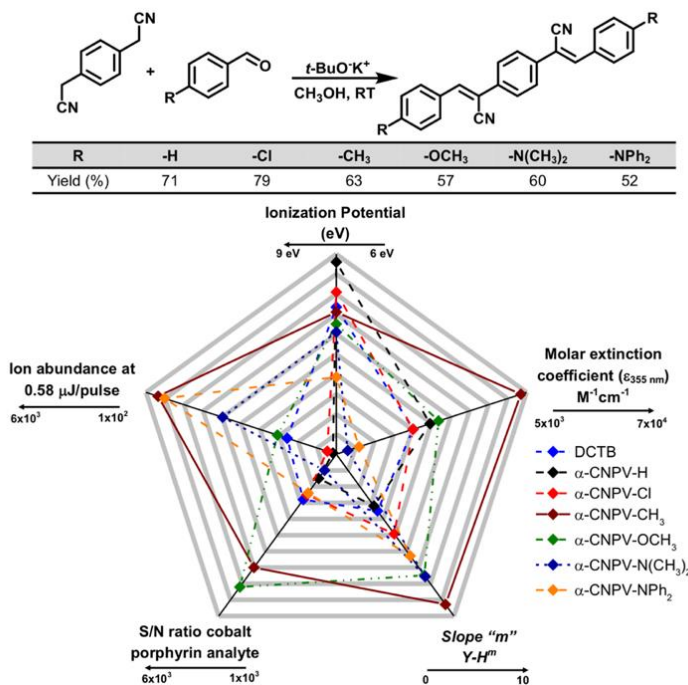


**Figure 6** A) Synthetic approach to  $\alpha$ -CNPV derivatives. B) Radar chart for the correlation between each synthesized  $\alpha$ -CNPVs and their physicochemical properties: molar extinction coefficients at 355 nm, experimental IP values by UPS, molecular ion  $[\text{M}^+\bullet]$  abundance a

The radar chart in Figure 1B compiles characterization information for the six  $\alpha$ -CNPV derivatives and DCTB in terms of molar extinction coefficients at  $\lambda_{355 \text{ nm}}$  from UV-Vis spectra, experimental ionization potential (IP) values obtained by UPS, molecular ion ( $\text{M}^+$ ) abundance at  $0.58 \mu\text{J}$  per pulse, slopes ( $m$ ) from ion abundance vs laser energy plots, and mass spectrometric

performance (S/N ratios) for a single analyte. The experimental data used for building the radar chart can be found in the Supporting Information Figures S1, S2, S3 and S4. Figure S1 of the Supporting Information shows characteristic UV-vis absorption bands in  $\alpha$ -CNPV derivatives, related mostly with  $\pi$ - $\pi^*$  transitions, located between 200 and 400 nm; as a reference point, the basic  $\alpha$ -cyanophenylenevinylene core ( $\alpha$ -CNPV-H) shows UV absorption maximum ( $\lambda_{\text{max}}$ ) at 349 nm. The inclusion of a soft EDG group such as  $-\text{CH}_3$ , in the phenylene *para*- position, induces a red shift to  $\lambda_{\text{max}}=355$  nm, the wavelength of the Nd:YAG laser; while a strong EDG group  $-\text{OCH}_3$ , causes an even more dramatic red shift to  $\lambda_{\text{max}}=365$  nm. In addition, the introduction of basic auxochromic substituents (also EDGs) in the  $\alpha$ -CNPV core, such as  $\text{N}(\text{CH}_3)_2$  and  $\text{NPh}_2$ , cause even stronger red shifts in the  $\lambda_{\text{max}}$  to 425 and 430 nm, respectively. Interestingly, as the red shift increases (by inclusion of EDG groups) the IP of the derivative decreases; UPS measurements show IP values of 8.30, 8.22, and 7.77 eV for derivatives with  $-\text{OCH}_3$ ,  $-\text{N}(\text{CH}_3)_2$  and  $-\text{NPh}_2$  groups in contrast with 8.92 eV for the  $\alpha$ -CNPV-H core. On the other hand, introduction of a EWG group ( $-\text{Cl}$ ) barely affects the  $\lambda_{\text{max}}$ , with a shift from 349 nm (in  $\alpha$ -CNPV-H) to 351 nm (for  $\alpha$ -CNPV-Cl). Finally, the  $\alpha$ -CNPV-Cl derivative exhibits the second highest IP value of the series, corresponding to 8.62 eV, in comparison with 8.92 eV for the  $\alpha$ -CNPV-H core.

Since the electron transfer process in MALDI strongly depends on matrix photoexcitation and primary ion formation (Eq 1.); molar absorptivity at 355 nm can be used as an initial approximation to weight the photophysical performance of the matrix candidates when compared with the standard DCTB. (Richard Knochenmuss, 2006) (Breuker, Knochenmuss, Zhang, Stortelder, & Zenobi, 2003) (R. Knochenmuss, 2016) UV-vis analysis (at 355 nm) in solution show for  $\alpha$ -CNPV-H,  $\alpha$ -CNPV- $\text{CH}_3$  and  $\alpha$ -CNPV- $\text{OCH}_3$ , molar absorptivities of 38.000, 70.000 and 41.000

$\text{M}^{-1}\text{cm}^{-1}$ , respectively (Figure 6B, Figure S2). These values are all above DCTB ( $32.000 \text{ M}^{-1}\text{cm}^{-1}$ ) indicating that these  $\alpha$ -CNPV derivatives have interesting UV absorption properties in the liquid phase. However, since primary ion formation in MALDI strongly depends on matrix photophysical properties in solid phase, in Figure S1 the diffuse reflectance spectra corresponding to all  $\alpha$ -CNPVs and the standard matrix DCTB reveal efficient photon absorption in the wavelength range of the Nd:YAG laser.

The performance of an ET MALDI matrix is also related to its ability to form a dense plume of primary ions at laser energies close to the matrix threshold. Figure S3 shows the ion yield in function of laser energy per pulse (from 0.39 to 2.80  $\mu\text{J}$ ) for  $\alpha$ -CNPV derivatives and DCTB. Logarithmic appearance curves of ion yield vs laser energy per pulse exhibit a well-known shape starting with a steep slope covering almost an order of magnitude along the energy per pulse axis and finishing with a plateau. Leveling off, in the ion abundance appearance curves, can be related to either detector saturation or fragmentation/decomposition of matrix's primary ions as a consequence of the high laser energy. (Dreisewerd, 2003) Four  $\alpha$ -CNPV derivatives plus the standard matrix (DCTB) showed ion yields in the range of  $10^2$  to  $10^3$  counts at low laser energy per pulse values (0.58  $\mu\text{J}$ ), interestingly these derivatives exhibit the lowest ionization potential of the series:  $\alpha$ -CNPV- $\text{CH}_3$  (8.42 eV),  $\alpha$ -CNPV- $\text{OCH}_3$  (8.30 eV),  $\alpha$ -CNPV- $\text{N}(\text{CH}_3)_2$  (8.22 eV) and  $\alpha$ -CNPV- $\text{NPh}_2$  (7.77 eV). The derivatives  $\alpha$ -CNPV- $\text{Cl}$  (IE: 8.62 eV) and  $\alpha$ -CNPV- $\text{H}$  (IP: 8.92 eV) show ion yields below  $10^2$  at 0.58  $\mu\text{J}$ . At laser energies above 0.89  $\mu\text{J}$  per pulse the ion yields for the standard DCTB matrix level off at 104 counts, while the  $\alpha$ -CNPV derivatives still show a linear dependence between laser energy and ion abundance up to 1.33  $\mu\text{J}$ . When reaching a plateau,

ion abundance for  $\alpha$ -CNPVs are 1.5 orders of magnitude above those of DCTB. These observations show abundant yields of matrix primary ions for the  $\alpha$ -CNPV derivatives, which in turn could promote gas-phase ion-molecule charge exchange reactions with analytes. To further support this assertion, the radar plot in Figure 6B, shows the slopes ( $m$ ) of linear sections of the ion abundance vs laser energy plots (Figure S3) when fitted to the form  $Y \sim H^m$ , where “Y” represents the ion yield, “H” the laser energy and “ $m$ ” indicates the molecule’s ability to form primary ions. Derivatives with the lowest IP values and highest molar absorptivity exhibit the highest “ $m$ ” values, as is the case with  $\alpha$ -CNPV-CH<sub>3</sub> ( $m = 7.64$ ). MALDI-MS matrices with “ $m$ ” values between 5-10 can efficiently form primary ions, which is of fundamental importance to form secondary ions according to Eq 1. (Dreisewerd, 2003) As an exploratory way to measure the performance of  $\alpha$ -CNPV derivatives as ET matrices, we selected the cobalt porphyrin (IP  $\sim$  6.58 eV) as standard analyte (Figure S4). As seen in Figure 6B,  $\alpha$ -CNPV-CH<sub>3</sub> and  $\alpha$ -CNPV-OCH<sub>3</sub> afforded the highest S/N ratios ( $4.5 \times 10^3$  and  $5.0 \times 10^3$ , respectively) for cobalt porphyrin [CoPP]<sup>+</sup>  $m/z$  791. These derivatives also exhibited the highest molar absorptivity, “ $m$ ” values, ion yields about  $\sim 10^3$  at 0.58  $\mu$ J/pulse and high ionization potentials, 8.42 and 8.30 eV, respectively.

Among the many requirements for an efficient MALDI matrix a clean and background-free spectrum is of paramount importance, especially for detection of low molecular weight compounds and for lowering the detection limits (LODs) of the technique. In Figure 7 the LDI MS spectra for all  $\alpha$ -CNPV derivatives and the standard matrix DCTB, using an energy laser output of 0.819  $\mu$ J and 2.5 pmol of each compound on target revealed high-abundance signals corresponding to the molecular ions ( $M^{+\bullet}$ ), with a small-to-large contribution of protonated molecules  $[M+H]^+$  and absence of clusters, fragments or adducts. Derivatives  $\alpha$ -CNPV-H,  $\alpha$ -CNPV-Cl,  $\alpha$ -CNPV-CH<sub>3</sub>,

and  $\alpha$ -CNPV-OCH<sub>3</sub> show the highest contributions of [M+H]<sup>+</sup> signals to the LDI spectra. For example, in the LDI spectrum of  $\alpha$ -CNPV-CH<sub>3</sub> the base peak apparently corresponds to the protonated molecule [M+H]<sup>+</sup> at  $m/z$  361. However, analysis of the experimental isotopic pattern for  $\alpha$ -CNPV-CH<sub>3</sub> (Figure 7) shows that abundances for both M<sup>+•</sup> ( $m/z$  360) and [M+H]<sup>+</sup> ( $m/z$  361) are equivalent; since the contribution of the monoisotopic [M+H]<sup>+</sup> to the measured M+1 signal is around 71%, with the remaining 29% corresponding to the radical cation of the  $\alpha$ -CNPV-CH<sub>3</sub> isotopologue <sup>13</sup>C<sup>12</sup>C<sub>25</sub>H<sub>20</sub>N<sub>2</sub>. Observation of [M+H]<sup>+</sup> species in  $\alpha$ -CNPV-CH<sub>3</sub> (and -H/-Cl/-OCH<sub>3</sub> derivatives) can be explained by two different reaction pathways: first the possibility of protonated matrix molecules preformed in the solid phase, as a result of the presence of -CN groups on the vinyl bridges which increase the acidity of adjacent  $\beta$ -hydrogens. Previously Lou and co-workers reported on the acidity of H- on  $\beta$  positions supporting this possibility. (Lou et al., 2010) Secondly, protonated matrix molecules can be the result of bimolecular reactions of the type M<sup>+•</sup> + M/S → [M-H]<sup>+</sup> + M<sup>•</sup>/S<sup>•</sup> (M= matrix neutral molecule, S=neutral solvent molecule) in the gas phase. This effects are also observed with the DCTB standard matrix where a high abundance of protonated species [M+H]<sup>+</sup> at  $m/z$  251 is also observed. In this case the M+1 signal in the isotopic pattern of Figure 2 corresponds to an overlapping of the monoisotopic [M+H]<sup>+</sup> (80%) and the radical cation of the DCTB isotopologue <sup>13</sup>C<sup>12</sup>C<sub>16</sub>H<sub>18</sub>N<sub>2</sub> (20%). Interestingly,  $\alpha$ -CNPV-N(CH<sub>3</sub>)<sub>2</sub> and  $\alpha$ -CNPV-NPh<sub>2</sub> do not show significant [M+H]<sup>+</sup> signals due perhaps to the stabilization of the matrix radical cations induced by resonance and delocalization of the lone electron pair(s) in these auxochromic groups.

Four of the tested  $\alpha$ -CNPV (-CH<sub>3</sub>, -OCH<sub>3</sub>, -N(CH<sub>3</sub>)<sub>2</sub>, NPh<sub>2</sub>) provide a clean and background-free spectrum as seen in Figure 7; in contrast, the standard ET matrix DCTB shows a complex

background were not only the radical cation signals were observed but also protonated molecules ( $[M+H]^+$ ,  $[2M+H]^+$ ,  $[3M+H]^+$ ,  $[4M+H]^+$ ), adducts ( $[M+Na/K]^+$ ) in addition to several signals corresponding to the matrix chemical decomposition and intermolecular reactions in the gas phase. The presence of these clusters and adducts may hinder detection of low molecular weight compounds and alter the isotopic patterns of the analytes (an issue in low to medium resolution analyzers).

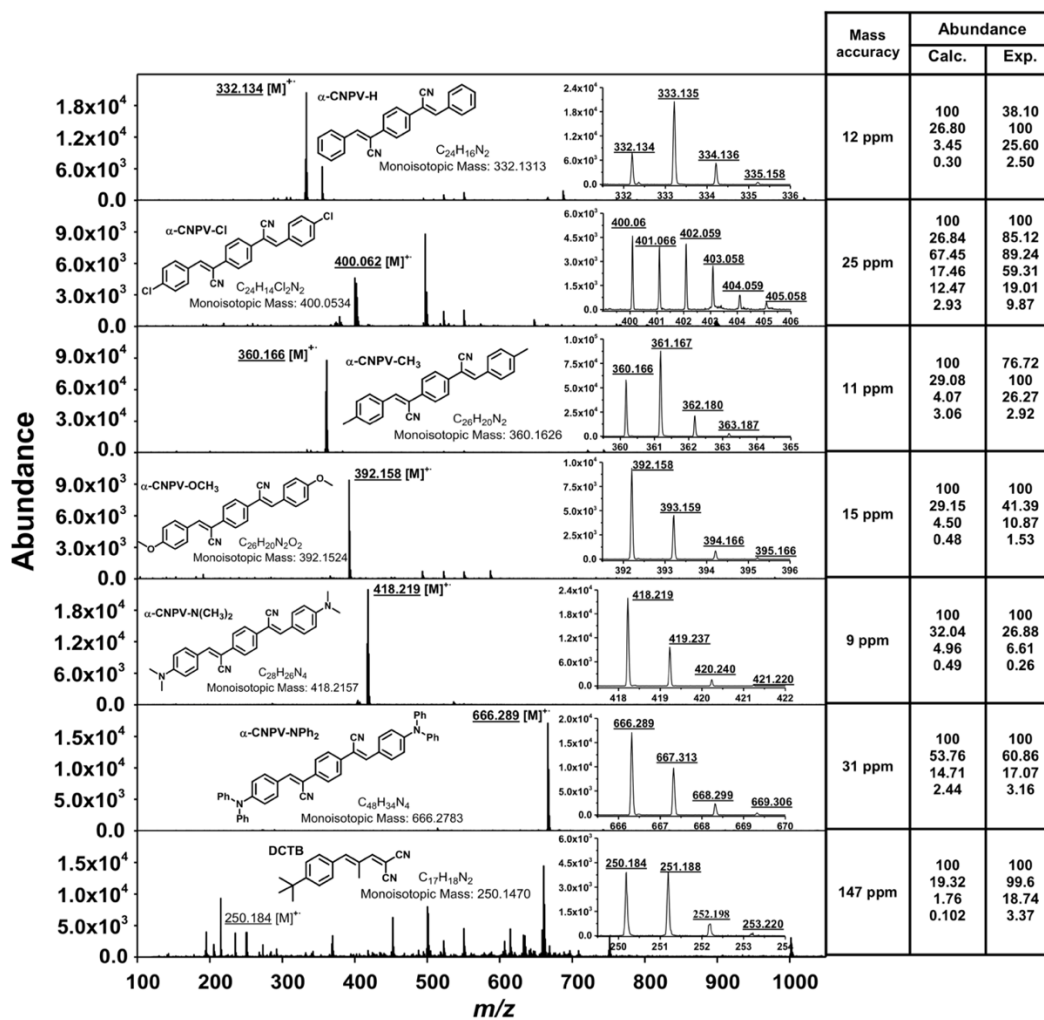


**Figure 7** LDI MS spectra for the  $\alpha$ -CNPV derivatives  $\alpha$ -CNPV-H,  $\alpha$ -CNPV-Cl,  $\alpha$ -CNPV-CH<sub>3</sub>,  $\alpha$ -CNPV-OCH<sub>3</sub>,  $\alpha$ -CNPV-N(CH<sub>3</sub>)<sub>2</sub>,  $\alpha$ -CNPV-NPh<sub>2</sub> and DCTB using 0.819  $\mu$ J of laser output and 2.5 pmol of each compound on target.

In addition to the above mentioned disadvantages, are the DCTB's well documented reactivity against analytes, in-source decomposition, low vacuum stability and chemical decomposition overtime.(Lou et al., 2010) Comparatively, the LDI spectra of  $\alpha$ -CNPV-H showed signals associated with  $[2M+H]^+$  ( $m/z$  661) and some adducts at  $m/z$  355 corresponding to  $[\alpha\text{-CNPV-H}+\text{CH}_3\text{OH}]^+$ . The  $\alpha$ -CNPV-Cl derivative exhibited signals related to hydrolysis products such as  $[\alpha\text{-CNPV-Cl}+t\text{-BuO}+\text{Na}]^+$  at  $m/z$  497, resulting of  $t\text{-BuO}^-$  addition to the  $-\text{CN}$  group due the high electrophilic character of the  $-\text{Cl}$  substituent due to the strong basic media used for the synthesis of these derivatives.

Considering the radar plot of Figure 6B and the LDI spectra in Figure 7, we selected  $\alpha$ -CNPV- $\text{CH}_3$  and  $\alpha$ -CNPV- $\text{OCH}_3$  derivatives to test further as ET matrices. These derivatives exhibit remarkable UV absorption properties ( $\epsilon_{355} = 70\ 000$  and  $41\ 000\ \text{M}^{-1}\text{cm}^{-1}$ ), ability to efficiently produce primary ions upon laser irradiation ( $m = 7.64$  and  $6.74$ ), high yields of primary ion at low laser thresholds ( $0.58\ \mu\text{J}/\text{pulse}$ ), high S/N values for a standard analyte and the absence of clusters, adducts and fragment in their LDI spectra.

**2.3.2. Vacuum stability  $\alpha$ -CNPV- $\text{CH}_3$  and  $\alpha$ -CNPV- $\text{OCH}_3$  derivatives.** Vacuum stability in a MALDI matrix is of fundamental importance, particularly for applications where the analyte:matrix mixture must stay for long periods of time at low pressure such as the case of high-throughput analysis and imaging MS.(Ibrahim, Jurcic, Wang, Whitehead, & Yeung, 2017) Traditional ET matrices, such as DCTB, rapidly decompose and sublime under vacuum. We tested the vacuum stability of  $\alpha$ -CNPV- $\text{CH}_3$  and  $\alpha$ -CNPV- $\text{OCH}_3$  against DCTB, for the analysis of Cobalt porphyrin (11) as a function of sample residence time in the MALDI ion source. Figure

8 shows the change in  $M^{+•}$  signal ( $m/z$  791.21) over a 240 min time period. As a general trend we observe, over time, a decrease in S/N ratios for the cobalt porphyrin with the three matrices. However, with  $\alpha$ -CNPV-CH<sub>3</sub> and  $\alpha$ -CNPV-OCH<sub>3</sub> this decrease corresponds to 21 and 34% of the initial S/N value after 240 min, respectively, while for DCTB the decrease reaches 87% after 240 min. Recently, Lou et al, reported on the disadvantages of DCTB, (Lou et al., 2010) among which reactivity with analytes and poor vacuum instability are of great concern. For applications requiring long residence times of the sample in the ion source, such as MALDI imaging, clearly  $\alpha$ -CNPV-CH<sub>3</sub> and  $\alpha$ -CNPV-OCH<sub>3</sub> could provide the necessary vacuum stability.

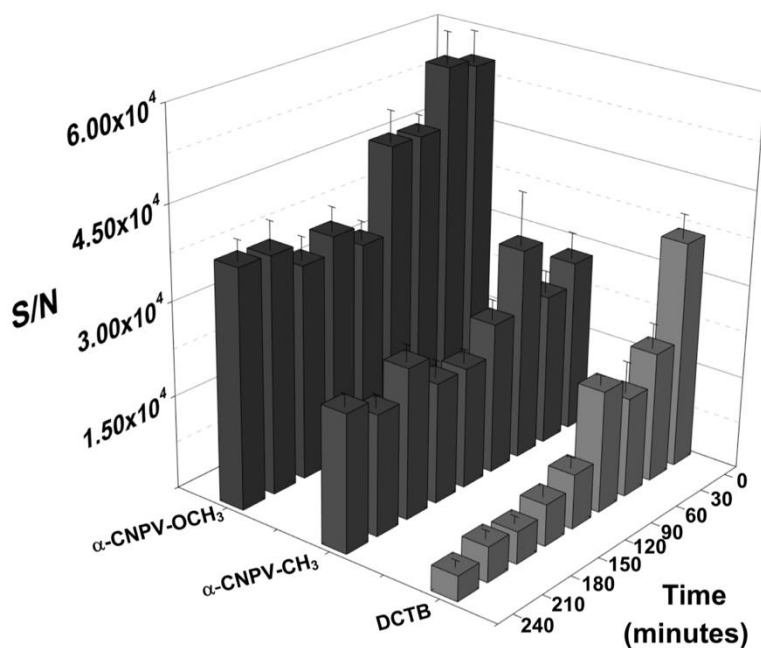


**Figure 8** Changes on  $[M]^{+•}$  S/N ratios for cobalt porphyrin as a function of residence time in the ion source using  $\alpha$ -CNPV-CH<sub>3</sub>,  $\alpha$ -CNPV-OCH<sub>3</sub> and DCTB as matrices. 1.25 pmol of analyte on target

**2.3.3. Analysis of polyaromatic hydrocarbons, porphyrins, phtalocyanines and solar cell sensitizers using  $\alpha$ -CNPV-CH<sub>3</sub>,  $\alpha$ -CNPV-OCH<sub>3</sub> as ET matrices.** Highly conjugated organic and organometallic compounds, such as porphyrins dyes, polyaromatics and optoelectronic materials are important structures for light harvesting applications.(Kay & Graetzel, 1993)(Mathew et al., 2014)(Gómez Esteban, de la Cruz, Aljarilla, Arellano, & Langa, 2011)(Tigreros et al., 2014) Porphyrins, for example are extensively studied for their ability to harvest photons in plants, transport oxygen in blood, and take part in catalytic processes.(Collman, Marrocco, Denisevich, Koval, & Anson, 1979) On the other hand, molecules based on triphenylamine and polyaromatics structures are extensively used as sensitizers, quantum dots dopants, and building blocks in electronic polymers for organic light emitting diode (OLED) technology, among other applications.(Arcos, Guimarães, Insuasty, Araki, & Ortiz, 2016)(G. Li et al., 2015) The analysis of compounds mentioned above by MS represents a great challenge because common ionization techniques such as electron ionization (EI) or electrospray (ESI) cause demetallation, fragmentation and intermolecular reactions which produce undesirable signals in the mass spectrum. To test the performance of  $\alpha$ -CNPVs as ET matrices we selected twenty compounds (see structures in Figure S5 supporting info) suitable for ionization via ET reactions and subjected the mixture to LDI and MALDI analysis using  $\alpha$ -CNPV-CH<sub>3</sub>,  $\alpha$ -CNPV-OCH<sub>3</sub> and commercial DCTB as matrices. The mixture includes organic materials such as polyaromatics: coronene (**1**), naphto[2,3-b]-pyrene (**2**), 1,9-diphenylanthracene (**3**), 1,2,3,4,5-pentaphenyl-1,3-cyclopentadiene (**4**), rubrene (**5**), and hexaphenylbenzene (**6**); porphyrins and phtalocyanines: compounds **7-15**; and triphenylamine-based dyes: compounds **16-20**.(Nazim Boutaghou & Cole, 2012)(Arcos et al., 2016)(Barlow, Scudiero, & Hipps, 2004)(Clar, Robertson, Schloegl, & Schmidt, 1981)(Clar & Schmidt, 1979)(Kiselev, Sakhabutdinov, Shakirov, Zverev, & Konovalov,

1992)·(Sato, Seki, & Inokuchi, 1981)·(Györösi, Hvistendahl, & Undheim, 1975)·(Dolgounitcheva, Zakrzewski, & Ortiz, 2005)·(Blase, Attaccalite, & Olevano, 2011) Figure 9 shows the MALDI spectra of the mixture, using 1.25 pmol of each analyte on target and laser energy of 0.89  $\mu\text{J}$  per pulse. In addition, Table S1 (see supporting material, Table S1) shows the S/N ratios for all observed signals in Figure 9. We calculated the percentage coverage of the mixture, the ratio between the number of observed analytes (with  $S/N > 3$ ) over the total number of analytes times 100, as a general way to determine how efficient the analytical approach is. For MALDI, using the standard DCTB matrix we detected 14 out of 20 analytes for a coverage of 70%. With  $\alpha$ -CNPV-OCH<sub>3</sub> and  $\alpha$ -CNPV-CH<sub>3</sub> as MALDI matrices we registered signals for 18 of the 20 compounds in the mixture for a 90% of analyte coverage. In Figure 9 we observed signals corresponding to radical cations for all analytes; interestingly, for analytes **16** and **19** (containing tertiary basic nitrogens) we also observed  $[M+H]^+$  species (with less than 5% of relative abundances, see Table S1). Porphyrins (**10**) and (**11**) are detected with high S/N ratios using  $\alpha$ -CNPV-CH<sub>3</sub> and  $\alpha$ -CNPV-OCH<sub>3</sub> as MALDI matrices (1342 and 1058; 517 and 504, respectively) in contrast with S/N of 270 and 491 when DCTB was used. The phthalocyanine (**13**) shows high S/N ratios with 78, 1395 and 1265 with  $\alpha$ -CNPV-CH<sub>3</sub>,  $\alpha$ -CNPV-OCH<sub>3</sub> and DCTB, respectively. Although, in general phthalocyanines have higher IPs than porphyrins (because the imino groups in the  $\alpha$ -position act as EWG substituents and decrease the available  $\pi$ -electrons on the conjugated  $\pi$ -backbone, in contrast with porphyrins that do not contain imino groups), the presence of EDG ( $-\text{OC}_4\text{H}_9$ ) groups in the phenyl ring of **13**, decreases the IP of the molecule and stabilizes charged species in the gas phase making this compound easily ionizable, even more so than porphyrins. Likewise, unsubstituted phthalocyanines **7**, **8**, **9** and **12** exhibit lower S/N values than the alkoxy substituted **13**, **14** and **15** analogues. The presence of these substituents, strong donating groups, cause a

decrease on IPs that favor electron transfer net energy release. Secondary ionization in electron transfer, depends strongly, as mentioned above, on energetically-favored  $M^{+}/A$  interactions.

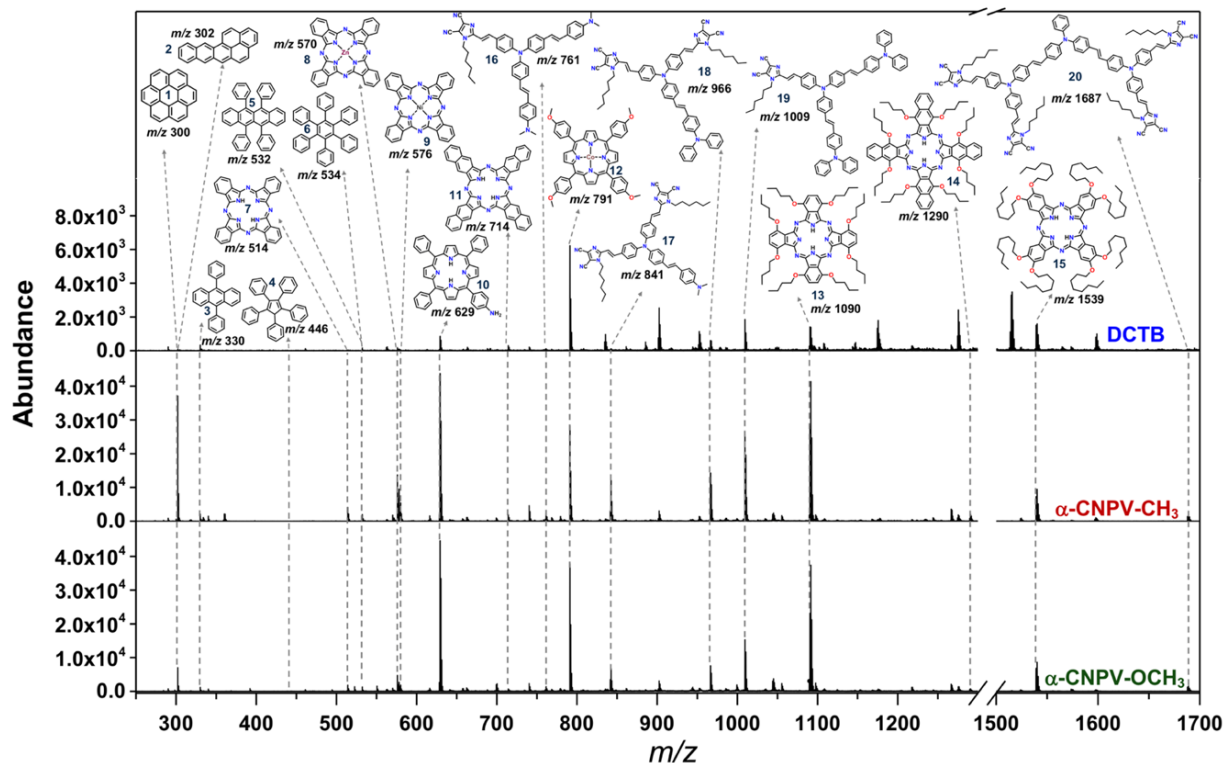


**Figure 9** MALDI spectra of polyaromatic hydrocarbons 1-6, porphyrins and phthalocyanines 7-15 and triphenylamine pigments 16-20. 1.25 pmol of each analyte on target and laser energy of 0.89  $\mu$ J per pulse.

Aromatic compounds **4** and **6** (1,2,3,4,5-pentaphenyl-1,3-cyclopentadiene and hexaphenylbenzene), with the highest IPs: 7.54 and 8.60 eV, respectively; were not observed during the electron transfer experiments. Secondary ion formation for compound **6** is not thermodynamically favored with any of the matrices used, hence this compound is not detected, while for compound **4** secondary ion formation is favored. However, due to the analyte suppression effect (ASE) compound **4** is not observed in the MALDI spectra. (Richard Knochenmuss, 2009)

Analytes with lower IPs than compound **4** (basically all of the analytes in the mixture except **6**) can react more favorably with the matrix, thus competing and decreasing the signal for compound **4**. (Richard Knochenmuss, 2009) Finally, triphenylamine-based (TPA) compounds (**16-20**), commonly used as solar cells sensitizers, exhibit the lowest IPs of the mixture ranging from 5.83 to 6.0 eV (theoretical DFT values (Arcos et al., 2016)). These five analytes were all efficiently ionized by  $\alpha$ -CNPV-CH<sub>3</sub> and  $\alpha$ -CNPV-OCH<sub>3</sub>, while DCTB only produced ions from compounds **17**, **18** and **19** with low S/N (Table S1). As a general conclusion we observe better analyte coverage, and overall signal enhancement and reduced background noise in the MALDI spectra when using  $\alpha$ -CNPV-OCH<sub>3</sub> and  $\alpha$ -CNPV-CH<sub>3</sub> matrices *versus* DCTB. In the following sections we feature exclusively the  $\alpha$ -CNPV-CH<sub>3</sub> as ET MALDI matrix.

#### **2.3.4. ET-MALDI applications to complex mixture analysis using $\alpha$ -CNPV-CH<sub>3</sub> as matrix:**

##### **2.3.4.1. Direct identification of biomarkers (nickel and vanadyl porphyrins) in crude oils.**

In geochemistry the presence of nickel and vanadyl porphyrins is related with the processes of diagenesis, kerogen formation and catagenesis. (Treibs, n.d.) (Hodgson & Peake, 1961) These compounds (Figure 10), structurally derived from biologically-active chlorophylls or heme groups, range from small to large complex structures incorporating everything from aromatic and heteroaromatic rings to variable length alkyl units in the peripheral tetrapyrrole structure. (X. Zhao, Shi, Gray, & Xu, 2014) Although useful as biomarkers for assessing oil maturation, among other geochemical characteristics, determining the presence of nickel and vanadyl porphyrins in feeds before the refining process is crucial, because these metals cause catalyst poisoning impacting negatively oil refineries worldwide. The characterization of metal porphyrins is typically achieved after lengthy isolation processes including open column chromatography, (X. Zhao et al., 2013)

HPLC(Kashiyama, Kitazato, & Ohkouchi, 2007) and solid phase extraction.(Putman, Rowland, Corilo, & McKenna, 2014) However, sometimes these methods overlook low concentration species such as nickel porphyrins which hold valuable information. We recently demonstrated the use of  $\alpha$ -CNPV-CH<sub>3</sub> as ET matrix for the ionization of metal porphyrins-enriched fractions, extracted from heavy American crude-oils using traditional chromatographic approaches.(Giraldo-Dávila, Chacón-Patiño, Ramirez-Pradilla, Blanco-Tirado, & Combariza, 2018) Complex mixture analysis, as discussed above, is regularly tackled from a solubility point of view (e.g. crude oil chromatographic fractionation SARA -Saturated, Aromatic, Resins and Asphaltenes); however, for analytical purposes one can take advantage of other physicochemical characteristics common to groups of compounds present on those complex mixtures.

Petroporphyrins in crude oils, due to structural similarities, have very similar IP values (ranging from 6.5 to 7.5 eV), therefore a strategy for selective ionization of these analytes can be devised from Eq 1. For instance, the use of a matrix with IP above 0.5 eV from that of the petroporphyrin group could be adopted for selective ionization. This rationale is demonstrated in Figure 10 where an ACN extract, from a heavy crude oil, is directly analyzed via ET ionization using both  $\alpha$ -CNPV-CH<sub>3</sub> and DCTB as MALDI matrices. Clearly, the group of nickel and vanadyl porphyrins in the  $m/z$  450-700 mass region is easily detected as radical cations when using  $\alpha$ -CNPV-CH<sub>3</sub> as matrix (100 porphyrins identified), while the standard DCTB matrix does not perform as well (30 porphyrins identified). A complete description and discussion of this new strategy for petroporphyrin analysis is presented in a submitted manuscript.(Ramírez-Pradilla et al., 2019) ET reactions between primary ions of the  $\alpha$ -CNPV-CH<sub>3</sub> and the nickel/vanadyl porphyrins are highly favored by a  $\Delta IP > 2$  eV.(Ogunrinde, Hipps, & Scudiero, 2006)(Scudiero, Barlow, & Hipps, 2002) Curiously, the selective ionization of porphyrins by DCTB (IP 8.54 eV) is dramatically hindered

by the presence in the ACN extract of species containing nucleophilic or high polar groups, which otherwise do not affect the  $\alpha$ -CNPV-CH<sub>3</sub> performance. This effect has been identified by Lou *et al.* (Lou et al., 2010) as the appearance of several signals that don't correspond with the DCTB's fingerprint in the MS spectrum. These signals, of the type [DCTB+Nu]<sup>+</sup>, are associated to nucleophilic reactions of DCTB with analytes with functional groups like -NH<sub>2</sub> or -SH.

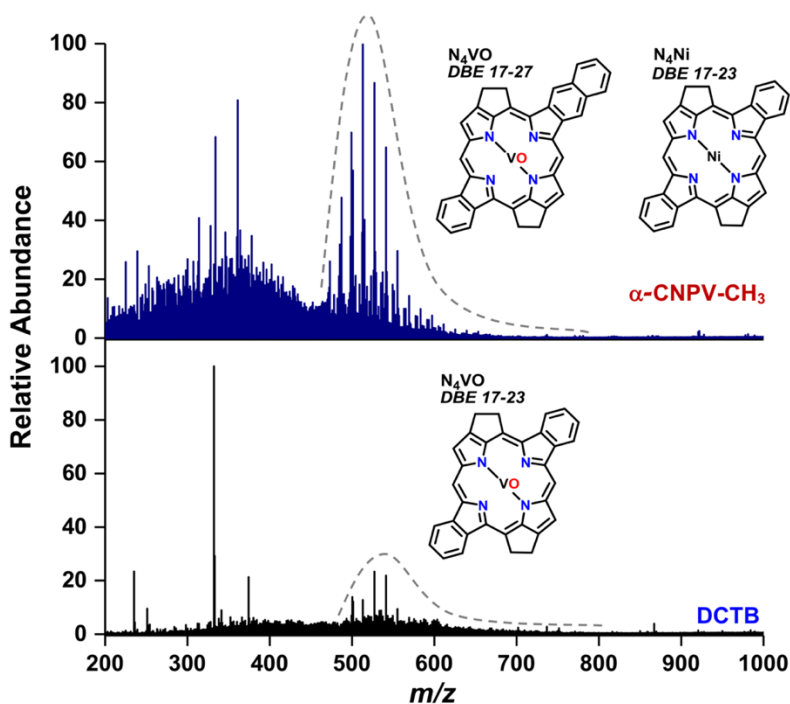


**Figure 10** ET-MALDI-TOF spectra showing selective ionization, when using  $\alpha$ -CNPV-CH<sub>3</sub> as matrix, of nickel and vanadyl porphyrins present in a heavy American crude-oil.

**2.3.4.2. Polymer analysis.** The development of novel polymeric materials based on polythiophene has increased significantly in recent years, due to their application as photoactive material in PLED technology, (Camurlu et al., 2009) (Ohshita, Tada, Kunai, Harima, & Kunugi, 2009) (Youn, Park, & Guo, 2015) polymer-sensitized solar cells, (Qin et al., 2016) (Zhang, Guo,

Ma, Ade, & Hou, 2014)(L. Zhao & Lin, 2012) and chemical sensors.(Nalwa et al., 2010) Ability to perform accurate measurement of molecular weight distributions and molecular weight averages ( $M_w$  and  $M_n$ ), as well as to follow decomposition and end group modification during synthesis and deposition steps, are analytical characteristics of fundamental importance during polythiophene analysis by MS.(Liu & McCullough, 2002)(Liu, Loewe, & McCullough, 1999) In a previous report, De Winter et al,(De Winter et al., 2011) found a significant correlation between the photophysical properties of three different matrices (DCTB, dithranol and terthiophene) and their performance during the ET ionization of polyhexylthiophene. Properties such as IP (8.54 eV),  $\lambda_{\max}$  (337 nm) and  $\epsilon_{355}$  determined the performance of DCTB as matrix, when compared with the other matrices for the ionization of P3HT<sub>3000</sub>.

Figure 11 shows the ET-MALDI-MS spectra of a 3-hexylpolythiophene (P3HT<sub>3000</sub>) standard using  $\alpha$ -CNPV-CH<sub>3</sub> and DCTB as matrices.  $\alpha$ -CNPV-CH<sub>3</sub> produced an ET spectrum where the molecular weight averages  $M_w$  and  $M_n$  were 3493.30 and 3196.95, respectively; while for DCTB the  $M_w$  and  $M_n$  were 3084.11 and 2682.04. MS data measured with  $\alpha$ -CNPV-CH<sub>3</sub> coincides with the reported standard's parameters, while the compositional information collected with DCTB do not (Figure 11). Interestingly, despite the fact that IP values for DCTB (8.47 eV) and  $\alpha$ -CNPV-CH<sub>3</sub> (8.42 eV) are very close -translating into energetically-favored ET processes in both cases with  $\Delta IP \sim 3.8$  eV ( $IP_{P3HT}$  4.7 eV),(De Winter et al., 2011) - the matrices' analytical performance is not comparable (as seen in Figure 6). We believe  $\alpha$ -CNPV-CH<sub>3</sub> outperforms DCTB due to a combination of factors such as UV absorption ( $\epsilon_{355}$  70 000 M<sup>-1</sup>cm<sup>-1</sup> for  $\alpha$ -CNPV-CH<sub>3</sub> vs 32 000 M<sup>-1</sup>cm<sup>-1</sup> for DCTB), high yield of primary ions upon laser interaction with the matrix ( $m=7.54$  for  $\alpha$ -CNPV-CH<sub>3</sub> vs  $m=4.64$  for DCTB) and absence of collateral processes (cluster and aggregate

formation, fragmentation, reactions with analytes, etc.) during primary and secondary ion formation.

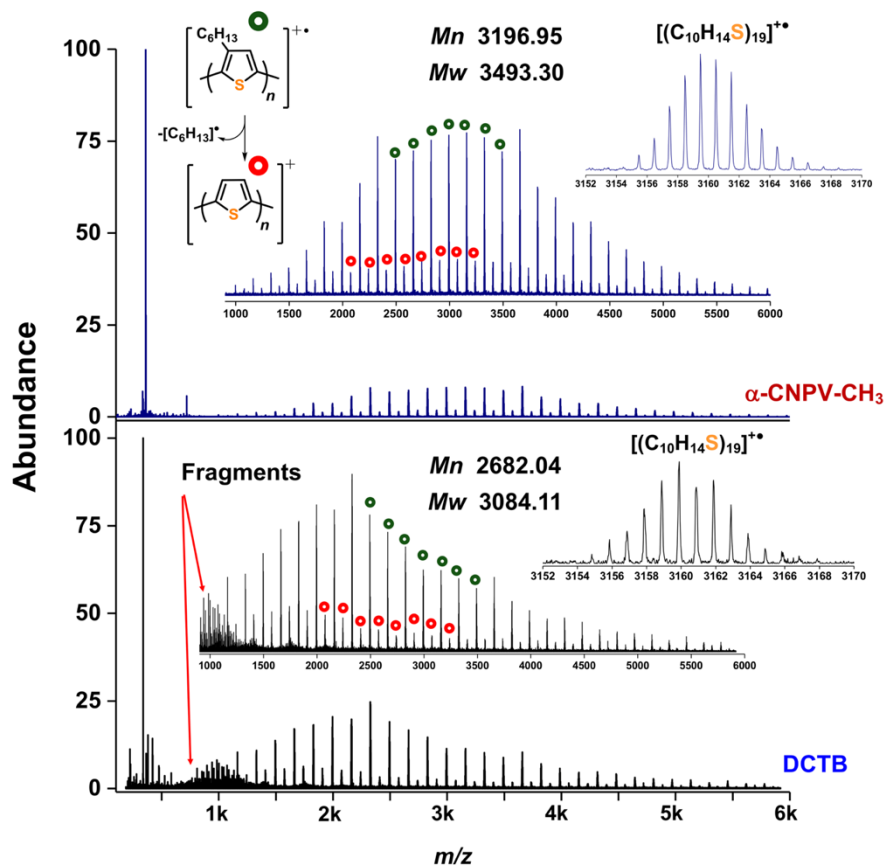


**Figure 11** ET-MALDI-TOF mass spectra of 3-hexylpolythiophene using  $\alpha$ -CNPV-CH<sub>3</sub> and DCTB as matrices, at 1.24  $\mu\text{J}$  per pulse of laser energy and 1:1000 matrix to analyte ratio.

In addition, we observed S/N ratios up to 1000 with  $\alpha$ -CNPV-CH<sub>3</sub> while DCTB afforded a maximum S/N of 200 under the same experimental conditions. Regarding molecular ion survival, Figure 11 shows abundant polymer fragmentation in the low-mass region when using DCTB, while the ET mass spectrum with  $\alpha$ -CNPV-CH<sub>3</sub> does not show analyte fragmentation. It has been

reported, by De Winter et al,(De Winter et al., 2011) that the use of DCTB induces hexyl groups excision and thiophene-thiophene bond cleavage.

**2.3.4.3. ET-MALDI analysis of labile materials using  $\alpha$ -CNPV-CH<sub>3</sub> as matrix: Gold Nanoparticles.** In recent years, the number of applications of ligand-protected gold nanoparticles and nanoclusters as nanozymes,(Wu et al., 2018) drug delivery materials,(Paciotti et al., 2016)(Nasrolahi Shirazi et al., 2013) photothermal cancer therapy agents,(Fazal et al., 2014) nanomaterials for memory storage,(Gupta, Kusuma, Lee, & Srinivasan, 2011) and a myriad other uses, have increased exponentially. Controlling gold nanoparticles size during synthesis, purification and isolation steps is crucial depending upon the target application. The small size of gold nanoclusters/nanoparticles in addition with their low IP,(Jin, 2015) make these materials ideal analytes for electron transfer ionization in MALDI-MS. Historically, MS analysis of gold nanoparticles has been performed using electrospray ionization ESI-TOF,(Qian & Jin, 2009) direct laser desorption ionization LDI-TOF and matrix assisted laser desorption ionization, MALDI-TOF using DCTB as matrix.(Chaki et al., 2008)(Dass, 2009)(Jin, 2015)

Figure 12 shows the ET-MALDI-TOF-MS spectra, using  $\alpha$ -CNPV-CH<sub>3</sub> (top left) and DCTB (bottom left) as matrices, of gold nanoclusters/nanoparticles with several core sizes synthesized following the Brust methodology.(Brust, Walker, Bethell, Schiffrin, & Whyman, 1994) The spectra, taken in positive reflectron ion mode, shows signals corresponding to gold nanoclusters with low core sizes; for instance, the distribution around 8 kDa was previously reported for Au<sub>25</sub>(SC<sub>12</sub>H<sub>25</sub>)<sub>18</sub> and other clusters with several core sizes; Au<sub>24</sub>, Au<sub>31</sub>, Au<sub>35</sub>. In material science, the targeted synthesis and isolation of gold nanoparticles of specific core sizes depends on

synthetic techniques, solvents, temperature, molar ratios, among others (Chaki et al., 2008) (Brust et al., 1994). The synthetic approach we used, under non-controlled conditions, produced gold nanoparticles with random sizes and not structures with magic numbers  $\text{Au}_{25}$ ,  $\text{Au}_{35}$ ,  $\text{Au}_{68}$ ,  $\text{Au}_{102}$  and  $\text{Au}_{144}$ . Nevertheless, this induced randomness allows us to demonstrate that  $\alpha\text{-CNPV-CH}_3$  matrix can be used for the simultaneous ionization of gold nanoparticles with several core sizes, and represents a new alternative –to DCTB– for the analysis of these materials.

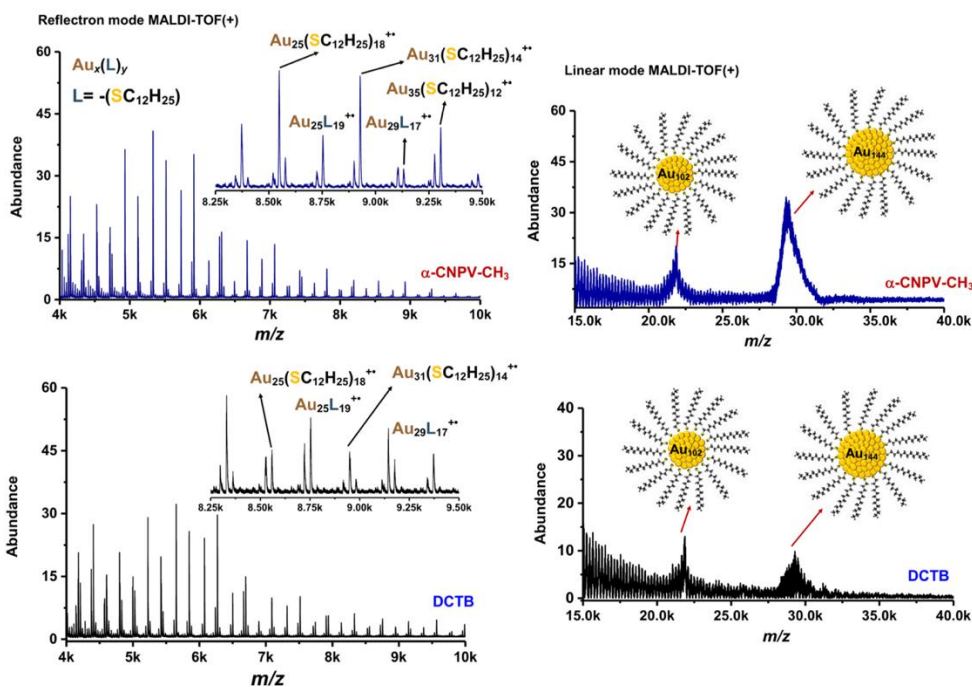


**Figure 12** ET-MALDI-TOF-(+) spectrum in reflectron (left) and linear modes (right) of thiolated gold nanoparticles using  $\alpha\text{-CNPV-CH}_3$  and DCTB as matrices.

The spectra in Figure 12 (right), taken in positive linear ion mode, shows a bimodal distribution centered around  $\sim 22$  kDa and  $\sim 30$  kDa, for the synthesized gold nanoparticle sample. These signals correspond mostly to  $\text{Au}_{102}$  and  $\text{Au}_{144}$  core sized nanoparticles. Previously, Martin, et

al,(Martin, Li, Dass, & Eah, 2012) reported the simultaneous detection of gold nanoparticles with core sizes of 25, 35, 68, 102 and 144 gold atoms using DCTB as matrix, however a high degree of fragmentation was observed. On the other hand, the use of LDI-TOF causes a high degree of fragmentation of gold nanoparticles with core sizes larger than 38 atoms.(Chaki et al., 2008) In contrast,  $\alpha$ -CNPV-CH<sub>3</sub> can efficiently ionize - in high yields- intact gold nanoparticles, as a consequence of a highly energetic electron transfer reactions, with  $\Delta IP$  larger than 4eV, and other advantageous properties of the  $\alpha$ -CNPV-CH<sub>3</sub> as discussed and demonstrated above. Besides, the matrix properties can merge synergistically with the high UV absorption properties of gold nanoparticles, resulting from the SPR effect, which are core size-dependent with, for instance, gap energy ( $E_g$ ) decreasing as the nanoparticle core increases.(Jin, 2015)

**2.3.4.4. Fullerene derivatives.** Fullerenes are important in materials science due to their applications in photovoltaics,(Giacalone & Martín, 2010) photochemistry,(Speller et al., 2017) and biochemistry,(T. Li et al., 2017) among others. DCTB was introduced in 2000 by Ulmer and co-workers as ET matrix for the analysis of substituted fullerenes and other labile compounds.(Ulmer et al., 2000) However, under MALDI-MS conditions fullerenes tend to fragment during the ionization step making it difficult, with most matrices, to observe their intact molecular ions. In Figure 13 (left), the MALDI-MS spectra in positive ion mode for a BODIPY-C<sub>60</sub> derivative (Ortiz, *et al.*,(Cabrera-Espinoza, Insuasty, & Ortiz, 2018)) using  $\alpha$ -CNPV-CH<sub>3</sub> and DCTB. Both matrices allow observation of the intact molecular ion at  $m/z$  1540;  $\alpha$ -CNPV-CH<sub>3</sub>, though, afforded a significant signal enhancement in terms of ion abundance, resolution and S/N ratio when compared with DCTB. The S/N ratio for the molecular ion with  $\alpha$ -CNPV-CH<sub>3</sub> is almost an order of magnitude higher than with DCTB (339.1 vs 42.3, respectively). The HOMO energy of the

BODIPY- $C_{60}$  derivative is under 5 eV, thus, the ET reaction between  $\alpha$ -CNPV-CH<sub>3</sub> or DCTB primary ions has a  $\Delta IP > 3\text{eV}$ , which may cause an excess of internal energy in the secondary analyte ion resulting in fragmentation, particularly loss of a NO' radical.

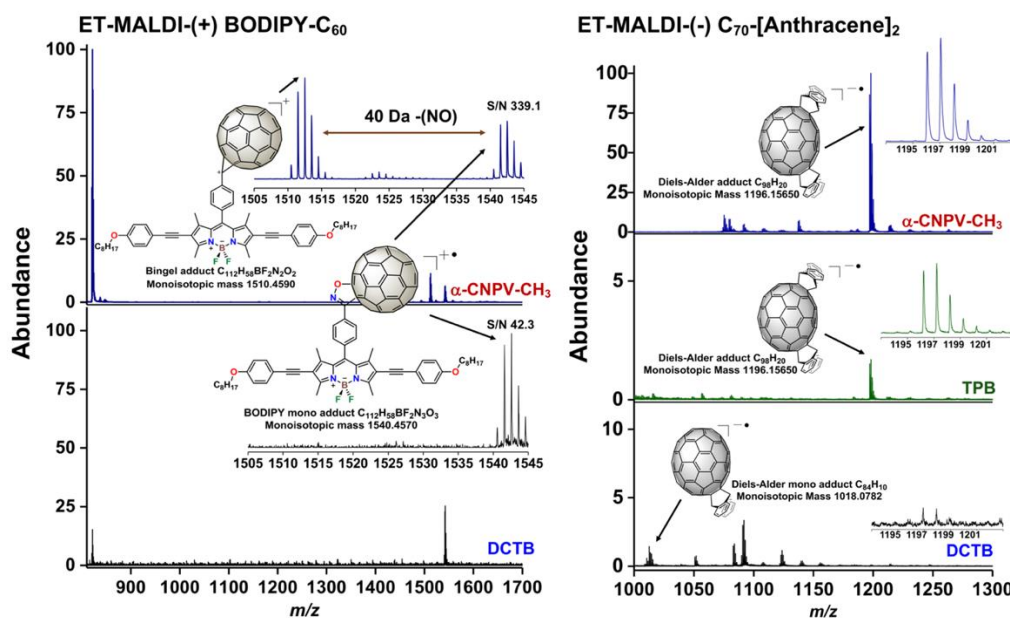


**Figure 13** Analysis of fullerene derivatives by electron transfer ionization using  $\alpha$ -CNPV-CH<sub>3</sub>, TPB and DCTB as MALDI matrices.

Recently, use of Diels-Alder reactions for introduction of anthracene units on fullerenes allows the regiochemically controlled synthesis of derivatives (regioisomers bis adducts), however, mass spectrometric analysis of these new compounds is still a challenge due to their extremely high lability. (Cerón, Castro, Neti, Dunk, & Echegoyen, 2017) An alternative charge-acquisition channel in ET involves formation of radical anions, where migration of an electron from a primary matrix radical anion to the neutral analyte produces a negatively-charged secondary ion. This process is possible only for analytes with electron affinities (EA) larger than the matrix's ( $M^{\bullet-} +$

$A \rightarrow A^{-\bullet} + M \therefore EA(A) > EA(M)$ ). Coincidentally, the EA of fullerene derivatives are above 2.0 eV, while HF calculations for  $\alpha$ -CNPV-CH<sub>3</sub> show an electron affinity of 1.52 eV and experimental measurements report 2.37 eV for DCTB. (Vasil'ev et al., 2006) Thus, the ET from  $\alpha$ -CNPV-CH<sub>3</sub> primary ions to fullerene derivatives will be energetically-favored, while the reaction with DCTB is not (see supporting information, Figure S6). This rationale is demonstrated in Figure 13 (right), where the ET-MALDI-TOF-MS spectra in negative ion mode of the bis-adduct C<sub>70</sub>-[anthracene]<sub>2</sub> shows the molecular ion as the base peak in the spectrum, when using  $\alpha$ -CNPV-CH<sub>3</sub> as matrix. In the same Figure, the use of TPB (tetraphenyl-1,1,3,3-butadiene) - a common matrix for fullerene analysis- produces a low-abundance signal for the bis-adduct C<sub>70</sub>-[anthracene]<sub>2</sub>, while the ET spectrum with DCTB only shows signals associated with fragments of the molecule.

#### 2.4. Conclusions

Electron transfer reactions in MALDI-MS strongly depend on matrix physicochemical and optoelectronic properties, among which ionization potentials and solid-phase photon absorption are of fundamental importance. (R. Knochenmuss, 2016) We report new  $\alpha$ -CNPV-based MALDI matrices with IP values ranging from 7.90 to 8.49 eV and the ability to efficiently harvest photons, as demonstrated by the low energy threshold needed to obtain primary ions. We observe that the introduction of -CN groups on the vinyl bridge of the PV core, greatly enhance the derivative solubility and also that introduction of -CH<sub>3</sub> and -OCH<sub>3</sub> groups on the phenyl ring greatly improves the matrix ability to efficiently form secondary ions. These new matrices also exhibit high vacuum stability, 79% for up to two hours of residence in the MALDI source, in contrast with DCTB with only 13%. Vacuum stability for a ET-MALDI matrix is of paramount importance for

applications requiring long residence times at low pressure such as imaging MS. In addition, we demonstrated the highly effective analytical performance of the  $\alpha$ -CNPV-CH<sub>3</sub> and  $\alpha$ -CNPV-OCH<sub>3</sub> as ET MALDI matrices for the analysis of mixtures of compounds including polyaromatics, porphyrins, phthalocyanines and triphenylamine dyes. Finally, we prove the versatility of  $\alpha$ -CNPV-CH<sub>3</sub> for the ionization of a wide range of advanced materials such as electronic polymers, gold nanoparticles and fullerene derivatives.

## References

- Ameri, T., Khoram, P., Min, J., & Brabec, C. J. (2013). Organic Ternary Solar Cells: A Review. *Advanced Materials*, 25(31), 4245–4266.
- Arcos, W. A., Guimarães, R. R., Insuasty, B., Araki, K., & Ortiz, A. (2016). Structural effects on the photoelectrochemical properties of new push-pull dyes based on vinazene acceptor triphenylamine donor. *Journal of Molecular Structure*, 1111(Supplement C), 157–165.
- Barlow, D. E., Scudiero, L., & Hipps, K. W. (2004). Scanning Tunneling Microscopy Study of the Structure and Orbital-Mediated Tunneling Spectra of Cobalt(II) Phthalocyanine and Cobalt(II) Tetraphenylporphyrin on Au(111): Mixed Composition Films. *Langmuir*, 20(11), 4413–4421.
- Blase, X., Attaccalite, C., & Olevano, V. (2011). First-principles GW calculations for fullerenes, porphyrins, phtalocyanine, and other molecules of interest for organic photovoltaic applications. *Physical Review B*, 83(11), 115103.
- Breuker, K., Knochenmuss, R., Zhang, J., Stortelder, A., & Zenobi, R. (2003). Thermodynamic control of final ion distributions in MALDI: in-plume proton transfer reactions. *International Journal of Mass Spectrometry*, 226(1), 211–222.
- Brust, M., Walker, M., Bethell, D., Schiffrin, D. J., & Whyman, R. (1994). Synthesis of thiol-derivatised gold nanoparticles in a two-phase Liquid–Liquid system. *Journal of the Chemical Society, Chemical Communications*, (7), 801–802.
- Bubeck, C., Kaltbeitzel, A., Lenz, R. W., Neher, D., Stenger-Smith, J. D., & Wegner, G. (1989). Nonlinear optical properties of poly (p-phenylene vinylene) thin films. In *Nonlinear Optical Effects in Organic Polymers* (pp. 143–147). Springer.

- Cabrera-Espinoza, A., Insuasty, B., & Ortiz, A. (2018). Novel BODIPY-C60 derivatives with tuned photophysical and electron-acceptor properties: Isoxazolino[60]fullerene and pyrrolidino[60]fullerene. *Journal of Luminescence*, *194*, 729–738.
- Calvano, C. D., Ventura, G., Cataldi, T. R. I., & Palmisano, F. (2015). Improvement of chlorophyll identification in foodstuffs by MALDI ToF/ToF mass spectrometry using 1, 5-diaminonaphthalene electron transfer secondary reaction matrix. *Analytical and Bioanalytical Chemistry*, *407*(21), 6369–6379.
- Calvano, C. D., Ventura, G., Trotta, M., Bianco, G., Cataldi, T. R. I., & Palmisano, F. (2017). Electron-Transfer Secondary Reaction Matrices for MALDI MS Analysis of Bacteriochlorophyll a in Rhodobacter sphaeroides and Its Zinc and Copper Analogue Pigments. *Journal of the American Society for Mass Spectrometry*, *28*(1), 125–135.
- Camposeo, A., Del Carro, P., Persano, L., & Pisignano, D. (2012). Electrically Tunable Organic Distributed Feedback Lasers Embedding Nonlinear Optical Molecules. *Advanced Materials*, *24*(35), OP221–OP225.
- Camurlu, P., Giovanella, U., Bolognesi, A., Botta, C., Cik, G., & Végh, Z. (2009). Polythiophene–polyoxyethylene copolymer in polyfluorene-based polymer blends for light-emitting devices. *Synthetic Metals*, *159*(1), 41–44.
- Castellanos-García, L. J., Agudelo, B. C., Rosales, H. F., Cely, M., Ochoa-Puentes, C., Blanco-Tirado, C., ... Combariza, M. Y. (2017). Oligo p-Phenylenevinylene Derivatives as Electron Transfer Matrices for UV-MALDI. *Journal of The American Society for Mass Spectrometry*.
- Cerón, M. R., Castro, E., Neti, V. S. P. K., Dunk, P. W., & Echegoyen, L. A. (2017). Regiochemically Controlled Synthesis of a  $\beta$ -4- $\beta'$  [70]Fullerene Bis-Adduct. *The Journal of Organic Chemistry*, *82*(2), 893–897.

- Chaki, N. K., Negishi, Y., Tsunoyama, H., Shichibu, Y., & Tsukuda, T. (2008). Ubiquitous 8 and 29 kDa gold:alkanethiolate cluster compounds: Mass-spectrometric determination of molecular formulas and structural implications. *Journal of the American Chemical Society*, *130*(27), 8608–8610.
- Chen, Y., Zhou, L., Wang, J., Liu, X., Lu, H., Liu, L., ... Wang, S. (2018). Photoactive Oligo(p-phenylenevinylene) Functionalized with Phospholipid Units for Control and Visualization of Delivery into Living Cells. *ACS Applied Materials & Interfaces*, *10*(33), 27555–27561.
- Chendo, C., Rollet, M., Phan, T. N. T., Viel, S., Gigmes, D., & Charles, L. (2015). Successful MALDI mass spectrometry of poly (4-vinylpyridine) using a solvent-free sample preparation. *International Journal of Mass Spectrometry*, *376*, 90–96.
- Chung, S.-J., Rumi, M., Alain, V., Barlow, S., Perry, J. W., & Marder, S. R. (2005). Strong, low-energy two-photon absorption in extended amine-terminated cyano-substituted phenylenevinylene oligomers. *Journal of the American Chemical Society*, *127*(31), 10844–10845.
- Clar, E., Robertson, J. M., Schloegl, R., & Schmidt, W. (1981). Photoelectron spectra of polynuclear aromatics. 6. Applications to structural elucidation: “circumanthracene.” *Journal of the American Chemical Society*, *103*(6), 1320–1328.
- Clar, E., & Schmidt, W. (1979). Correlations between photoelectron and UV absorption spectra of polycyclic hydrocarbons. The pyrene series. *Tetrahedron*, *35*(8), 1027–1032.
- Collman, J. P., Marrocco, M., Denisevich, P., Koval, C., & Anson, F. C. (1979). Potent catalysis of the electroreduction of oxygen to water by dicobalt porphyrin dimers adsorbed on graphite electrodes. *Journal of Electroanalytical Chemistry and Interfacial Electrochemistry*, *101*(1), 117–122.

- Cornil, J., Heeger, A. J., & Bredas, J. L. (1997). Effects of intermolecular interactions on the lowest excited state in luminescent conjugated polymers and oligomers. *Chemical Physics Letters*, 272(5–6), 463–470.
- Dass, A. (2009). Mass spectrometric identification of Au<sub>68</sub>(SR)<sub>34</sub> molecular gold nanoclusters with 34-electron shell closing. *Journal of the American Chemical Society*, 131(33), 11666–11667.
- De Winter, J., Deshayes, G., Boon, F., Coulembier, O., Dubois, P., & Gerbaux, P. (2011). MALDI-ToF analysis of polythiophene: Use of trans-2-[3-(4-t-butyl-phenyl)-2-methyl-2-propenyldene]malononitrile - DCTB - as matrix. *Journal of Mass Spectrometry*, 46(3), 237–246.
- Ding, R., Wang, X.-P., Feng, J., Li, X.-B., Dong, F.-X., Tian, W.-Q., ... Sun, H.-B. (2018). Clarification of the Molecular Doping Mechanism in Organic Single-Crystalline Semiconductors and their Application in Color-Tunable Light-Emitting Devices. *Advanced Materials*, 0(0), 1801078.
- Dolgounitcheva, O., Zakrzewski, V. G., & Ortiz, J. V. (2005). Electron propagator calculations show that alkyl substituents alter porphyrin ionization energies. *Journal of the American Chemical Society*, 127(23), 8240–8241.
- Dreisewerd, K. (2003). The Desorption Process in MALDI. *Chemical Reviews*, 103(2), 395–426.
- Fang, H.-H., Chen, Q.-D., Yang, J., Xia, H., Gao, B.-R., Feng, J., ... Sun, H.-B. (2010). Two-Photon Pumped Amplified Spontaneous Emission from Cyano-Substituted Oligo(p-phenylenevinylene) Crystals with Aggregation-Induced Emission Enhancement. *The Journal of Physical Chemistry C*, 114(27), 11958–11961.
- Fazal, S., Jayasree, A., Sasidharan, S., Koyakutty, M., Nair, S. V, & Menon, D. (2014). Green

- Synthesis of Anisotropic Gold Nanoparticles for Photothermal Therapy of Cancer. *ACS Applied Materials & Interfaces*, 6(11), 8080–8089.
- Feng, Y., Wang, N., & Ju, H. (2018). Highly Efficient Electrochemiluminescence of Cyanovinylene-Contained Polymer Dots in Aqueous Medium and Its Application in Imaging Analysis. *Analytical Chemistry*, 90(2), 1202–1208.
- Giacalone, F., & Martín, N. (2010). New Concepts and Applications in the Macromolecular Chemistry of Fullerenes. *Advanced Materials*, 22(38), 4220–4248.
- Giraldo-Dávila, D., Chacón-Patiño, M. L., Ramirez-Pradilla, J. S., Blanco-Tirado, C., & Combariza, M. Y. (2018). Selective ionization by electron-transfer MALDI-MS of vanadyl porphyrins from crude oils. *Fuel*, 226(March), 103–111.
- Gómez Esteban, S., de la Cruz, P., Aljarilla, A., Arellano, L. M., & Langa, F. (2011). Panchromatic push–pull chromophores based on triphenylamine as donors for molecular solar cells. *Organic Letters*, 13(19), 5362–5365.
- Gupta, R. K., Kusuma, D. Y., Lee, P. S., & Srinivasan, M. P. (2011). Covalent Assembly of Gold Nanoparticles for Nonvolatile Memory Applications. *ACS Applied Materials & Interfaces*, 3(12), 4619–4625.
- Györösi, P., Hvistendahl, G., & Undheim, K. (1975). Mass spectrometry of some triphenylcyclopropenium salts. Competition between dimerisation and adduct formation. *Journal of Mass Spectrometry*, 10(9), 744–747.
- Hodgson, G. W., & Peake, E. (1961). Metal Chlorin Complexes in Recent Sediments as Initial Precursors to Petroleum Porphyrin Pigments. *Nature*, 191, 766. Retrieved from
- Ibrahim, H., Jurcic, K., Wang, J. S.-H., Whitehead, S. N., & Yeung, K. K.-C. (2017). 1,6-Diphenyl-1,3,5-hexatriene (DPH) as a Novel Matrix for MALDI MS Imaging of Fatty Acids,

- Phospholipids, and Sulfatides in Brain Tissues. *Analytical Chemistry*, 89(23), 12828–12836.
- Jandke, M., Strohhriegl, P., Gmeiner, J., Brütting, W., & Schwoerer, M. (1999). Polarized Electroluminescence from Rubbing-Aligned Poly (p-phenylenevinylene). *Advanced Materials*, 11(18), 1518–1521.
- Jaskolla, T. W., Lehmann, W.-D., & Karas, M. (2008). 4-Chloro-alpha-cyanocinnamic acid is an advanced, rationally designed MALDI matrix. *Proceedings of the National Academy of Sciences of the United States of America*, 105(34), 12200–12205.
- Jin, R. (2015). Atomically precise metal nanoclusters: Stable sizes and optical properties. *Nanoscale*, 7(5), 1549–1565.
- Juhász, P., & Costello, C. E. (1993). Generation of large radical ions from oligometalloenes by matrix-assisted laser desorption ionization. *Rapid Communications in Mass Spectrometry*, 7(5), 343–351.
- Kashiyama, Y., Kitazato, H., & Ohkouchi, N. (2007). An improved method for isolation and purification of sedimentary porphyrins by high-performance liquid chromatography for compound-specific isotopic analysis. *Journal of Chromatography A*, 1138(1–2), 73–83.
- Kay, A., & Graetzel, M. (1993). Artificial photosynthesis. 1. Photosensitization of TiO<sub>2</sub> solar cells with chlorophyll derivatives and related natural porphyrins. *Journal of Physical Chemistry;(United States)*, 97(23).
- Kiselev, V. D., Sakhabutdinov, A. G., Shakirov, I. M., Zverev, V. V., & Konovalov, A. I. (1992). BIS-REAGENTS IN DIELS-ALDER REACTION. 7. PREPARATION AND PROPERTIES OF POLYADDUCTS OF BISPOLYMETHYLCYCLOPENTADIENES AND BISMALEIMIDES REACTION. *ZHURNAL ORGANICHESKOI KHIMII*, 28(11), 2244–2252.

- Knochenmuss, R. (2016). *The Coupled Chemical and Physical Dynamics Model of MALDI. Annual Review of Analytical Chemistry* (Vol. 9).
- Knochenmuss, Richard. (2006). Ion formation mechanisms in UV-MALDI. *Analyst*, 131(9), 966–986.
- Knochenmuss, Richard. (2009). A bipolar rate equation model of MALDI primary and secondary ionization processes, with application to positive/negative analyte ion ratios and suppression effects. *International Journal of Mass Spectrometry*, 285(3), 105–113.
- Kotsiris, S. G., Vasil'ev, Y. V., Streletskii, A. V., Han, M., Mark, L. P., Boltalina, O. V, ... Drewello, T. (2006). Application and evaluation of solvent-free matrix-assisted laser desorption/ionization mass spectrometry for the analysis of derivatized fullerenes. *European Journal of Mass Spectrometry*, 12(6), 397–408.
- Li, G., Zhao, Y., Li, J., Cao, J., Zhu, J., Sun, X. W., & Zhang, Q. (2015). Synthesis, Characterization, Physical Properties, and OLED Application of Single BN-Fused Perylene Diimide. *The Journal of Organic Chemistry*, 80(1), 196–203.
- Li, J.-J., Chen, Y., Yu, J., Cheng, N., & Liu, Y. (2018). A Supramolecular Artificial Light-Harvesting System with an Ultrahigh Antenna Effect. *Advanced Materials*, 29(30), 1701905.
- Li, T., Xiao, L., Yang, J., Ding, M., Zhou, Z., LaConte, L., ... Li, X. (2017). Trimetallic Nitride Endohedral Fullerenes Carboxyl-Gd<sub>3</sub>N@C<sub>80</sub>: A New Theranostic Agent for Combating Oxidative Stress and Resolving Inflammation. *ACS Applied Materials & Interfaces*, 9(21), 17681–17687.
- Liu, J., Loewe, R. S., & McCullough, R. D. (1999). Employing MALDI-MS on Poly(alkylthiophenes): Analysis of Molecular Weights, Molecular Weight Distributions, End-Group Structures, and End-Group Modifications. *Macromolecules*, 32(18), 5777–5785.

- Liu, J., & McCullough, R. D. (2002). End Group Modification of Regioregular Polythiophene through Postpolymerization Functionalization. *Macromolecules*, 35(27), 9882–9889.
- Lou, X., de Waal, B. F. M., van Dongen, J. L. J., Vekemans, J. A. J. M., & Meijer, E. W. (2010). A pitfall of using 2-[(2E)-3-(4-tert-butylphenyl)-2-methylprop-2-enylidene] malononitrile as a matrix in MALDI TOF MS: chemical adduction of matrix to analyte amino groups. *Journal of Mass Spectrometry*, 45(10), 1195–1202.
- Macha, S. F., & Limbach, P. A. (2002). Matrix-assisted laser desorption/ionization (MALDI) mass spectrometry of polymers. *Current Opinion in Solid State and Materials Science*, 6(3), 213–220.
- Martin, M. N., Li, D., Dass, A., & Eah, S.-K. (2012). Ultrafast, 2 min synthesis of monolayer-protected gold nanoclusters ( $d < 2$  nm). *Nanoscale*, 4(14), 4091–4094.
- Masuda, K., Ikeda, Y., Ogawa, M., Benten, H., Ohkita, H., & Ito, S. (2010). Exciton Generation and Diffusion in Multilayered Organic Solar Cells Designed by Layer-by-Layer Assembly of Poly(p-phenylenevinylene). *ACS Applied Materials & Interfaces*, 2(1), 236–245.
- Mathew, S., Yella, A., Gao, P., Humphry-Baker, R., Curchod, B. F. E., Ashari-Astani, N., ... Grätzel, M. (2014). Dye-sensitized solar cells with 13% efficiency achieved through the molecular engineering of porphyrin sensitizers. *Nature Chemistry*, 6(3), 242–247.
- McCarley, T. D., McCarley, R. L., & Limbach, P. A. (1998). Electron-transfer ionization in matrix-assisted laser desorption/ionization mass spectrometry. *Analytical Chemistry*, 70(20), 4376–4379.
- Mikroyannidis, J. A., Kabanakis, A. N., Suresh, P., & Sharma, G. D. (2011). Efficient Bulk Heterojunction Solar Cells Based on a Broadly Absorbing Phenylenevinylene Copolymer Containing Thiophene and Pyrrole Rings. *The Journal of Physical Chemistry C*, 115(14),

7056–7066.

- Moorthy, J. N., Venkatakrisnan, P., Natarajan, P., Lin, Z., & Chow, T. J. (2010). Nondoped Pure-Blue OLEDs Based on Amorphous Phenylenevinylene-Functionalized Twisted Bimesitylenes. *The Journal of Organic Chemistry*, 75(8), 2599–2609.
- Nalwa, K. S., Cai, Y., Thoeming, A. L., Shinar, J., Shinar, R., & Chaudhary, S. (2010). Polythiophene-Fullerene Based Photodetectors: Tuning of Spectral Response and Application in Photoluminescence Based (Bio)Chemical Sensors. *Advanced Materials*, 22(37), 4157–4161.
- Nasrolahi Shirazi, A., Mandal, D., Tiwari, R. K., Guo, L., Lu, W., & Parang, K. (2013). Cyclic Peptide-Capped Gold Nanoparticles as Drug Delivery Systems. *Molecular Pharmaceutics*, 10(2), 500–511.
- Nazim Boutaghou, M., & Cole, R. B. (2012). 9, 10-Diphenylanthracene as a matrix for MALDI-MS electron transfer secondary reactions. *Journal of Mass Spectrometry*, 47(8), 995–1003.
- Ogunrinde, A., Hipps, K. W., & Scudiero, L. (2006). A Scanning Tunneling Microscopy Study of Self-Assembled Nickel(II) Octaethylporphyrin Deposited from Solutions on HOPG. *Langmuir*, 22(13), 5697–5701.
- Ohshita, J., Tada, Y., Kunai, A., Harima, Y., & Kunugi, Y. (2009). Hole-injection properties of annealed polythiophene films to replace PEDOT–PSS in multilayered OLED systems. *Synthetic Metals*, 159(3), 214–217.
- Paciotti, G. F., Zhao, J., Cao, S., Brodie, P. J., Tamarkin, L., Huhta, M., ... Kingston, D. G. I. (2016). Synthesis and Evaluation of Paclitaxel-Loaded Gold Nanoparticles for Tumor-Targeted Drug Delivery. *Bioconjugate Chemistry*, 27(11), 2646–2657.
- Patiny, L., & Borel, A. (2013). ChemCalc: A Building Block for Tomorrow's Chemical

- Infrastructure. *Journal of Chemical Information and Modeling*, 53(5), 1223–1228.
- Pond, S. J. K., Rumi, M., Levin, M. D., Parker, T. C., Beljonne, D., Day, M. W., ... Perry, J. W. (2002). One- and two-photon spectroscopy of donor–acceptor–donor distyrylbenzene derivatives: effect of cyano substitution and distortion from planarity. *The Journal of Physical Chemistry A*, 106(47), 11470–11480.
- Putman, J. C., Rowland, S. M., Corilo, Y. E., & McKenna, A. M. (2014). Chromatographic enrichment and subsequent separation of nickel and vanadyl porphyrins from natural seeps and molecular characterization by positive electrospray ionization FT-ICR mass spectrometry. *Analytical Chemistry*, 86(21), 10708–10715.
- Qian, H., & Jin, R. (2009). Controlling nanoparticles with atomic precision: The case of Au<sub>144</sub>(SCH<sub>2</sub>CH<sub>2</sub>Ph)<sub>60</sub>. *Nano Letters*, 9(12), 4083–4087.
- Qin, Y., Uddin, M. A., Chen, Y., Jang, B., Zhao, K., Zheng, Z., ... Hou, J. (2016). Highly Efficient Fullerene-Free Polymer Solar Cells Fabricated with Polythiophene Derivative. *Advanced Materials*, 28(42), 9416–9422.
- Ramírez-Pradilla, J. S., Blanco-Tirado, C., Hubert-Roux, M., Giusti, P., Afonso, C., & Combariza, M. Y. (2019). No Title. *Energy & Fuels*, Submitted.
- Sato, N., Seki, K., & Inokuchi, H. (1981). Polarization energies of organic solids determined by ultraviolet photoelectron spectroscopy. *Journal of the Chemical Society, Faraday Transactions 2: Molecular and Chemical Physics*, 77(9), 1621–1633.
- Scotognella, F., Puzzo, D. P., Zavelani-Rossi, M., Clark, J., Sebastian, M., Ozin, G. A., & Lanzani, G. (2011). Two-Photon Poly(phenylenevinylene) DFB Laser. *Chemistry of Materials*, 23(3), 805–809.
- Scudiero, L., Barlow, D. E., & Hipps, K. W. (2002). Scanning Tunneling Microscopy, Orbital-

- Mediated Tunneling Spectroscopy, and Ultraviolet Photoelectron Spectroscopy of Nickel(II) Octaethylporphyrin Deposited from Vapor. *The Journal of Physical Chemistry B*, 106(5), 996–1003.
- Speller, E. M., McGettrick, J. D., Rice, B., Telford, A. M., Lee, H. K. H., Tan, C.-H., ... Tsoi, W. C. (2017). Impact of Aggregation on the Photochemistry of Fullerene Films: Correlating Stability to Triplet Exciton Kinetics. *ACS Applied Materials & Interfaces*, 9(27), 22739–22747.
- Tigeros, A., Dhas, V., Ortiz, A., Insuasty, B., Martín, N., & Echegoyen, L. (2014). Influence of acetylene-linked  $\pi$ -spacers on triphenylamine–fluorene dye sensitized solar cells performance. *Solar Energy Materials and Solar Cells*, 121, 61–68.
- Treibs, A. (n.d.). Chlorophyll- und Hämin-Derivate in bituminösen Gesteinen, Erdölen, Kohlen, Phosphoriten. *Justus Liebigs Annalen Der Chemie*, 517(1), 172–196.
- Ulmer, L., Mattay, J., Torres-Garcia, H. G., & Luftmann, H. (2000). Letter: The use of 2-[(2E)-3-(4-tert-butylphenyl)-2-methylprop-2-enylidene] malononitrile as a matrix for matrix-assisted laser desorption/ionization mass spectrometry. *European Journal of Mass Spectrometry*, 6(1), 49–52.
- Vandenbergh, J., Conings, B., Bertho, S., Kesters, J., Spoltore, D., Esiner, S., ... Vanderzande, D. J. M. (2011). Thermal Stability of Poly[2-methoxy-5-(2'-phenylethoxy)-1,4-phenylenevinylene] (MPE-PPV):Fullerene Bulk Heterojunction Solar Cells. *Macromolecules*, 44(21), 8470–8478.
- Vasil'ev, Y. V, Khvostenko, O. G., Streletskii, A. V, Boltalina, O. V, Kotsiris, S. G., & Drewello, T. (2006). Electron transfer reactivity in matrix-assisted laser desorption/ionization (MALDI): ionization energy, electron affinity and performance of the DCTB matrix within

- the thermochemical framework. *The Journal of Physical Chemistry A*, 110(18), 5967–5972.
- Wang, P., Collison, C. J., & Rothberg, L. J. (2001). Origins of aggregation quenching in luminescent phenylenevinylene polymers. *Journal of Photochemistry and Photobiology A: Chemistry*, 144(1), 63–68.
- Wu, J., Qin, K., Yuan, D., Tan, J., Qin, L., Zhang, X., & Wei, H. (2018). Rational Design of Au@Pt Multibranching Nanostructures as Bifunctional Nanozymes. *ACS Applied Materials & Interfaces*, 10(15), 12954–12959.
- Wyatt, M. F., Stein, B. K., & Brenton, A. G. (2006). Characterization of Various Analytes Using Matrix-Assisted Laser Desorption/Ionization Time-of-Flight Mass Spectrometry and 2-[2-E)-3-(4-tert-Butylphenyl)-2-methylprop-2-enylidene] malononitrile Matrix. *Analytical Chemistry*, 78(1), 199–206.
- Xu, Y., Xie, Z., Zhang, H., Shen, F., & Ma, Y. (2016). Conformational polymorphism of a twisted conjugated molecule: controllable torsional motion for crystal growth selectivity. *CrystEngComm*, 18(36), 6824–6829.
- Yoo, J., Yang, S. K., Jeong, M.-Y., Ahn, H. C., Jeon, S.-J., & Cho, B. R. (2003). Bis-1, 4-(p-diarylaminostryl)-2, 5-dicyanobenzene derivatives with large two-photon absorption cross-sections. *Organic Letters*, 5(5), 645–648.
- Youn, H., Park, H. J., & Guo, L. J. (2015). Printed Nanostructures for Organic Photovoltaic Cells and Solution-Processed Polymer Light-Emitting Diodes. *Energy Technology*, 3(4), 340–350.
- Zhang, M., Guo, X., Ma, W., Ade, H., & Hou, J. (2014). A Polythiophene Derivative with Superior Properties for Practical Application in Polymer Solar Cells. *Advanced Materials*, 26(33), 5880–5885.
- Zhao, L., & Lin, Z. (2012). Crafting Semiconductor Organic–Inorganic Nanocomposites via

Placing Conjugated Polymers in Intimate Contact with Nanocrystals for Hybrid Solar Cells.

*Advanced Materials*, 24(32), 4353–4368.

Zhao, X., Liu, Y., Xu, C., Yan, Y., Zhang, Y., Zhang, Q., ... Shi, Q. (2013). Separation and characterization of vanadyl porphyrins in Venezuela Orinoco heavy crude oil. *Energy and Fuels*, 27(6), 2874–2882.

Zhao, X., Shi, Q., Gray, M. R., & Xu, C. (2014). New Vanadium Compounds in Venezuela Heavy Crude Oil Detected by. *Scientific Reports*, 4, 1–6.

### **3. Tunable Fluorene-based light-harvesting materials as MALDI MS matrices for macrocyclic ligands and metal complexes analysis *via* Electron-Transfer Ionization**

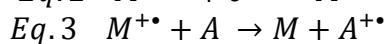
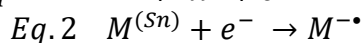
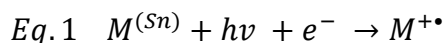
#### **3.1. Abstract**

Macrocyclic ligands and their metal complexes are fundamental structures, in both nature and technology. Molecular characterization of these compounds can be easily performed via secondary ion formation by electron-transfer (ET) reactions in the gas phase, using synthetically-tunable molecules based on Fluorene (FL) as UV MALDI matrices. Five FL derivatives, synthesized from 2,7-dibromofluorene via Knoevenagel reaction, were characterized in terms of physicochemical properties such as IE, UV absorption in solution and solid phase, gap energy  $E_{gap}$  and primary ion energy thresholds. ET-MALDI MS experiments using the FLs provided a significant signal enhancing based on analytical descriptors such as ion abundance and signal-to-noise ratios and a 100% of analyte coverage in a mixture of porphyrins/phthalocyanines/chlorophyll when compared with standard matrix DCTB. Finally, we evaluate the performance of FLs for the ionization of crude-oil lithology markers (vanadyl porphyrins) in a real complex oil mixture; FLs exhibited high selectivity and a significant signal increase when compared with the LDI and DCTB standard matrix.

#### **3.2. Introduction**

Macrocyclic ligands and their metal complexes such as the tetrapyrrole-based porphyrins, porphyrazines, phtalocyanins, hemes and the chlorin-based chlorophylls are compounds of

fundamental importance in nature and technology as photosensitizers,(Lovell et al., 2009)(Shen et al., 2011) light harvesters,(Hiroto, Miyake, & Shinokubo, 2017)(Economopoulos & Tagmatarchis, 2015) oxygen and electron carriers,(Nishide, Tsukahara, & Tsuchida, 1998)(Marydasan, Nair, & Ramaiah, 2013) dyes, pigments, biomarkers,(Gourier et al., 2010)(Giraldo-Dávila, Chacón-Patiño, Ramirez-Pradilla, Blanco-Tirado, & Combariza, 2018) and photocatalyst,(Murphy et al., 2014)(Nayak et al., 2016) among others. Molecular identification of these species, alone or in complex mixtures, is vital in many research fields, *e.g.* biochemistry,(Hitchcock et al., 2016)(Davison et al., 2005) material sciences,(Hosseini, Hodgson, Tham, Reed, & Boyd, 2006)(Bera, Jana, Mondal, & Patra, 2017) petrochemistry.(Giraldo-Dávila et al., 2018)(Putman, Rowland, Corilo, & McKenna, 2014) Mass spectrometric analysis of macrocyclic ligands and their metal complexes afford compound identification, molecular weight measurement and study of gas-phase reactivity, among other properties. However, due to the labile nature of most of these complexes MS analysis, even using “soft” ionization methods such as ESI or APCI, often result in compound degradation, demetallation, fragmentation, oxidation and decomposition.(Müller, Vergeiner, & Kräutler, 2014),(Schoefs, 2002) Electron transfer (ET) ionization in MALDI-MS is a powerful technique able to yield single charged species in the form of radicals ( $M^{+\bullet}$ ,  $M^{-\bullet}$ ) from labile species. (R. Knochenmuss, 2016)(Richard Knochenmuss, 2006) These species are formed by secondary charge-transfer reactions with a matrix primary ion according to Eq 1-3, where M refers to matrix and A to analyte.



Primary ion formation in ET-MALDI majorly depends on effective interactions between a solid matrix and photons emitted from a light source, typically a Nd-YAG laser (355 nm) for UV-MALDI. Thus, a compound acting as ET matrix must form crystalline networks able to efficiently harvest photons, withstand low pressure environments, be chemically inert and exhibit relatively high ionization energy, among other characteristics. (Richard Knochenmuss, 2006)(Richard Knochenmuss, 2009) According to the coupled physical and chemical dynamics model (CPCD) proposed by R. Knochenmuss,(R. Knochenmuss, 2016) primary ionization in MALDI-MS occurs by energy pooling where adjacent excited species ( $S_0$ ,  $S_1$  and  $S_2$ ) are involved in the process of absorption/emission of photons. Matrix electronic structure is of fundamental importance to create molecular “excitons” where enough energy can be stored by pooling to reach an ionized state. Once matrix primary ions are formed, the ET reaction (Eq 3) involving a matrix radical cation  $[M]^{+\bullet}$  and a neutral analyte  $[A]$  takes place only if the ionization energy (IE) of A is at least 0.5 eV lower than the matrix', according to McCarley and Co-workers statement.(McCarley, McCarley, & Limbach, 1998)(Vasil'ev et al., 2006)

As mentioned above, the role of porphyrin derivatives in biochemistry, material science, and petrochemistry, has prompted the development of several matrices for their analysis using ET reactions in MALDI-MS, which decreases the rate of metal loss, fragmentation and decomposition. In 2012, the 1,9-diphenylanthracene (9,10-DPA) was reported as electron transfer matrix for the ionization of chlorophyll *a*, with an outstanding performance when compared with traditional MALDI matrices, DHB, dithranol or CHCA. Such matrices drive the ionization of chlorophylls via proton transfer reactions, dramatically affecting the integrity of the molecular ion, as a result, the observed ions corresponded to fragments  $[Chla-Mg]^+ m/z$  870 and  $[Chla-phytol]^+ m/z$  614 while

9,10-DPA showed the signal corresponding to intact chlorophyll *a* at  $m/z$  892 as a radical cation  $[\text{Chl}a]^{+\bullet}$ .(Nazim Boutaghou & Cole, 2012) Because chlorophylls are of great importance in food industry and biochemistry field, the detection of those metal complexes as intact ions using ET ionization has received a special efforts, recently, Calvano, et al, reported the use of 1,5-diaminonaphthalene (1,5-DAN) for the selective ionization of chlorophylls in foodstuff and bacteria; interestingly the basic character in addition with low energy threshold and high yield of primary ions, conducted to their effective ionization without metal or phytol losses.(Calvano, Ventura, Cataldi, & Palmisano, 2015)(Calvano et al., 2017) Chlorophyll-derived porphyrins occurring in fossil fuels, are partially degraded biomarkers carrying information about origin, kerogen formation and maturity, additionally, these compounds are commonly responsible of nickel(II) and vanadium(IV) bounding, deleterious metals for catalyst during the refining process. The detection, identification and characterization of these compounds have been achieved after several chromatographic approaches, using ESI or APPI ion sources, however, their limitations in ionization efficiency, sample amounts, purity and dynamic range of the instruments, inhibit a comprehensive characterization. Recently, we reported an approach for the identification of petroporphyrins in Colombian heavy crude-oils using a *p*-cyanophenylenevinylene matrix, demonstrating that rationally designed electron transfer experiments in MALDI, can address a comprehensive analysis of these important molecules.(Giraldo-Dávila et al., 2018) As far, the electron transfer ionization in MALDI-MS is still a matrix-dependent phenomena and strongly relies in physicochemical properties such as UV-absorption, chemical stability, vacuum pressure, solubility, crystallization and ionization energy. Reasonably, the fluorene core, which has been widely used as starting material in light harvesting, electronic polymers, OLEDs, solar cell sensitizers and photoswitch technology, using bottom up synthesis, represent a potential organic

material for the design and synthesis of matrices to be used in electron transfer MALDI mass spectrometry. The advantages of fluorene core are based on its synthetically-tunable structure which enable the introduction of chromophores, EDG and EWG substituents and extension on conjugation by current approaches like heck reactions, aldol condensations via acidic hydrogen activation, sonogashira coupling, among others.

### **3.3. Experimental Section**

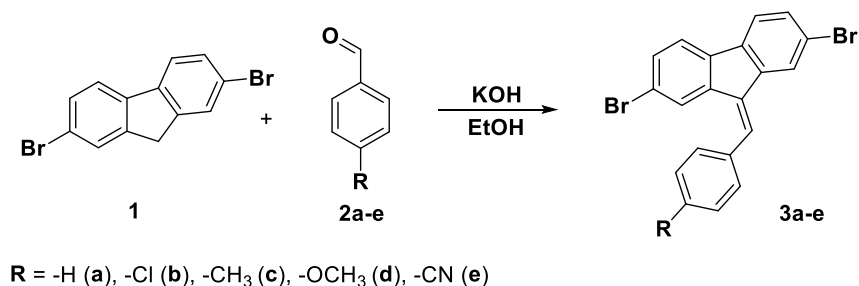
**3.3.1. UV-vis spectroscopy measurements and Ionization Energy measurement.** UV-Vis properties of FL derivatives and the standard matrix DCTB were measured by UV-Vis experiments in solution and solid state using a Shimadzu UV-2401PC instrument; 15 mg of each matrix was dispersed in 200 mg of BaSO<sub>4</sub> and subjected to irradiation in a range of 200-900 nm with a slit of 0.5 nm. For molar extinction coefficients, stock solutions of all compounds in the range of 5.0 – 30  $\mu$ M in THF were measured at 355 nm in a double channel Shimadzu UV-2401PC spectrophotometer (Kyoto, Japan) using the Beer-Lambert law to fit the data. A scanning range of 200 to 800 nm was used in order to obtain all spectra focusing the region of interest close to 355 nm. The ionization potentials of fluorene (IPs) were theoretically determined by Koopmans theory using the Gaussian 09 software suite

**3.3.2. LDI and UV-MALDI sample preparation.** For all experiments 5.0 mM stock solutions of the FL derivatives and analytes in THF were prepared and sonicated in a Bransonic ultrasonic bath (Danbury CT, USA) at 40 KHz and 130 W during 30 seconds. For MALDI experiments, FLs and analyte solutions were mixed in several analyte:matrix molar ratios from 1:10 to 1:10<sup>6</sup> and 1.0  $\mu$ L, resulting solution was placed on stainless steel target by dried droplet method.

**3.3.3. Mass Spectrometry.** Bruker Ultraflex extreme MALDI TOF-TOF instrument (Bruker Daltonics, Billerica, MA) equipped with a 1 kHz Smart Beam Nd:YAG laser (355 nm) was used to LDI and MALDI experiments. The energy of Nd:YAG laser was measured employing a PowerMax<sup>TM</sup> – USB/RS Sensor System (Coherent, Santa Clara, USA); ranging the attenuator from 0% to 60% in order to obtain the threshold energies. Mass spectra of fluorenes were acquired in positive ion reflectron mode from m/z 100 to 2000, with delayed extraction set at 100 ns and an accelerating voltage of 25 kV.  $\alpha$ -CHCA and standard peptide as leu-enkephaline, bradykinin, bombesin and renin substrate purchased from Sigma Aldrich (St. Louis, MO) were used for internal calibration. Autoexecute mode in FlexControl Software (Bruker Daltonics, Billerica, MA) was used to randomize the acquisition data over spot and is based on a 10-shots walk algorithm over spot. For each analysis 2000 spectrum were accumulated, and the analysis of all experiments was carried out using FlexAnalysis software (Bruker Daltonics, Billerica MA, USA) that automatically reports analytical figures of merit such as ion abundances, S/N ratios and resolution.

### 3.4. Results and Discussions

Historically, fluorene derivatives have demonstrated a great versatility in material science with large applications in biochemistry,(Yue et al., 2015) molecular electronics,(Lian, Liu, & Chen, 2011) display technology,(Tang et al., 2006)(Feng et al., 2015) photocatalysis,(Stergiou & Tagmatarchis, 2016) solar cells,(Liu, Li, et al., 2014)(Liu, Xiong, et al., 2014) and chemoresponsive sensors.(Peterson, Davis, Werre, Coughlin, & Carter, 2011)(Sui, Kim, Zhang, Frazer, & Belfield, 2013) Extending the conjugation on C-9 position consists in an accessible reaction which creates a new C-C bond, yielding substituted derivatives containing chromophores, biologically active moieties or conjugated extensions with specific physicochemical properties. Because organic materials for applications as electron transfer matrices in MALDI-MS need to attach some well-known physicochemical properties such as liquid and solid UV absorption, gap energy  $E_g$ , ionization energy (IE) and high yield on the formation of matrix's primary ions, the fluorene derivatives emerges as ideal candidates due to its synthetic versatility and optoelectronically-tunable structure. In Scheme 1, a straightforward methodology using the Knoevenagel condensation from 2,7-dibromofluorene and 4-substituted benzaldehydes, resulted in five fluorene derivatives (**3a-e**); (**a**) FL-H, (**b**) FL-Cl, (**c**) FL-CH<sub>3</sub>, (**d**) FL-OCH<sub>3</sub> and (**e**) FL-CN. In supporting information a detailed procedure including NMR-<sup>1</sup>H data is shown (See figure S1).



According to the coupled physical and chemical dynamics mechanism “CPCD” introduced by R. Knochenmuss, (R. Knochenmuss, 2016) the desorption process and primary ion formation in MALDI-MS is likely a photon-mediated event. Primary ionization is a consecutive pooling mechanism started by the absorption of UV laser photons (Nd:YAG 355 nm) followed by annihilation of excited species, resulting in the formation of primary ions of the matrix. As seen in Figure 14 (middle), all tested compounds showed  $\lambda_{\max}$  values ranging from 250 to 360 nm; the observed absorption bands are mostly related with the  $\pi$ - $\pi^*$  transitions with *hypso* shifts for EWG (-H, -Cl, -CN) and *batho* shift for the EDG -OCH<sub>3</sub> group, taking 355 nm as a reference (Nd:YAG laser emitted photon wavelength). The ability to harvest photons was measured using the Beer-Lambert law at 355 nm. Insets in figure 14 show values from 5600 to 16400 M<sup>-1</sup>.cm<sup>-1</sup>, in which molecules like FL-CN, FL-OCH<sub>3</sub> and FL-CH<sub>3</sub> appeared as excellent candidates for ET matrices with molar extinction coefficients above 10000 M<sup>-1</sup>.cm<sup>-1</sup>. As far, the UV absorption in solution cannot be considered as a descriptor to determine the absorption properties of a matrix candidate since MALDI process is a solid/semi-condensed-gas-phase phenomenon, therefore, diffuse reflection (DR) experiments can be used to obtain valuable information about photon absorption properties in the solid phase. In Figure 15, the DR spectra revealed a strong photon absorption in the range of 400-250 nm for all FLs and DCTB standard matrix with a minimum percentage of reflectance close to 355 nm; in solid state, all the fluorenes efficiently absorbs photons and appeared to be good matrix candidates. Additionally, data obtained from DR experiments were treated using the Kubelka-Munk approximation; in material science, the Kubelka-Munk estimates the gap energy; referring to the energy between valence (HOMO) and conduction (LUMO) band. In figure 15, those give us information about the exciton energy (gap energy between HOMO and LUMO “ $E_g$ ”) for insulators like fluorene derivatives. (Brimmer & Griffiths, 1988) (Morikawa,

Asahi, Ohwaki, Aoki, & Taga, 2001);(Jeong, Jin, So, Lim, & Lee, 2009) As seen in figure 3, we observed low exciton energies for all tested matrices: FL-H (2.69 eV), FI-Cl (2.65 eV), FL-CN (2.44 eV), FI-CH<sub>3</sub> (2.55 eV), FI-OCH<sub>3</sub> (2.42 eV) and DCTB (3.05 eV). Because pooling mechanism is mediated by the annihilation of excited species, matrices like FL-CN and FL-OCH<sub>3</sub> with a low  $E_g$  ensures a higher population, thus, the annihilation of two excited molecules “S<sub>1</sub>” promotes the formation of a double excited state “S<sub>n</sub>” in a key step.

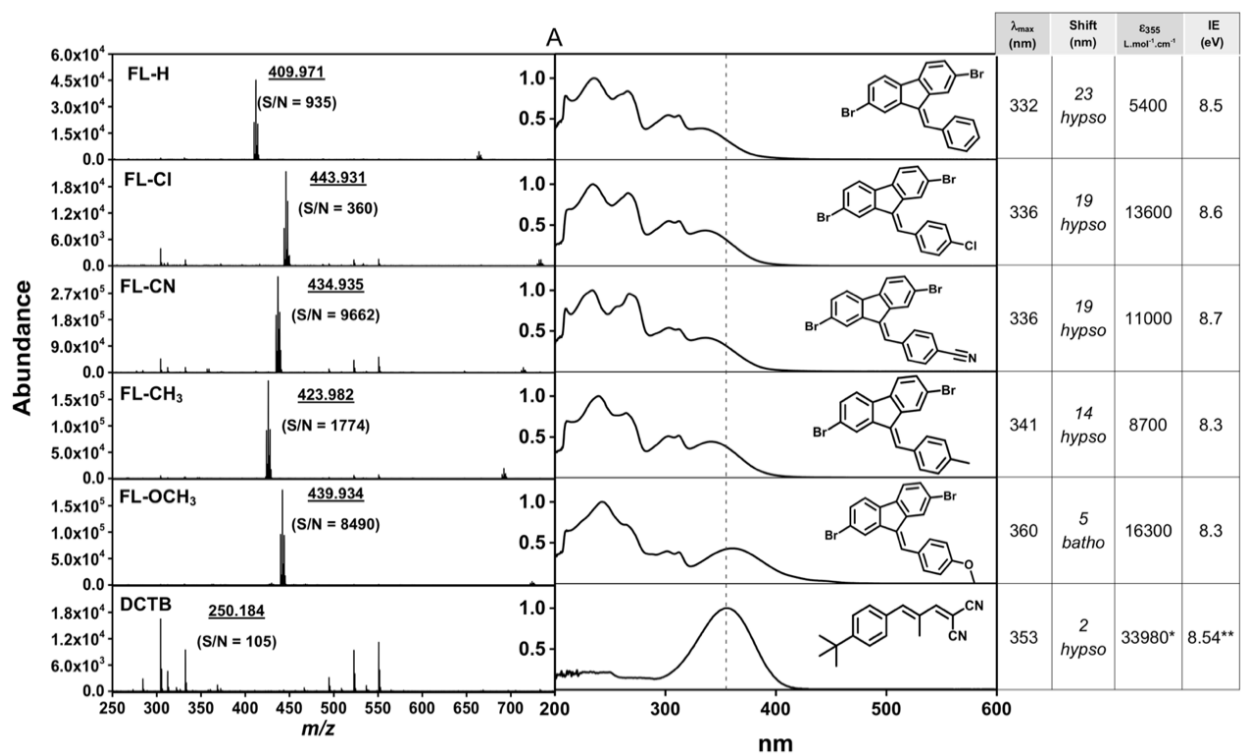


**Figure 14** LDI-MS spectra of all fluorene derivatives in comparison with standar matrix DCTB, 5 pmol on target and 1.24  $\mu$ J per pulse. (middle) UV-Vis absorption screening of fluorene derivatives; inset dot line refers to 355 nm (Nd:YAG photon wavelength).

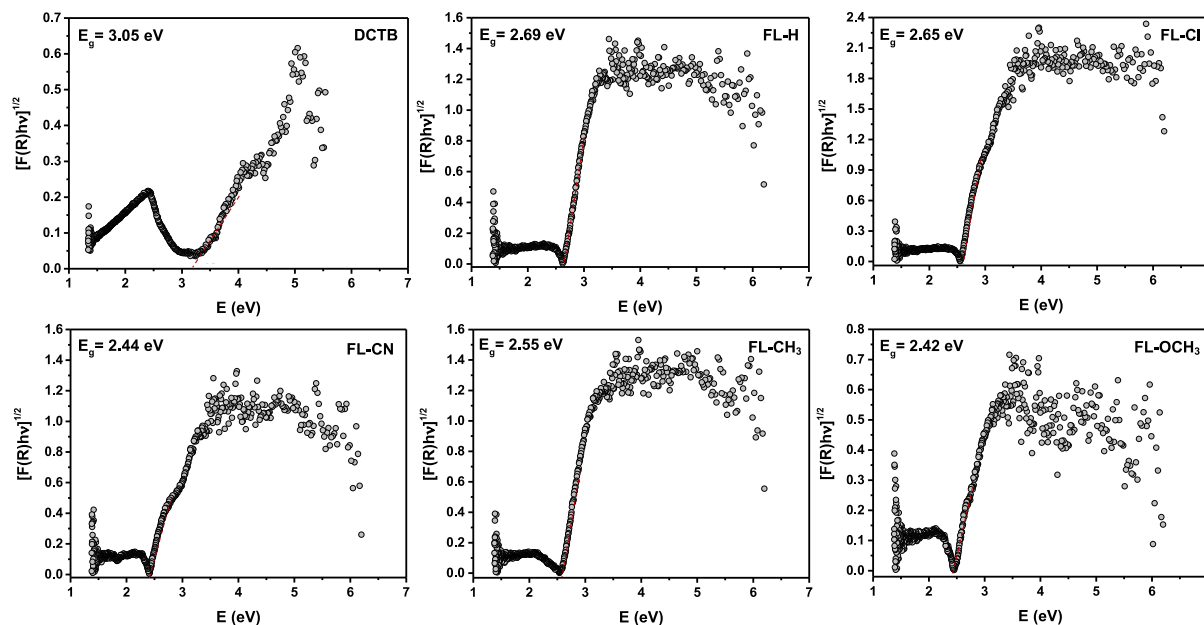


**Figure 15** (TOP) Diffuse reflection (DR) spectra for all FL derivatives and standard matrix DCTB taken in BaSO<sub>4</sub>. (BOTTON) Kubelka-Munk transformation for FL derivatives. Insets correspond to a linear fit and the cut on x-axis denotes the  $E_g$  of each derivative.

Contrarily, the FL-H, FL-Cl and DCTB exhibited a higher exciton energy, interestingly, these derivatives possess a higher ionization energy when compared with other derivatives. Here, the presence of EDGs or EWGs play an important role since the enrichment or reducing the  $\pi$ -electron cloud decreases or increases the ionization energy. These physicochemical aspects are fundamental in the formation of primary ions and need to be considered in a whole mechanism, therefore, ensuring a good UV absorption, desorption, exciton formation and annihilation between species result in a high yield of matrix's ions. The correlation between physicochemical properties and primary ion yield can be summarized in the ion appearance curves; the ion abundance in function of laser energy ( $\square J$ ) explain better the correlation between photons from the Nd:YAG laser and matrices in solid state. The ability to form a dense plume at low laser energies is one of

the requirements of a MALDI matrix candidate; a great ion count increases the probability for the electron transfer reaction between matrix and analytes, improving figures of merit such as signal to noise ratio and ion abundance. (Dreisewerd, 2003) (Knochenmuss, Stortelder, Breuker, & Zenobi, 2000) We studied the behavior of our FL derivatives and DCTB in function of laser energy by ranging the values from 0.65 to 3.37  $\mu\text{J}$  per pulse. As seen in figure 16, at laser threshold energy (0.43  $\mu\text{J}$  per pulse) FL-CN and FL-OCH<sub>3</sub> showed the highest ion abundance for the formation of primary ions as radical cation  $m/z$  434 [FL-CN]<sup>+•</sup>,  $m/z$  439 [FL-OCH<sub>3</sub>]<sup>+•</sup>; those with the lowest  $E_g$  of the series. Curiously, the DCTB exhibited a high ion abundance at the energy threshold despite the  $E_g$  value which goes up 3 eV; the high volatility under vacuum help during the desorption process after laser irradiance, in addition, the high absorption showed by the DCTB at 355 nm plays a crucial role for the primary ion formation.

As a general trend, we observed a linear dependence between 0.65 and 1.49  $\mu\text{J}$ , reaching the plateau between 1.49 and 3.27  $\mu\text{J}$ , in contrast, the DCTB matrix, exhibited the worst behavior of teste compounds without a clear tendency. Interestingly, at high energies, the fluorene derivatives keeps the radical cation signals without fragmentation process when compared with DCTB, see supporting info S3, probably related with the stabilization of the positive charge along the conjugated core. In previous reports, Dreissewerd, (Dreisewerd, 2003)

Respecting to the signal-to-noise values, we observed the same trend for fluorene derivatives; due to energy dependence the S/N ratios at low energies exhibited values under  $1.0^3$  observing the highest value at 1.24  $\mu\text{J}$ . With the laser increment, the noise levels augmenting (See supporting info S4) and the S/N dramatically decreases until values below  $2 \times 10^3$ . For DCTB using, we

observed a high noise levels even at low energies, obtaining for all determinations, values under  $1 \times 10^3$ . Because the electron transfer in MALDI-MS relies on the ability to form a dense plume of primary ions, we decide to discard the FL-H and FL-Cl compounds due to their poor results in LDI experiments when compared with the analogues. Based on figures of merit such as ion abundance, S/N ratio and signal resolution FL-CN, FL-CH<sub>3</sub> and FL-OCH<sub>3</sub> are shown as excellent candidate for ET-MALDI.

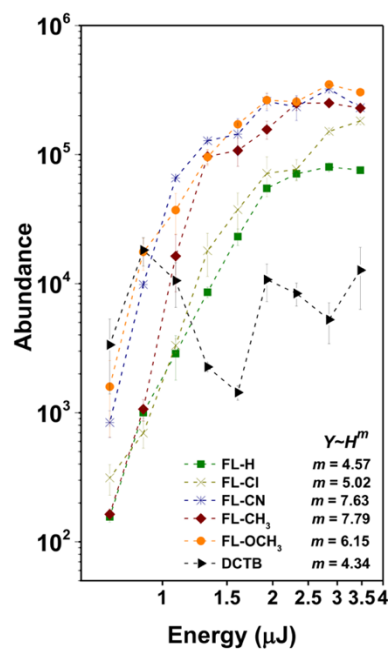


**Figure 16** Ion appearance curve for FL derivatives and DCTB.

**3.4.1. Fluorene derivatives as Electron transfer in MALDI-MS.** Since its introduction by Karas and Hillenkamp, (Karas & Hillenkamp, 1988) MALDI-MS has been a suitable, rapid and robust technique for the analysis of organic molecules, organometallic complexes, macromolecules and biomolecules. In general, many compounds can be analyzed using proton or transfer reaction in positive and negative ion mode, however, non-protonable and labile compounds such as porphyrins, polymers, polyaromatics, fullerene derivatives and organic dyes

are of great importance in the growing field of organic materials and cannot be ionized using the current ionization methods, accordingly, the electron transfer (ET) in MALDI-MS becomes as an adequate technique for the ionization of such compounds. Porphyrins and phthalocyanines are compounds based on a tetrapyrrole core, with several applications in photodynamic therapy,(Bonnett, 1995) petroleum chemistry,(Giraldo-Dávila, Chacón-Patiño, Orrego-Ruiz, Blanco-Tirado, & Combariza, 2016) organic solar cells,(Mathew et al., 2014) and supramolecular chemistry.(Moscatelli, 2015) For instance, some porphyrins containing a metallic nucleus (MPps) like Mg, Fe or Zn, which are involved in redox process, oxygen transport or simply stabilization of tetrapyrrole structure, thus, when MPps are analyzed in acidic media, the tetrapyrrole core undergoes demetallation or metal exchange, given unwanted results of MS analysis. Considering the importance of porphyrins and phthalocyanines, we decided to test the ability of our synthesized fluorenes for the ionization of cobalt porphyrin and a mixture of MPps and phthalocyanines derived from synthesis and purification process (from *spinacia olearacea*). As seen in figure 17, we tested the ability of FI-CN, FI-CH<sub>3</sub>, FI-OCH<sub>3</sub> and DCTB to form the radical cation of cobalt porphyrin [CoPp]<sup>+•</sup>, at 1.25 μJ per pulse of laser energy and 1000:1 (matrix to analyte ratio, 2.5 pmol of analyte on target). The FI-CN, FI-CH<sub>3</sub>, FI-OCH<sub>3</sub> show the signal associated with the intact CoPp molecule with a clean background and matrix suppression effect, in contrast, the use of DCTB shows the [CoPp]<sup>+•</sup> with signals in the range of m/z 400 to 700 directly related with DCTB background spectrum (zoomed DCTB spectrum is shown in supporting info, Figure S5). Up to this point, we decided to take a look onto the thermodynamics in the gas phase for the electron transfer reaction between CoPp and FI-CN, FI-CH<sub>3</sub> and FI-OCH<sub>3</sub>. As shown in figure 17, we followed the signal associated with [CoPp]<sup>+•</sup> and [FI]<sup>+•</sup> in function of laser energy from 0.34 to 2.37 μJ per pulse. At the threshold energy, we observed the matrix suppression effect phenomena,

(ref) meaning that secondary matrix-analyte reaction is thermodynamically favored; determinations by ultraviolet photoelectron spectroscopy, showed that compounds like CoPp exhibits ionization energy values of 6.5 eV. Taking as reference the IP values for Fls, 8.7, 8.3 and 8.3 eV for FL-CN, FL-CH<sub>3</sub> and FL-OCH<sub>3</sub>, the observed MSE is in accord with the condition established by McCarley and co-workers; in our particular case, the secondary matrix-analyte reaction is favored by a value of 2.2, 1.8 and 1.8 eV. Interestingly, with laser increasing we still observed the MSE (See figure S6, supporting info) for all matrices, nevertheless, for FL-CN, this trend is more pronounced, probably due to the high ionization potential.

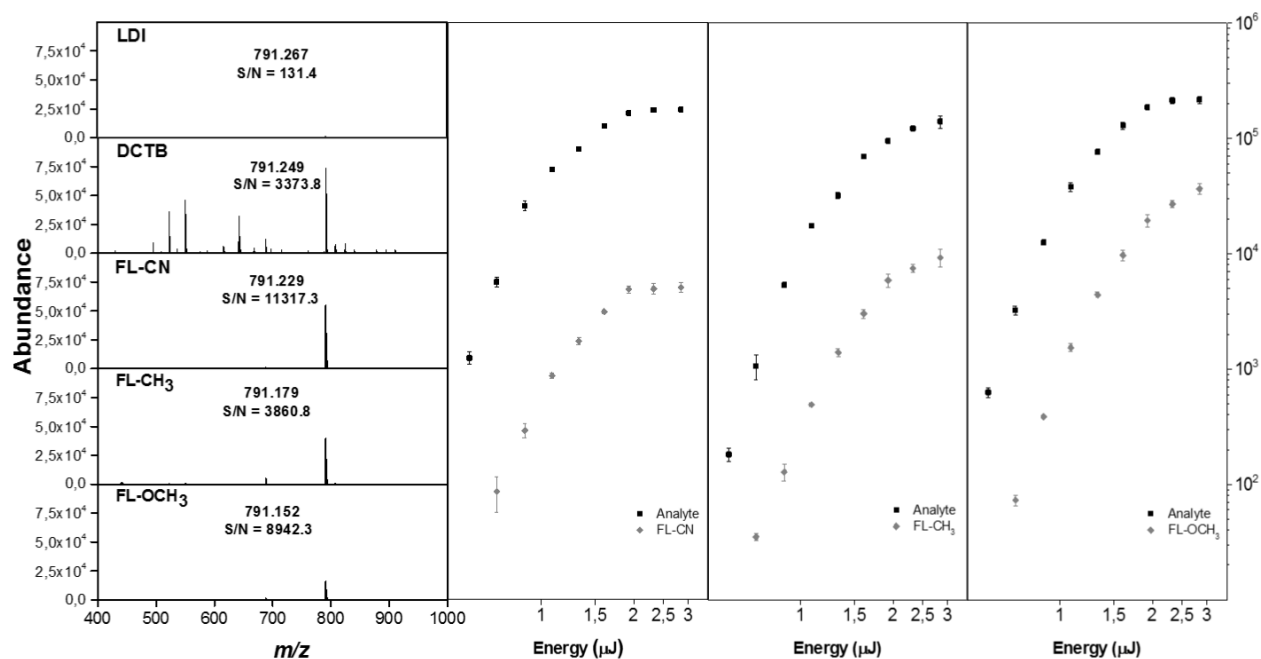


**Figure 17** (left) ET-MALDI spectra for the ionization of cobalt porphyrin (CoPp) using FL-CN, FL-CH<sub>3</sub>, FL-OCH<sub>3</sub> and DCTB as matrices. (right) ion appearance curves following the analyte radical cation signal [CoPp]<sup>+</sup>• and [M]<sup>+</sup>• ranging the laser energy from 0.34 to 2.16 μJ per pulse.

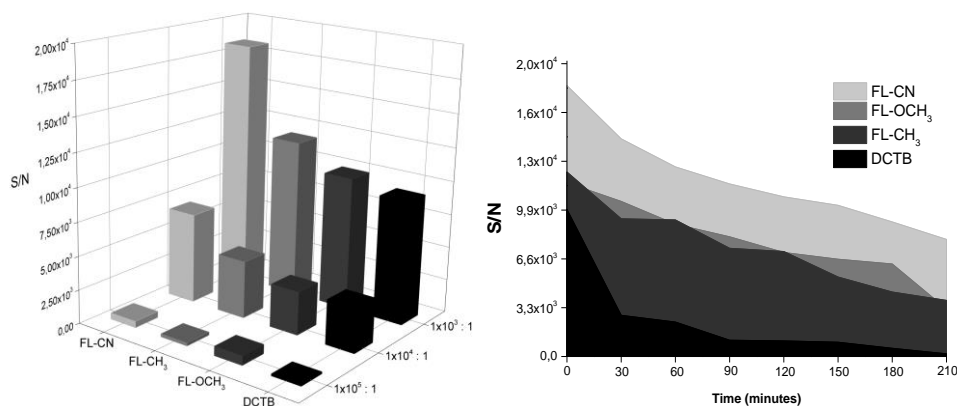


**Figure 18** (left) Limit of detection for the ionization of CoPp using FL-CN, FL-CH<sub>3</sub>, FL-OCH<sub>3</sub> and DCTB. (right) vacuum stability of FL-CN, FL-CH<sub>3</sub>, FL-OCH<sub>3</sub> and DCTB during a long time experiment following the [CoPp]<sup>+</sup>• signal.

Because our objective is to analyze a mixture of porphyrins and phtalocyanines with a possible application to petroporphyrins analysis (compounds that are present in crude oils at low concentrations), we decided to test the limit of detections (LODs) following the [CoPp]<sup>+</sup>• signal at several matrix to analyte ratios; 1x10<sup>3</sup>:1, 1x10<sup>4</sup>:1 and 1x10<sup>5</sup>:1. Figure 18, shows the LODS for FL-CN, FL-CH<sub>3</sub>, FL-OCH<sub>3</sub> and DCTB, interestingly, at low concentration of analyte, 12.5 fmol on target, we observed S/N ratios in the range of 1x10<sup>2</sup> to 5x10<sup>2</sup>. We concluded that FIs could exhibit good performance as matrices for low concentrated analytes such as petroporphyrins in crude-oils and porphyrinoids in plants.

Some analysis such as MALDI imaging and time scale experiments needs to retain the matrix over sample or MALDI target, especially when experiments go under vacuum condition; matrices with high vapor pressures have critical disadvantages due to sublimation resulting in a signal loss. In figure 18 (right) the analysis of [CoPp]<sup>+</sup>• in function of time at 1x10<sup>3</sup>:1 M:A molar ratio, shows

a dramatic decrease of the S/N value when DCTB was used; from  $1 \times 10^4$  to  $3 \times 10^3$  during the first 60 minutes of analysis. In contrast, the use of FI-CN, FI-CH<sub>3</sub> and FI-OCH<sub>3</sub> keep the S/N in almost the 70% of the initial value;  $1.8 \times 10^4$  to  $1.3 \times 10^4$ ,  $1.3 \times 10^4$  to  $1.0 \times 10^4$  and  $1.2 \times 10^4$  to  $9.8 \times 10^4$ , respectively.

In brief, we have determined several physicochemical and mass spectrometric properties with the expected results, thus, the FI-CN, FI-CH<sub>3</sub> and FI-OCH<sub>3</sub> compounds appear as promising matrices for the electron transfer ionization of complex mixtures containing porphyrin-like compounds. To evaluate the efficiency of FIs for the ionization of complex samples, we used a mixture of ten porphyrins and phthalocyanines as analytes listed as; phthalocyanine IP = 7.36 eV (**1**), nickel phthalocyanine IP = 6.56eV (**2**), zinc phthalocyanine IP = 6.46 (**3**), pheophorbide *b* IP = unknown (**4**), *p*-aminotetraphenylporphyrin IP = unknown (**5**), naphthalocyanine IP = unknown (**6**), cobalt porphyrin IP = unknown (**7**), octabutoxyphtalocyanine IP = unknown (**8**), octabutoxynaphthalocyanine IP = unknown (**9**) and octaoctyloxyphtalocyanine IP = unknown (**10**), mixed in a matrix to analyte molar ratio of  $1 \times 10^3$ :1. Figure 19 highlights the LDI and MALDI spectra in positive ion mode for the ionization of the porphyrin mixture using DCTB (B), FI-CN (C) and FI-OCH<sub>3</sub> (D) as matrices, we decided to discard the FI-CH<sub>3</sub> matrix based on its figures of merit, being overcome by FI-CN and FI-OCH<sub>3</sub> performance. According to figure 19 and table 1, we observed in the LDI spectrum the signal of compound (**6**), interestingly, the UV absorption in naphthalocyanines exhibits a blue-shift, when compared with phthalocyanines and porphyrins, which normally absorbs at visible wavelengths. Moreover, some signals for compounds **9** and **10** are observed in small amounts, probably by a secondary analyte-analyte electron transfer reactions; the ionization energy of raw naphthalocyanine apparently overcome the value of phthalocyanines **9**

and **10**, which present strong donor groups like butoxy and octyloxy in their structures. Regarding MALDI experiments, with the use of DCTB we coverage the 70% of tested analytes, in which compounds **1**, **4** and **6** were not observed. In contrast, when FI-CN a were used, we coverage the 100% of tested analytes, being porphyrin **4** and **7** with phtalocyanines **8** and **10** the signals with higher ion abundances and S/N ratios. Apparently, the presence of strong donor substituents like alcoxy chains, affects the HOMO energy causing a decreasing on ionization energies for compounds **4**, **7**, **8** and **10**. It phenomena was plenty observed for porphyrin **4**, which contains the strong donor group  $-NH_2$  on phenyl *p*-position and probably the lowest ionization energy; the  $-NH_2$  act as donor group by delocalization of the lone pair of electrons. Taking a look onto the phtalocyanine and naphtalocyanine structure, these compounds have a common characteristic: the presence of imino like segments on the tetrapyrrole skeleton which act as an electron acceptor groups producing an increase on the ionization energy; raw phtalocyanine (**1**) exhibited an IP value of 7.36 eV. It means that structures like **2**, **3** and **6** which do not have donor substituents, apparently possess higher IP values when compared with the analogues **8**, **9** and **10**.

The mass accuracy in MALDI-MS depends on many factors; sample preparation, acquisition parameters, internal and external calibration and signal resolution. We have stablished the same protocol for sample preparation and have used the same instrumental parameters for spectrum acquisition leaving the mass accuracy depending directly on matrix performance. As seen in figure 18 we obtained a clean spectrum of the mixture when FI-CN and FI-OCH<sub>3</sub> were used, hence, the mass accuracy for all analytes were in the range of 3.0 to 17.5 ppm and 2.52 to 9.16, respectively. In contrast, the use of DCTB exhibited mass accuracy values in the range of 11.6 to 97.7 ppm.

The outstanding analytical performance exhibited by FI-CN and FI-OCH<sub>3</sub> over the DCTB, motivated us to test the matrices for the ionization of complex mixtures such vanadyl porphyrins extracted from Colombian crude oils. We previously reported the ionization of these mixtures using the  $\alpha$ -CNPV-CH<sub>3</sub> matrix, obtaining excellent results in terms of signal resolution, appearance of the spectrum and ion abundances. Figure S7 (see supporting info) shows the petroporphyrins spectra at 1.49  $\mu$ J per pulse of laser energy and matrix to analyte molar ratio 100:1 approx. With the use of FIs, we observed a clear molecular weight distribution in the range of  $m/z$  480 to 600 assigned to vanadyl porphyrins, previously demonstrated by APPI-FT-ICR experiments, (Giraldo-Dávila et al., 2018) contrarily to the DCTB matrix, which shows a complex spectrum with molecular distribution unlike the MWD for vanadyl porphyrins. Based on molecular formula assignments by FT-ICR, (Ramírez-Pradilla et al., n.d.) we extracted the signal associated with  $m/z$  501 (C<sub>29</sub>H<sub>30</sub>N<sub>4</sub>O<sub>V</sub>); insets in figure 6s, demonstrated that experimental isotope patterns obtained using the FIs are similar to theoretical isotope patterns, also, the signal resolution and ion abundance open a new window for future analysis using MALDI-FT-ICR.

**Table 1** Mass accuracy and signal-to-noise ratio for porphyrins and phthalocyanines

	<b>Molecular formula</b>	<b>Mass</b>	<b>Mass Accuracy (ppm)</b>			<b>S/N</b>			
			<b>DCTB</b>	<b>FL-CN</b>	<b>FL-OCH<sub>3</sub></b>	<b>LDI</b>	<b>DCTB</b>	<b>FL-CN</b>	<b>FL-OCH<sub>3</sub></b>
<b>1</b>	C <sub>32</sub> H <sub>18</sub> N <sub>8</sub>	514.165	-	9.7	-	-	-	39	-
<b>2</b>	C <sub>32</sub> H <sub>16</sub> N <sub>8</sub> Ni	570.085	71.9	17.5	3.5	-	25	62	112
<b>3</b>	C <sub>32</sub> H <sub>16</sub> N <sub>8</sub> Zn	576.078	88.5	17.5	5.2	-	20	347	491
<b>4</b>	C <sub>35</sub> H <sub>34</sub> N <sub>4</sub> O <sub>6</sub>	606.247	-	12.8	6.4	-	-	237	339
<b>5</b>	C <sub>44</sub> H <sub>31</sub> N <sub>5</sub>	629.257	79.4	7.9	6.35	-	455	2087	1104
<b>6</b>	C <sub>48</sub> H <sub>26</sub> N <sub>8</sub>	714.228	-	11.4	-	82	-	211	-
<b>7</b>	C <sub>48</sub> H <sub>36</sub> CoN <sub>4</sub> O <sub>4</sub>	791.206	94.7	6.3	2.52	-	734	2104	1901
<b>8</b>	C <sub>64</sub> H <sub>82</sub> N <sub>8</sub> O <sub>8</sub>	1090.625	22.9	11	9.16	17	1704	2226	1137
<b>9</b>	C <sub>80</sub> H <sub>90</sub> N <sub>8</sub> O <sub>8</sub>	1290.688	15.4	3.0	7.7	-	416	678	389
<b>10</b>	C <sub>96</sub> H <sub>146</sub> N <sub>8</sub> O <sub>8</sub>	1539.126	11.6	13.7	6.8	21	702	1147	938

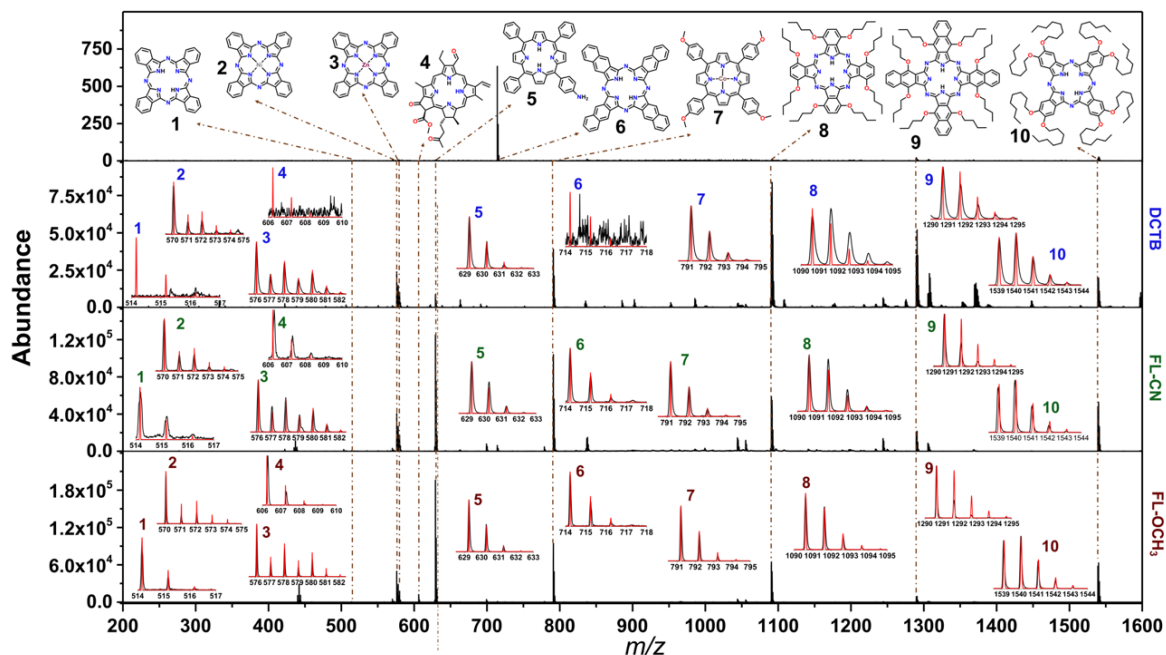


**Figure 19** LDI and MALDI spectra using the FI-CN and FI-CH<sub>3</sub> of a mixture of ten porphyrins at 1.24  $\mu$ J per pulse and 1000:1 matrix to analyte molar ratio.

### 3.5. Conclusions

We report a new set of ET matrices based on the fluorene core with well-defined physicochemical properties; good UV absorption in the solid phase, low exciton energy and ionization potentials above 8.0 eV. We demonstrated the high ability to yield primary ions after laser irradiance, one of the critical issues in MALDI-MS. The fluorene derivatives showed an outstanding performance for the ionization of porphyrin-like compounds reaching the LOD at femtomole level, also, exhibited high vacuum, chemical stability and low fragmentation, even, at high laser energies. The fluorene derivatives FI-CN and FI-OCH<sub>3</sub>, proved the excellent performance for the ionization of mixtures containing porphyrins and phtalocyanines with coverages of 100 and 90% when compared with 70% exhibited by DCTB.

## References

- Bera, R., Jana, B., Mondal, B., & Patra, A. (2017). Design of CdTeSe–Porphyrin–Graphene Composite for Photoinduced Electron Transfer and Photocurrent Generation. *ACS Sustainable Chemistry & Engineering*, 5(4), 3002–3010.
- Bonnett, R. (1995). Photosensitizers of the porphyrin and phthalocyanine series for photodynamic therapy. *Chem. Soc. Rev.*, 24(1), 19–33.
- Brimmer, P. J., & Griffiths, P. R. (1988). Angular Dependence of Diffuse Reflectance Infrared Spectra. Part III: Linearity of Kubelka-Munk Plots. *Appl. Spectrosc.*, 42(2), 242–247.
- Calvano, C. D., Ventura, G., Cataldi, T. R. I., & Palmisano, F. (2015). Improvement of chlorophyll identification in foodstuffs by MALDI ToF/ToF mass spectrometry using 1, 5-diaminonaphthalene electron transfer secondary reaction matrix. *Analytical and Bioanalytical Chemistry*, 407(21), 6369–6379.
- Calvano, C. D., Ventura, G., Trotta, M., Bianco, G., Cataldi, T. R. I., & Palmisano, F. (2017). Electron-Transfer Secondary Reaction Matrices for MALDI MS Analysis of Bacteriochlorophyll a in *Rhodobacter sphaeroides* and Its Zinc and Copper Analogue Pigments. *Journal of the American Society for Mass Spectrometry*, 28(1), 125–135.
- Davison, P. A., Schubert, H. L., Reid, J. D., Iorg, C. D., Heroux, A., Hill, C. P., & Hunter, C. N. (2005). Structural and Biochemical Characterization of Gun4 Suggests a Mechanism for Its Role in Chlorophyll Biosynthesis. *Biochemistry*, 44(21), 7603–7612.
- Dreisewerd, K. (2003). The Desorption Process in MALDI. *Chemical Reviews*, 103(2), 395–426.

- Economopoulos, S. P., & Tagmatarchis, N. (2015). Multichromophores Onto Graphene: Supramolecular Non-Covalent Approaches for Efficient Light Harvesting. *The Journal of Physical Chemistry C*, 119(15), 8046–8053.
- Feng, X. J., Peng, J., Xu, Z., Fang, R., Zhang, H., Xu, X., ... Wong, M. S. (2015). AIE-Active Fluorene Derivatives for Solution-Processable Nondoped Blue Organic Light-Emitting Devices (OLEDs). *ACS Applied Materials & Interfaces*, 7(51), 28156–28165.
- Giraldo-Dávila, D., Chacón-Patiño, M. L., Orrego-Ruiz, J. A., Blanco-Tirado, C., & Combariza, M. Y. (2016). Improving compositional space accessibility in (+) APPI FT-ICR mass spectrometric analysis of crude oils by extrography and column chromatography fractionation. *Fuel*, 185, 45–58.
- Giraldo-Dávila, D., Chacón-Patiño, M. L., Ramirez-Pradilla, J. S., Blanco-Tirado, C., & Combariza, M. Y. (2018). Selective ionization by electron-transfer MALDI-MS of vanadyl porphyrins from crude oils. *Fuel*, 226(March), 103–111.
- Gourier, D., Delpoux, O., Bonduelle, A., Binet, L., Ciofini, I., & Vezin, H. (2010). EPR, ENDOR, and HYSCORE Study of the Structure and the Stability of Vanadyl–Porphyrin Complexes Encapsulated in Silica: Potential Paramagnetic Biomarkers for the Origin of Life. *The Journal of Physical Chemistry B*, 114(10), 3714–3725.
- Hiroto, S., Miyake, Y., & Shinokubo, H. (2017). Synthesis and Functionalization of Porphyrins through Organometallic Methodologies. *Chemical Reviews*, 117(4), 2910–3043.
- Hitchcock, A., Jackson, P. J., Chidgey, J. W., Dickman, M. J., Hunter, C. N., & Canniffe, D. P. (2016). Biosynthesis of Chlorophyll a in a Purple Bacterial Phototroph and Assembly into a Plant Chlorophyll–Protein Complex. *ACS Synthetic Biology*, 5(9), 948–954.

- Hosseini, A., Hodgson, M. C., Tham, F. S., Reed, C. A., & Boyd, P. D. W. (2006). Tapes, Sheets, and Prisms. Identification of the Weak C–F Interactions that Steer Fullerene–Porphyrin Cocrystallization. *Crystal Growth & Design*, 6(2), 397–403.
- Jeong, H. K., Jin, M. H., So, K. P., Lim, S. C., & Lee, Y. H. (2009). Tailoring the characteristics of graphite oxides by different oxidation times. *Journal of Physics D: Applied Physics*, 42(6), 65418.
- Karas, M., & Hillenkamp, F. (1988). Laser desorption ionization of proteins with molecular masses exceeding 10,000 daltons. *Analytical Chemistry*, 60(20), 2299–2301.
- Knochenmuss, R. (2016). *The Coupled Chemical and Physical Dynamics Model of MALDI*. *Annual Review of Analytical Chemistry* (Vol. 9).
- Knochenmuss, Richard. (2006). Ion formation mechanisms in UV-MALDI. *Analyst*, 131(9), 966–986.
- Knochenmuss, Richard. (2009). A bipolar rate equation model of MALDI primary and secondary ionization processes, with application to positive/negative analyte ion ratios and suppression effects. *International Journal of Mass Spectrometry*, 285(3), 105–113.
- Knochenmuss, Stortelder, Breuker, & Zenobi. (2000). Secondary ion-molecule reactions in matrix-assisted laser desorption/ionization. *Journal of Mass Spectrometry: JMS*, 35(11), 1237–1245.
- Lian, S.-L., Liu, C.-L., & Chen, W.-C. (2011). Conjugated Fluorene Based Rod–Coil Block Copolymers and Their PCBM Composites for Resistive Memory Switching Devices. *ACS Applied Materials & Interfaces*, 3(11), 4504–4511.

- Liu, Z., Li, W., Topa, S., Xu, X., Zeng, X., Zhao, Z., ... He, H. (2014). Fine Tuning of Fluorene-Based Dye Structures for High-Efficiency p-Type Dye-Sensitized Solar Cells. *ACS Applied Materials & Interfaces*, 6(13), 10614–10622.
- Liu, Z., Xiong, D., Xu, X., Arooj, Q., Wang, H., Yin, L., ... He, H. (2014). Modulated Charge Injection in p-Type Dye-Sensitized Solar Cells Using Fluorene-Based Light Absorbers. *ACS Applied Materials & Interfaces*, 6(5), 3448–3454.
- Lovell, J. F., Chen, J., Jarvi, M. T., Cao, W.-G., Allen, A. D., Liu, Y., ... Zheng, G. (2009). FRET Quenching of Photosensitizer Singlet Oxygen Generation. *The Journal of Physical Chemistry B*, 113(10), 3203–3211.
- Marydasan, B., Nair, A. K., & Ramaiah, D. (2013). Optimization of Triplet Excited State and Singlet Oxygen Quantum Yields of Picolylamine–Porphyrin Conjugates through Zinc Insertion. *The Journal of Physical Chemistry B*, 117(43), 13515–13522.
- Mathew, S., Yella, A., Gao, P., Humphry-Baker, R., Curchod, B. F. E., Ashari-Astani, N., ... Grätzel, M. (2014). Dye-sensitized solar cells with 13% efficiency achieved through the molecular engineering of porphyrin sensitizers. *Nature Chemistry*, 6(3), 242–247.
- McCarley, T. D., McCarley, R. L., & Limbach, P. A. (1998). Electron-transfer ionization in matrix-assisted laser desorption/ionization mass spectrometry. *Analytical Chemistry*, 70(20), 4376–4379.
- Morikawa, T., Asahi, R., Ohwaki, T., Aoki, K., & Taga, Y. (2001). Band-Gap Narrowing of Titanium Dioxide by Nitrogen Doping. *Japanese Journal of Applied Physics*, 40(6A), L561.
- Moscatelli, A. (2015). Supramolecular chemistry: Porphyrins on the move. *Nature*

*Nanotechnology*. Retrieved from <http://dx.doi.org/10.1038/nano.2015.82>

Müller, T., Vergeiner, S., & Kräutler, B. (2014). Structure elucidation of chlorophyll catabolites (phyllobilins) by ESI-mass spectrometry—Pseudo-molecular ions and fragmentation analysis of a nonfluorescent chlorophyll catabolite (NCC). *International Journal of Mass Spectrometry*, 365–366, 48–55.

Murphy, B. E., Krasnikov, S. A., Sergeeva, N. N., Cafolla, A. A., Preobrajenski, A. B., Chaika, A. N., ... Shvets, I. V. (2014). Homolytic Cleavage of Molecular Oxygen by Manganese Porphyrins Supported on Ag(111). *ACS Nano*, 8(5), 5190–5198.

Nayak, A., Roy, S., Sherman, B. D., Alibabaei, L., Lapides, A. M., Brennaman, M. K., ... Meyer, T. J. (2016). Phosphonate-Derivatized Porphyrins for Photoelectrochemical Applications. *ACS Applied Materials & Interfaces*, 8(6), 3853–3860.

Nazim Boutaghou, M., & Cole, R. B. (2012). 9, 10-Diphenylanthracene as a matrix for MALDI-MS electron transfer secondary reactions. *Journal of Mass Spectrometry*, 47(8), 995–1003.

Nishide, H., Tsukahara, Y., & Tsuchida, E. (1998). Highly Selective Oxygen Permeation through a Poly(vinylidene dichloride)–Cobalt Porphyrin Membrane: Hopping Transport of Oxygen via the Fixed Cobalt Porphyrin Carrier. *The Journal of Physical Chemistry B*, 102(44), 8766–8770.

Peterson, J. J., Davis, A. R., Werre, M., Coughlin, E. B., & Carter, K. R. (2011). Carborane-Containing Poly(fluorene): Response to Solvent Vapors and Amines. *ACS Applied Materials & Interfaces*, 3(6), 1796–1799.

Putman, J. C., Rowland, S. M., Corilo, Y. E., & McKenna, A. M. (2014). Chromatographic

enrichment and subsequent separation of nickel and vanadyl porphyrins from natural seeps and molecular characterization by positive electrospray ionization FT-ICR mass spectrometry. *Analytical Chemistry*, 86(21), 10708–10715.

Ramírez-Pradilla, J. S., Blanco-Tirado, C., Hubert-Roux, M., Giusti, P., Afonso, C., & Combariza, M. Y. (n.d.). Comprehensive Petroporphyrin Identification in Crude Oils Using Highly Selective Electron Transfer Reactions in MALDI-FTICR MS. *Energy & Fuels*, 0(ja), null.

Schoefs, B. (2002). Chlorophyll and carotenoid analysis in food products. Properties of the pigments and methods of analysis. *Trends in Food Science & Technology*, 13(11), 361–371. [https://doi.org/https://doi.org/10.1016/S0924-2244\(02\)00182-6](https://doi.org/https://doi.org/10.1016/S0924-2244(02)00182-6)

Shen, X., He, F., Wu, J., Xu, G. Q., Yao, S. Q., & Xu, Q.-H. (2011). Enhanced Two-Photon Singlet Oxygen Generation by Photosensitizer-Doped Conjugated Polymer Nanoparticles. *Langmuir*, 27(5), 1739–1744.

Stergiou, A., & Tagmatarchis, N. (2016). Fluorene–Perylene Diimide Arrays onto Graphene Sheets for Photocatalysis. *ACS Applied Materials & Interfaces*, 8(33), 21576–21584.

Sui, B., Kim, B., Zhang, Y., Frazer, A., & Belfield, K. D. (2013). Highly Selective Fluorescence Turn-On Sensor for Fluoride Detection. *ACS Applied Materials & Interfaces*, 5(8), 2920–2923.

Tang, C., Liu, F., Xia, Y.-J., Lin, J., Xie, L.-H., Zhong, G.-Y., ... Huang, W. (2006). Fluorene-substituted pyrenes—Novel pyrene derivatives as emitters in nondoped blue OLEDs. *Organic Electronics*, 7(3), 155–162.

Vasil'ev, Y. V, Khvostenko, O. G., Streletskii, A. V, Boltalina, O. V, Kotsiris, S. G., & Drewello,

- T. (2006). Electron transfer reactivity in matrix-assisted laser desorption/ionization (MALDI): ionization energy, electron affinity and performance of the DCTB matrix within the thermochemical framework. *The Journal of Physical Chemistry A*, 110(18), 5967–5972.
- Yue, X., Armijo, Z., King, K., Bondar, M. V, Morales, A. R., Frazer, A., ... Belfield, K. D. (2015). Steady-State and Femtosecond Transient Absorption Spectroscopy of New Two-Photon Absorbing Fluorene-Containing Quinolizinium Cation Membrane Probes. *ACS Applied Materials & Interfaces*, 7(4), 2833–2846.

#### 4. Electron Transfer in MALDI-FTICR-MS: a non-chromatographic approach for the targeted analysis of Nickel and Vanadyl Porphyrins in complex mixtures

##### 4.1. Abstract

The electron transfer (ET) ionization in matrix-assisted laser desorption ionization MALDI-MS, is a powerful technique scarcely explored nowadays which consist in the electron transfer from an analyte with a low ionization potential (IP) to a preformed radical cation of the MALDI matrix. With the use of ET ionization, we report here a novel methodology for the targeted analysis of nickel and vanadium porphyrins in complex mixtures without purification steps or chromatographic sample enrichment. The ET-MALDI-FTICR MS experiment of a simple liquid-liquid (L-L) acetonitrile fraction directly extracted from a middle-eastern crude-oil and using our newly reported matrix ( $\alpha$ -CNPV-CH<sub>3</sub>), revealed a selective ionization of the nickel and vanadyl porphyrins, contrarily to currently used ion sources in petroleomics APPI, and LDI. A discriminatory data refinement by Kendrick mass defect in function of the ion abundance enabled the direct identification of the homologous series; DBE 17-26 for vanadyl porphyrins, and DBE 17-23 for nickel porphyrins. The remarkable resolving power of  $m/m_{50\%}$  1 000 000 at  $m/z$  500 and mass accuracy under 50 ppb, provided a detailed molecular formula assignment within the isotopologues determination (<sup>13</sup>C, <sup>15</sup>N, <sup>51</sup>V, <sup>58</sup>Ni, <sup>60</sup>Ni). This straightforward methodology allows the direct identification of more than 350 petroporphyrins in crude-oils (N<sub>4</sub>VO, N<sub>4</sub>VO<sub>2</sub>, N<sub>4</sub>VO<sub>3</sub>, N<sub>4</sub>VOS, and N<sub>4</sub>Ni) without chromatographic sample enrichment and represents the first rational electron transfer experiments in MALDI-FTICR applied for petroleomics.

## 4.2. Introduction

The analysis of crude-oils and its components represent one of the most challenging tasks in mass spectrometry due to the inherent complexity of the sample. In petroleomics, the high-resolution mass spectrometry (HRMS) has become progressively the most powerful technique to assess the compositional space and molecular-level characterization of crude-oils components.(Rodgers & McKenna, 2011)(Fernandez-Lima et al., 2009)(Hughey, Rodgers, & Marshall, 2002)(K. Qian, Rodgers, Hendrickson, Emmett, & Marshall, 2001) The use of Fourier Transform Ion Cyclotron Resonance Mass Spectrometry (FTICR-MS), provides the sufficient resolving power and mass accuracy to differentiate ion peaks from isobaric interferences and isotopic contributions, augmenting the knowledge about the molecular composition of asphaltenes,(Chacón-Patiño, Rowland, & Rodgers, 2017)(Chacón-Patiño et al., 2016) interfacial material,(Jarvis, Robbins, Corilo, & Rodgers, 2015)(Clingenpeel, Robbins, Corilo, & Rodgers, 2015) naphthenic acids,(Valencia-Dávila, Witt, Blanco-Tirado, & Combariza, 2018)(Colati et al., 2013) and petroporphyrins.(Giraldo-Dávila, Chacón-Patiño, Orrego-Ruiz, Blanco-Tirado, & Combariza, 2016)(Mckenna, Purcell, Rodgers, & Marshall, 2009)(Zhao et al., 2013)(Liu et al., 2015)

In crude-oils, petroporphyrins (PPs) represent a small group of compounds responsible of nickel (Ni) and vanadium (V) bounding, derived from chlorophylls, bacteriochlorophyll or heme group depending upon its origin.(Treibs, n.d.)(Barwise, 1990)(Baker, William Louda, & Orr, 1987) The main characteristic of PPs lies in maintaining the tetrapyrrole core despite the maturation process yielding a well-classified and low-polydispersed homologous series; etio porphyrins (DBE = **17** / Etio), deoxophylloerythroetioporphyrins (DBE = **18** / DPEP), dicyclic-deoxophylloerythroetio

porphyrins (DBE = **19** / Di-DPEP), Rhodo-etio porphyrins (DBE = **20** / Rhodo-Etio), Rhodo-deoxophylloerythroetioporphyrins (DBE = **21** / Rhodo-DPEP), and Rhododicyclicdeoxophylloerythroetio (DBE = **22** / Rhodo-Di-DPEP).(Zhao, Shi, Gray, & Xu, 2014) Naturally occurring Ni and VO porphyrins are in a concentration less than 1% and their characterization normally involves extensive chromatographic techniques.(Vorapalawut et al., 2012)(Kuangnan Qian, Edwards, Mennito, Walters, & Kushnerick, 2010)

Rodgers et al,(Rodgers et al., 2001) introducing by the first time in 2001 the analysis of oxovanadium (IV) porphyrins by ESI-(+)-FTICR from a chromatographed crude-oil, detecting 30 VOPPs from DBE 17 to 21 as [VOPP+H]<sup>+</sup> ions. In 2008 Qian et al,(Kuangnan Qian, Mennito, Edwards, & Ferrughelli, n.d.) observed sulfur-containing and high DBE ring-fused vanadyl porphyrins using APPI-(+)-FTICR from raw asphaltenes, interestingly, the presence of these high DBE species suggest that the structure of porphyrins added condensed phenyl and naphthalene rings during the catagenesis/diagenesis. Lately, an extensive porphyrin characterization by cyclograph sample enrichment followed by APPI-(+)-FTICR experiments addressed the identification of nickel porphyrins with the same structural growing than vanadyl porphyrins.(Kuangnan Qian et al., 2010) In crude-oils nickel is present in a concentration rate of 1:3 Ni:V,(Vorapalawut et al., 2012) being necessary an extensive sample enrichment using several strategies like chromatography,(Zhao et al., 2013) cyclograph,(Kuangnan Qian et al., 2010) or solid-phase extraction (SPE) with specific amino-coated stationary phase.(Putman, Rowland, Corilo, & McKenna, 2014) These methodologies which yield enriched fractions and efficiently separates the nickel, vanadyl, sulfur vanadyl and acidic porphyrins represent an exhaustive and time-consuming procedures. Consequently, the comprehensive identification of nickel and vanadyl porphyrins from raw complex mixtures without sample enrichment is still a challenge.

Recently, the simultaneous identification of Ni/VO porphyrins from natural seeps was reported using APPI-(+) and ultrahigh resolution mass spectrometry,(McKenna et al., 2014) nevertheless, the ionization efficiencies of these species - which are common in low concentration - are critically affected by the inherent complexity of the mixture, aggregation, the occlusion on asphaltenes, and the presence of other ionizable species in higher concentrations.(McKenna et al., 2014) Interestingly, the ionization efficiency of vanadyl porphyrins has been proved to be three times more by using APPI-(+) than nickel analogues, in addition with its low concentration when compared with vanadium (1:3 Ni:V as mentioned above).(Kuangnan Qian et al., 2010) Consequently, the use of an additional non-discriminatory ionization strategy that increases the ionization efficiencies and sensitivity for low occurring porphyrins, is desired.

In MALDI-MS, the electron transfer (ET) ionization which consists in a gas-phase charge transfer between primary ions of a matrix (commonly a photoactive material) and neutral analytes, is a promising approach for the direct analysis of porphyrins occurring in complex mixtures. In a recent contribution, we observed a high selectivity for the ionization of vanadyl porphyrins from enriched fractions using MALDI-TOF,(Giraldo-Dávila, Chacón-Patiño, Ramirez-Pradilla, Blanco-Tirado, & Combariza, 2018) and nickel/vanadyl porphyrins using the ET ionization in a (MALDI-FTICR) instrument.(Ramírez-Pradilla, Blanco-Tirado, Hubert-Roux, et al., n.d.) The high selectivity observed in electron transfer was attributed to the thermodynamics of the gas-phase; accordingly to McCarley et al,(McCarley, McCarley, & Limbach, 1998) these electron transfer reactions were favored because the matrix's ionization potential was almost 1.5 eV larger than analyte's value which is in the order of ~6.5-7.0 eV.

In figure 1, several model analytes corresponding to thiophene (S<sub>1</sub>-Class), carbazole (N<sub>1</sub>-Class), quinoline (N<sub>1</sub>-Class), benzopyrene (CH-Class), tetralin (CH-Class), phenol (O<sub>1</sub>-Class) and Nickel and Vanadium porphyrins (N<sub>4</sub>Ni and N<sub>4</sub>V) - commonly occurring in crude-oils fractions - exhibit theoretical and experimental ionization energies starting from 6.5 eV and going up to 10 eV.(Scudiero, Barlow, Mazur, & Hipps, 2001)(Ogunrinde, Hipps, & Scudiero, 2006) Interestingly, the lowest ionization potential of the series correspond to Ni/VO porphyrins; the high aromaticity caused by electron current over the peripheral tetrapyrrole core promotes a decreasing on IPs by affecting the HOMO energy.(Ramírez-Pradilla, Blanco-Tirado, & Combariza, n.d.) Our recently introduced  $\alpha$ -CNPV-CH<sub>3</sub> matrix,(Giraldo-Dávila et al., 2018)(Ramírez-Pradilla, Blanco-Tirado, Hubert-Roux, et al., n.d.)(Ramírez-Pradilla, Blanco-Tirado, & Combariza, n.d.) has an ionization potential of 8.42 eV (measured by ultraviolet photoelectron spectroscopy, UPS), in consequence, the use of  $\alpha$ -CNPV-CH<sub>3</sub> favors the ionization of Ni/VO porphyrins by a  $\Delta$ IP in the range of the 1.5-2.0 eV, while compounds with saturated rings, polar species and less conjugated of the CH, N<sub>1</sub> and S<sub>1</sub> class are less favored (See figure S1, supporting info).

In this contribution, we introduced the electron transfer ionization in MALDI-FTICR-MS for the direct analysis of Nickel and Vanadyl porphyrins in crude-oils. For the best of our knowledge, this approach represents the first rationally designed MALDI experiments applied for petroleomics and allows the simultaneous detection of NiPPs and VOPPs without chromatographic sample enrichment.

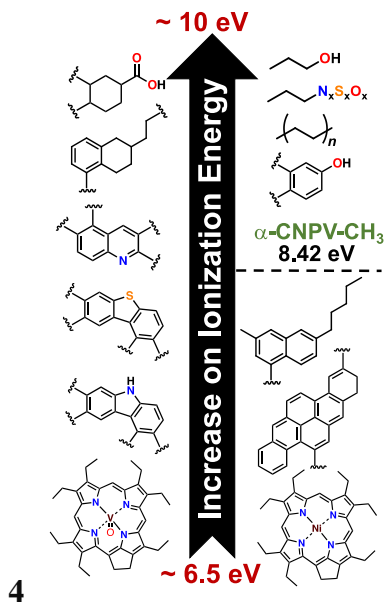


**Figure 20** Ionization potential values for N<sub>1</sub>, S<sub>1</sub>, O<sub>1</sub>, N<sub>4</sub>VO, N<sub>4</sub>Ni core extracted from NIST.

Inset at 8.42 eV corresponds to  $\alpha$ -CNPV-CH<sub>3</sub>'s ionization potential.

### 4.3. Experimental section

**4.3.1. Materials.** The  $\alpha$ -cyanophenylenevinylene matrix ( $\alpha$ -CNPV-CH<sub>3</sub>) was synthesized following our previously reported procedure, (Giraldo-Dávila et al., 2016) PAH mixture, Nickel octaethylporphyrin and Vanadyl octaethylporphyrin were purchased from Sigma-Aldrich. Analytical grade (99.5%) acetonitrile (ACN), tetrahydrofuran (THF) and Toluene (Tol), were purchased from Merck Millipore (Darmstadt, Germany).

**4.3.2. Sample preparation.** For extraction process (Scheme 1), 1 mL of a middle east crude-oil was placed in a glass flask, then, 1.5 mL of acetonitrile (ACN) was added and the resulting two-layer mixture was stirred using a Vortex apparatus during 5 minutes and sonicated during 1 minute. The upper ACN layer was carefully separated. This procedure was repeated six times, then, E1-E6 were monitored by MALDI-TOF with the  $\alpha$ -CNPV-CH<sub>3</sub> matrix (See supporting

information, figure SX), the last extract **E<sub>6</sub>** exhibited the highest ion abundance on porphyrin region ( $m/z$  450 – 600) and was chosen for further analysis. For LDI experiments, 5  $\mu\text{L}$  of **E<sub>6</sub>** were placed on a MALDI polished steel target by dried droplet method. Samples for MALDI were prepared mixing a 5 mM matrix's solution with an equivolume of **E<sub>6</sub>**, then, 1  $\mu\text{L}$  of the resulting solution was seeded on the MALDI polished steel target. For APPI experiments, **E<sub>6</sub>** extract was dried and diluted in 1 mL of toluene as solvent.

**4.3.3. Mass spectrometry.** APPI, LDI and ET-MALDI-HRMS experiments were performed in a Bruker Solarix XR 12T (Paracell<sup>TM</sup>) instrument operated in positive ion mode and equipped with a tripled Nd:YAG solid state laser (355 nm). 200 scans were accumulated for LDI, APPI and ET-MALDI experiments in 8M size, using a selective accumulation parameter ( $8.0 \times 10^8$  -  $9.0 \times 10^8$ ) for data collecting. LDI and MALDI experiments were obtained using 28% and 18% of laser power, respectively. Ions were conducted to the ICR cell using a sweep energy of 38.5% and 0.800 ms time of flight, 0.05 seconds of acquisition time with an average transient of 4.42 seconds. The external calibration was performed using a mixture of PAHs and standard Ni and VO porphyrins (Figure S3, supporting information).

**4.3.4. Data processing.** Raw spectra obtained after APPI and LDI/MALDI-FTICR experiments were internally calibrated following a  $\text{CH}^{\text{R}}$  class series with an average RMS of 50 ppb. Resolving power of  $m/\Delta m_{50\%}$  700 000 – 1 000 000 at  $m/z$  500 was observed for MALDI and APPI experiments, in contrast with LDI which exhibited values between 400 000 and 600 000. After peak peaking, raw data output was filtered by relative abundance in order to perform the discriminatory Kendrick Mass Defect plots. Molecular formula assignments for NiPPs and VOPPs after Kendrick refinement were performed using the SmartFormula tool in DataAnalysis (Bruker

Daltonics, Bremen, Germany) with an error window of 0.3 ppm. DBE vs carbon number diagrams and mass spectra data were plotted using OriginPro Software (North Hampton, MA).

#### 4.4. Results and Discussion

**4.4.1. ET-MALDI, LDI, and APPI analysis.** The sixth extract (**E<sub>6</sub>**) after the subsequent liquid-liquid extraction directly from a middle-eastern crude-oil using ACN as a solvent, was subjected to APPI, LDI and ET-MALDI FTICR-MS experiments. As seen in figure 20, the broadband spectra obtained by APPI-FTICR consisted of more than 12 000 assigned formulas corresponding to radical cations; since protonated ions can be generated by APPI, all the contribution of  $[M+H]^+$  were discarded. (Raffaelli & Saba, n.d.) (Purcell, Hendrickson, Rodgers, & Marshall, 2006) In LDI-FTICR, the formation of  $[M]^{+\bullet}$  and  $[M+H]^+$  species is a process which follows the primary ion formation mechanism proposed by R. Knochenmuss (Coupled Physical and Chemical Dynamics, CPCD). (R. Knochenmuss, 2016) By LDI, the compounds which effectively absorb the photon from Nd:YAG laser can be ionized, in fact, the number of signals corresponding to  $[M]^{+\bullet}$  were reduced to  $\sim 9\,000$ , figure 20. In electron transfer ionization, the mechanism follows the CPCD model and all the analytes with an ionization potential 0.5 eV below the matrix's IP can be ionized, consequently, the signals in the spectrum corresponding to the **E<sub>6</sub>** fraction were significantly reduced to about 40% ( $\sim 3500$ ) of the signals corresponding to radical cations  $[M]^{+\bullet}$  observed by APPI. (Figure 20).

The main differences between APPI, LDI, and ET-MALDI are the gas-phase energetics during the ionization process. In APPI, the use of toluene as dopant set a capped energy of 8.86 eV and components within the sample with lower ionization potential can be ionized, (Purcell et al., 2006) this strategy has extensively applied to restrict the number of ionized species and drive a partial

selective ionization, however, we still observed a broadband spectrum with a contribution of more than 10k signals in  $E_6$  (Figure 20). In LDI, the photons from the Nd:YAG laser (355 nm) with an energy of 3.5 eV are irradiated on sample and molecules absorbing the UV radiation can be ionized.(Richard Knochenmuss, 2004) However, the LDI addressed a partial selective ionization with an important reduction from 12k to 7.5k signals corresponding to the radical cation  $[M]^{+\bullet}$ ; in previous reports, molecules like asphaltenes and aromatics demonstrated high ionization efficiencies using LDI as ion source.(Cho et al., 2014)(Witt, Godejohann, Oltmanns, Moir, & Rogel, 2017)

As LDI, in ET-MALDI the sample is irradiated with photons from the Nd:YAG laser (3.5 eV), however, the ionization step is mediated by the use of the matrix, in our particular case, our previously reported  $\alpha$ -CNPV-CH<sub>3</sub> with an IP of 8.42 eV).(Giraldo-Dávila et al., 2018)(Ramírez-Pradilla, Blanco-Tirado, Hubert-Roux, et al., n.d.)(Ramírez-Pradilla, Blanco-Tirado, & Combariza, n.d.) We previously demonstrated that secondary ion-molecule electron transfer reactions during the evolution of MALDI plume are restricted to the thermodynamics in the gas-phase; a  $\Delta IP > 0.5$  eV ensures the efficient ionization of neutral analytes by charge transfer with primary ions of the matrix.(McCarley et al., 1998)(Knochenmuss, Stortelder, Breuker, & Zenobi, 2000) As discussed above, in figure 1, the ionization potential values corresponding to naturally occurring compounds of the CH, heteroatomic aromatic classes and saturates, span from 7 to 10 eV, while IP values of highly conjugated nickel and vanadyl porphyrins exhibit the lowest value.(Ogunrinde et al., 2006)(Scudiero et al., 2001)(Scudiero, Barlow, & Hippius, 2002) As we expected, the electron transfer reactions between  $\alpha$ -CNPV-CH<sub>3</sub> and nickel/vanadyl porphyrins were highly favored and the typical molecular weight distributions corresponding to NiPPs and

VOPPs exhibited an important increasing on total ion abundance with a high selectivity when compared with APPI and LDI, Figure 2.(Giraldo-Dávila et al., 2018)

Interestingly, during the ET-MALDI-FTICR-(+) experiments not only the NiPPs and VOPPs were ionized, but also, a molecular weight distribution centered to  $m/z$  350 was observed. In general, the ionization potential of organic compounds is directly related with the HOMO energy,(Blase, Attacalite, & Olevano, 2011)(Djurovich, Mayo, Forrest, & Thompson, 2009) and closely linked with the electronic structure and  $\pi$ -electron cloud, meaning that organic molecules with condensed aromatic rings and heterocyclic compounds with  $\pi$ -excedent electrons such as pyrrole or thiophene can be ionized by electron transfer in MALDI.

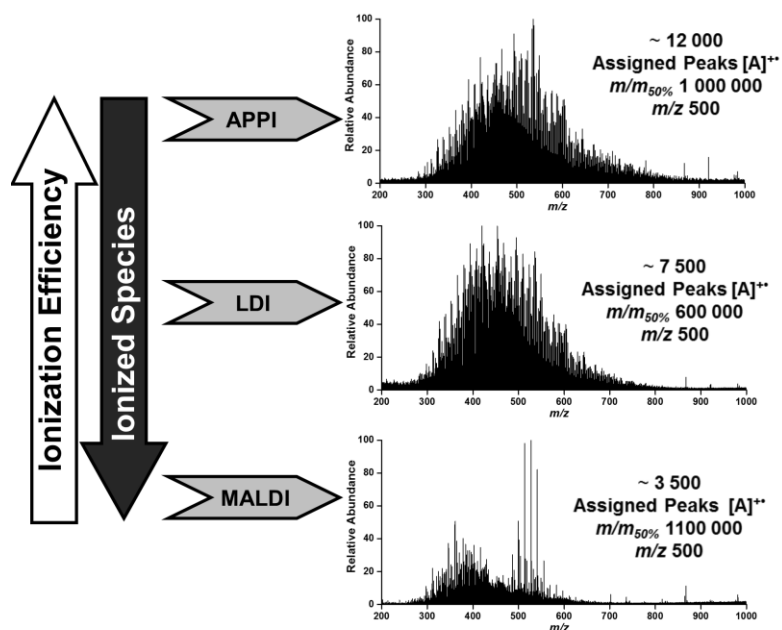


**Figure 21** Extract E6 APPI, LDI and ET-MALDI spectra in positive ion mode.

In a recent paper, we observed in a mixture of 20 analytes including PAH, nitrogen-containing aromatics and porphyrins analyzed by MALDI-TOF, larger differences on the ionization efficiencies; the S/N ratios for porphyrins (IP 6.5-7.0 eV) were several times larger than PAH (IP

~ 7.0-7.5 eV) and nitrogen-containing aromatics (IP 6.5-7.5 eV). Consequently, the heteroatom class distribution for extract **E<sub>6</sub>** using APPI, LDI and ET-MALDI, Figure 21, shows that compounds of the CH, N<sub>1</sub>, N<sub>2</sub>, S<sub>1</sub>, S<sub>2</sub> and N<sub>1</sub>S<sub>1</sub>, associated with aromatic-like structures were ionized when ET-MALDI was used, in contrast, APPI promotes the ionization of polar compounds (N<sub>x</sub>O<sub>y</sub>S<sub>z</sub> class) with high heteroatom content; these compounds exhibit the highest ionization energies. (Jaramillo, Domingo, Chamorro, & Pérez, 2008)

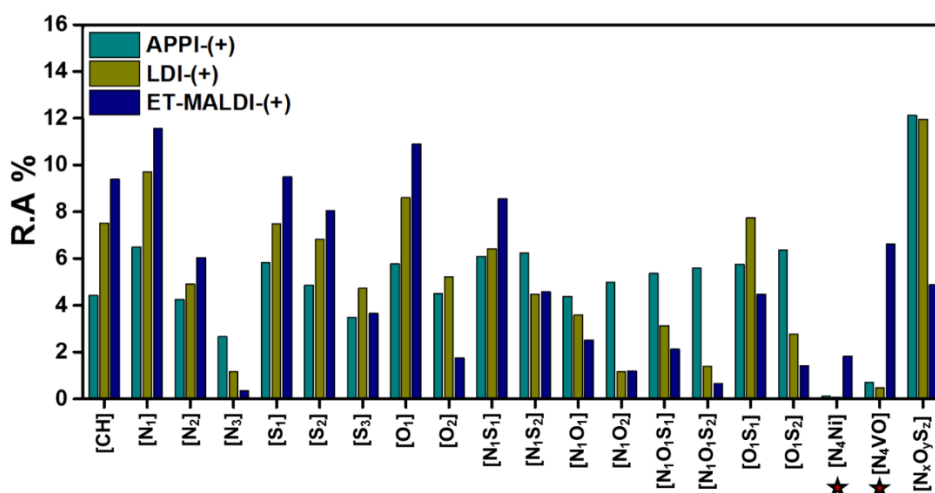


**Figure 22** Heteroatom class distribution in E6 for APPI-(+), LDI-(+) and ET-MALDI-(+).

In figure 22, the double bond equivalent (DBE) vs carbon number plots for the most abundant species (CH, N<sub>1</sub>, S<sub>1</sub>, O<sub>1</sub>, S<sub>2</sub> and N<sub>1</sub>S<sub>1</sub>) explain better the gas-phase energetics for APPI, LDI and ET-MALDI. As observed in Figure 21, the ET-MALDI favored the ionization of most aromatic species; an enriched  $\pi$ -cloud causes a decreasing on ionization energies, in fact, molecules with high grade of unsaturation were efficiently ionized and a shape close to the planar limit was observed for all classes. As a trend, LDI revealed several signals corresponding to high aromatic species, however, without the use of a matrix, the ionization step relies on the efficient photon

absorption, even with the presence of peripheral alkyl chains. This observation proves that species with high DBE and carbon number exhibited the highest relative abundance. Since the ionization step in APPI is controlled by the presence of toluene as a dopant, reactive species are generated and polar molecules with a low grade of unsaturation can be ionized. Hence, DBE plots for APPI revealed a major contribution of high carbon number and low DBE species when compared with LDI and ET-MALDI.

Avoiding the ionization of polar and saturated species while favoring the ionization of aromatic compounds including nickel and vanadyl porphyrins in ET-MALDI, causes an unprecedented increasing on the analytical descriptors such as signal-to-noise ratio and ion abundance corresponding to such signals. In figure S4 (supporting material), an expanded-scale view at  $m/z$  513, revealed that S/N ratios corresponding to the vanadyl porphyrin  $[C_{30}H_{30}N_4OV]^+$  were positively affected when compared with S/N for the same signal using APPI and LDI. Clearly, figure S3 is closely related with the ionization efficiency, being several times larger for vanadyl porphyrins using ET-MALDI in contrast of APPI or LDI, discarding as a result, almost the 50% of assigned classes per nominal mass.

**4.4.2. Nickel and Vanadyl porphyrin molecular formula assignments.** As mentioned previously, the larger differences on ionization efficiencies revealed by APPI, LDI, and ET-MALDI, enabled a discriminatory data refinement by Kendrick mass defect [KMD]. In Figure S5 (supporting material), all families classified in function of nominal mass showed a complex data output, however, when we plotted [KMD] vs nominal mass as a function of the relative ion abundance in a color-map form, all the families corresponding to Nickel and Vanadyl porphyrins

were easily identified, additionally, all signals below 5% of relative ion abundance were settled as grey/white scale to show up the signals of interest.

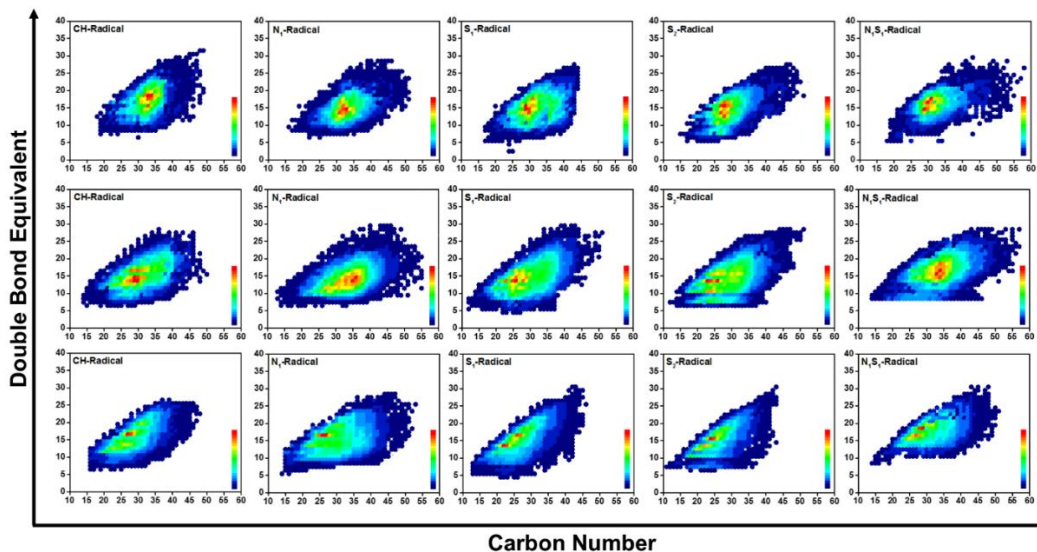


**Figure 23** DBE vs Carbon Number plots for most abundant species in extract E6, using APPI, LDI and ET-MALDI.

Once the signals corresponding to nickel/vanadyl porphyrins were extracted, the analysis of isotopologues for relevant signals was performed in order to corroborate our findings. In direct analysis from raw samples without sample enrichment, the molecular formula assignments relies in instrument resolving power, as previously discussed by McKenna and co-workers, (McKenna et al., 2014) in which almost  $m/\Delta m_{50\%} > 1\,000\,000$  is needed to separate porphyrins signals from isobaric interferences, fortunately, the ET-MALDI spectrum revealed enough resolving power and significantly decreased the isobaric interferences. In figure 23, the expanded scale ET-MALDI spectrum at  $m/z$  513-518 for E6, revealed the peak at  $m/z$  513 corresponding to the DBE 17 vanadyl porphyrin  $[C_{30}H_{30}N_4VO]^{+}$  with a mass accuracy of 4 ppb and  $m/\Delta m_{50\%}$  980 000, in addition,  $^{13}C$

isotopologue  $[^{13}\text{C}_1\text{C}_{29}\text{H}_{30}\text{N}_4\text{VO}]^{++}$  was differentiated from the contribution of the protonated ion  $[\text{C}_{30}\text{H}_{30}\text{N}_4\text{VO}+\text{H}]^+$ . Advantageously, the significant increasing on ion abundances using ET-MALDI, allowed the detection of the  $^{15}\text{N}$  isotopologue  $[\text{C}_{39}\text{H}_{30}\text{N}_3\text{VO}^{15}\text{N}_1]^{++}$  with a 74 ppb of mass accuracy.

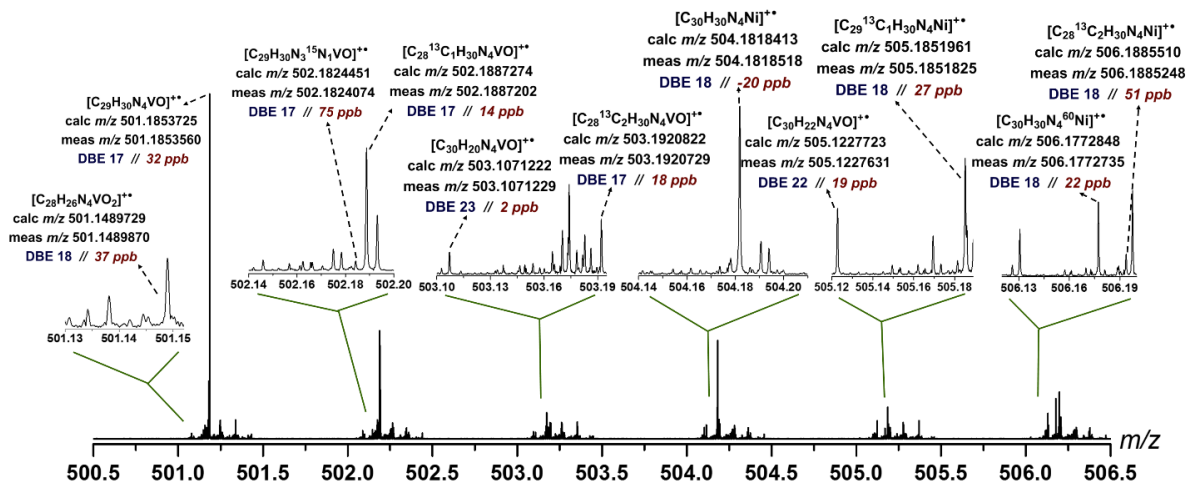


**Figure 24** Mass scale expanded-scale spectrum ( $m/z$  513 – 518) of extract E6 using ET-MALDI- (+). Insets show the isotopic fine structure determination,  $^{13}\text{C}$ ,  $^{15}\text{N}$  and  $^{60}\text{Ni}$  contribution corroborate the molecular formula assignments.

At  $m/z$  504 and 506, the peaks corresponding to monoisotopic DBE 18 nickel porphyrin  $[\text{C}_{31}\text{H}_{30}\text{N}_4^{58}\text{Ni}]^{++}$  and  $^{60}\text{Ni}$  isotopologue  $[\text{C}_{31}\text{H}_{30}\text{N}_4^{60}\text{Ni}]^{++}$  with -21 and 22 ppb of mass accuracy validated the molecular formula assignments for nickel porphyrins. Starting from correct isotopic determinations, all porphyrin families were classified by DBE and Kendrick mass defect, showing the relative ion abundance and mass accuracy, table S1 (Supporting Information).

**4.4.3. Porphyrin Diversity.** In figure 24 (TOP), double bond equivalent (DBE) vs carbon number plots, highlight all the porphyrin classes found in extract **E<sub>6</sub>** after ET-MALDI experiments. Without chromatographic sample enrichment, more than 150 vanadyl porphyrins were detected with an average error of 31 ppb, furthermore, about 100 nickel porphyrins including high DBE 22 and 23 classes were observed with a RMS of 102 ppb within isotopic fine structure determinations. Historically, vanadyl porphyrins with two or three oxygen atoms  $N_4VO_2$  or acidic porphyrins  $N_4VO_3$  have been detected after chromatography enrichment and co-elution with mobile phase containing formic acid.(Putman et al., 2014) Without chromatography sample enrichment, oxygen-containing porphyrins are also diluted in the ACN **E<sub>6</sub>** extract and can be ionized by the  $\alpha$ -CNPV-CH<sub>3</sub> in ET-MALDI. The homologous series for  $N_4VO_2$  and  $N_4VO_3$  families were detected with RMS of 50 and 51 ppb, respectively, (Supporting info table S1). Molecular insights about porphyrins have been reported based on MS/MS experiments and theoretical calculations, suggesting that structure growing specially for high DBE structures, attach phenyl or naphthyl rings on peripheral porphyrin core. Regarding sulfur vanadyl porphyrins, introducing a benzothiophene group explain the fact that VOS porphyrins starts at DBE 22 to 26 with a dibenzothiophene-like structure. Regarding oxygenated porphyrins  $VO_2$  and  $VO_3$ , several reports suggested the presence of ketone groups and free carboxylic acid groups, commonly based on more abundant Etio and DPEP structures. In a recent contribution, we discovered a new series of  $N_4VO_2$  and  $N_4VO_3$  species which exhibited low polarities by HPTLC separation and ET-MALDI experiments, however, these unknown species requires tandem MS/MS experiments in MALDI-FTICR for structure-insights determination.

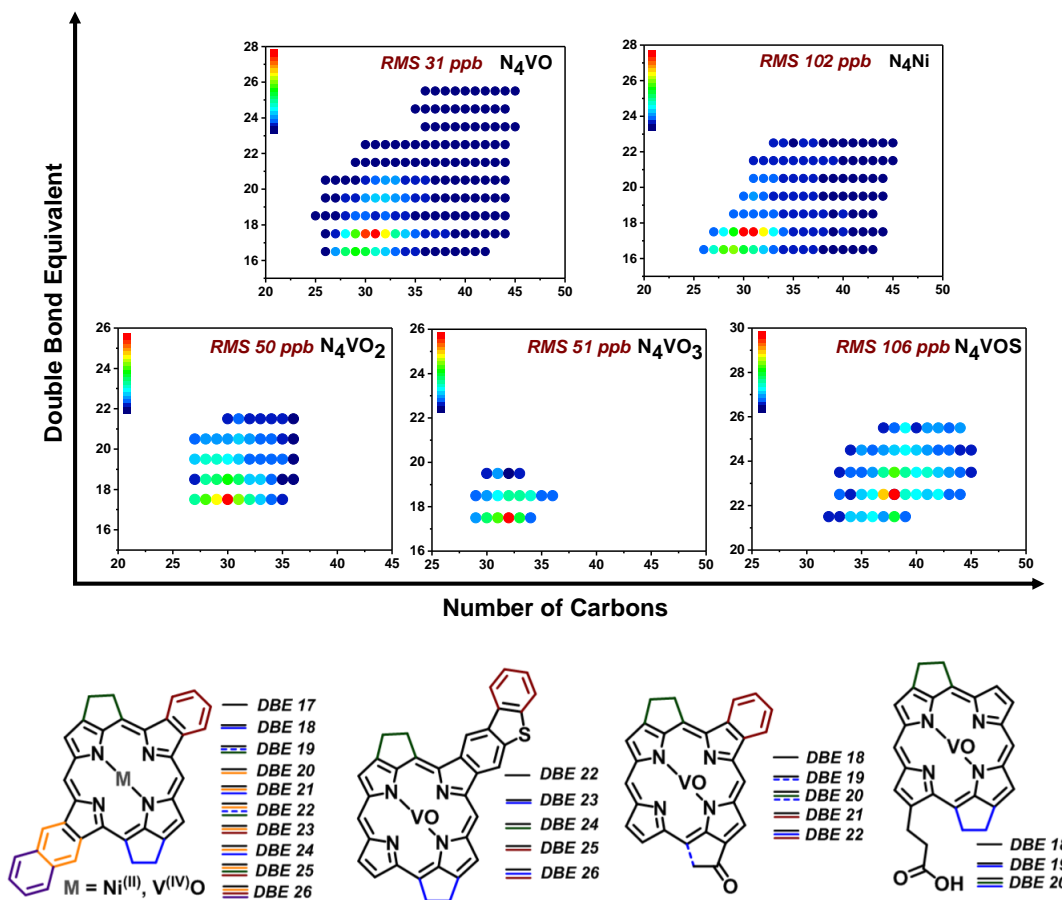


**Figure 25 (TOP)** Double Bond Equivalent (DBE) vs Number of Carbon plots for Vanadyl and Nickel porphyrins observed in extract **E<sub>6</sub>**. **(BOTTOM)** Proposed structures for Vanadyl and Nickel porphyrins founded in extract **E<sub>6</sub>**.

#### 4.5. Conclusions

We presented a straightforward analytical approach for the detection and classification of Nickel and Vanadyl porphyrins from crude-oils using the electron transfer (ET) ionization in MALDI-FTICR-MS. For the best of our knowledge, this novel methodology represents the first rational design of MALDI experiments for targeted analysis of porphyrins in crude-oils without

chromatographic sample enrichment or exhaustive purification procedures. The ET-MALDI approach not only increased the number of identified Ni/VO porphyrins, also, improved the analytical descriptors corresponding to low occurring nickel porphyrins, oxygen-containing VO<sub>2</sub> and VO<sub>3</sub> vanadyl porphyrins. This work explains how ET-MALDI works in complex mixtures and open a new window for Petroleomics.

## References

- Baker, E. W., William Louda, J., & Orr, W. L. (1987). Application of metalloporphyrin biomarkers as petroleum maturity indicators: The importance of quantitation. *Organic Geochemistry*, *11*(4), 303–309. [https://doi.org/10.1016/0146-6380\(87\)90041-6](https://doi.org/10.1016/0146-6380(87)90041-6)
- Barwise, A. J. G. (1990). Role of Nickel and Vanadium in Petroleum Classification. *Energy and Fuels*, *4*(6), 647–652.
- Blase, X., Attaccalite, C., & Olevano, V. (2011). First-principles GW calculations for fullerenes, porphyrins, phthalocyanine, and other molecules of interest for organic photovoltaic applications. *Physical Review B*, *83*(11), 115103.
- Chacón-Patiño, M. L., Rowland, S. M., & Rodgers, R. P. (2017). Advances in Asphaltene Petroleomics. Part 1: Asphaltenes Are Composed of Abundant Island and Archipelago Structural Motifs. *Energy and Fuels*, *31*(12), 13509–13518.
- Chacón-Patiño, M. L., Vesga-Martínez, S. J., Blanco-Tirado, C., Orrego-Ruiz, J. A., Gómez-Escudero, A., & Combariza, M. Y. (2016). Exploring Occluded Compounds and Their Interactions with Asphaltene Networks Using High-Resolution Mass Spectrometry. *Energy & Fuels*, *30*(6), 4550–4561.
- Cho, Y., Witt, M., Jin, J. M., Kim, Y. H., Nho, N.-S., & Kim, S. (2014). Evaluation of Laser Desorption Ionization Coupled to Fourier Transform Ion Cyclotron Resonance Mass Spectrometry To Study Metalloporphyrin Complexes. *Energy & Fuels*, *28*(11), 6699–6706.
- Clingenpeel, A. C., Robbins, W. K., Corilo, Y. E., & Rodgers, R. P. (2015). Effect of the Water Content on Silica Gel for the Isolation of Interfacial Material from Athabasca Bitumen. *Energy and Fuels*, *29*(11), 7150–7155.
- Colati, K. A. P., Dalmascio, G. P., De Castro, E. V. R., Gomes, A. O., Vaz, B. G., & Romão, W.

- (2013). Monitoring the liquid/liquid extraction of naphthenic acids in Brazilian crude oil using electrospray ionization FT-ICR mass spectrometry (ESI FT-ICR MS). *Fuel*, *108*, 647–655.
- Djurovich, P. I., Mayo, E. I., Forrest, S. R., & Thompson, M. E. (2009). Measurement of the lowest unoccupied molecular orbital energies of molecular organic semiconductors. *Organic Electronics: Physics, Materials, Applications*, *10*(3), 515–520.
- Fernandez-Lima, F. A., Becker, C., McKenna, A. M., Rodgers, R. P., Marshall, A. G., & Russell, D. H. (2009). Petroleum crude oil characterization by IMS-MS and FTICR MS. *Analytical Chemistry*, *81*(24), 9941–9947.
- Giraldo-Dávila, D., Chacón-Patiño, M. L., Orrego-Ruiz, J. A., Blanco-Tirado, C., & Combariza, M. Y. (2016). Improving compositional space accessibility in (+) APPI FT-ICR mass spectrometric analysis of crude oils by extrography and column chromatography fractionation. *Fuel*, *185*, 45–58.
- Giraldo-Dávila, D., Chacón-Patiño, M. L., Ramirez-Pradilla, J. S., Blanco-Tirado, C., & Combariza, M. Y. (2018). Selective ionization by electron-transfer MALDI-MS of vanadyl porphyrins from crude oils. *Fuel*, *226*(March), 103–111.
- Hughey, C. A., Rodgers, R. P., & Marshall, A. G. (2002). Resolution of 11 000 compositionally distinct components in a single electrospray ionization fourier transform ion cyclotron resonance mass spectrum of crude oil. *Analytical Chemistry*, *74*(16), 4145–4149.
- Jaramillo, P., Domingo, L. R., Chamorro, E., & Pérez, P. (2008). A further exploration of a nucleophilicity index based on the gas-phase ionization potentials. *Journal of Molecular Structure: THEOCHEM*, *865*(1–3), 68–72.
- Jarvis, J. M., Robbins, W. K., Corilo, Y. E., & Rodgers, R. P. (2015). Novel Method to Isolate Interfacial Material. *Energy and Fuels*, *29*(11), 7058–7064.

- Knochenmuss, R. (2016). *The Coupled Chemical and Physical Dynamics Model of MALDI. Annual Review of Analytical Chemistry* (Vol. 9).
- Knochenmuss, Richard. (2004). Photoionization pathways and free electrons in UV-MALDI. *Analytical Chemistry*, 76(11), 3179–3184.
- Knochenmuss, Stortelder, Breuker, & Zenobi. (2000). Secondary ion-molecule reactions in matrix-assisted laser desorption/ionization. *Journal of Mass Spectrometry: JMS*, 35(11), 1237–1245.
- Liu, H., Mu, J., Wang, Z., Ji, S., Shi, Q., Guo, A., ... Lu, J. (2015). Characterization of Vanadyl and Nickel Porphyrins Enriched from Heavy Residues by Positive-Ion Electrospray Ionization FT-ICR Mass Spectrometry. *Energy and Fuels*, 29(8), 4803–4813.
- McCarley, T. D., McCarley, R. L., & Limbach, P. A. (1998). Electron-transfer ionization in matrix-assisted laser desorption/ionization mass spectrometry. *Analytical Chemistry*, 70(20), 4376–4379.
- Mckenna, A. M., Purcell, J. M., Rodgers, R. P., & Marshall, A. G. (2009). Identification of Vanadyl porphyrins in a heavy crude oil and raw asphaltene by Atmospheric pressure photoionization Fourier transform ion cyclotron resonance (ft-icr) mass spectrometry. *Energy & Fuels*, 23(4), 2122–2128.
- McKenna, A. M., Williams, J. T., Putman, J. C., Aeppli, C., Reddy, C. M., Valentine, D. L., ... Rodgers, R. P. (2014). Unprecedented ultrahigh resolution FT-ICR mass spectrometry and parts-per-billion mass accuracy enable direct characterization of nickel and vanadyl porphyrins in petroleum from natural seeps. *Energy and Fuels*, 28(4), 2454–2464.
- Ogunrinde, A., Hips, K. W., & Scudiero, L. (2006). A Scanning Tunneling Microscopy Study of Self-Assembled Nickel(II) Octaethylporphyrin Deposited from Solutions on HOPG.

*Langmuir*, 22(13), 5697–5701.

Purcell, J. M., Hendrickson, C. L., Rodgers, R. P., & Marshall, A. G. (2006). Atmospheric Pressure Photoionization Fourier Transform Ion Cyclotron Resonance Mass Spectrometry for Complex Mixture Analysis. *Analytical Chemistry*, 78(16), 5906–5912.

Putman, J. C., Rowland, S. M., Corilo, Y. E., & McKenna, A. M. (2014). Chromatographic enrichment and subsequent separation of nickel and vanadyl porphyrins from natural seeps and molecular characterization by positive electrospray ionization FT-ICR mass spectrometry. *Analytical Chemistry*, 86(21), 10708–10715.

Qian, K., Rodgers, R. P., Hendrickson, C. L., Emmett, M. R., & Marshall, A. G. (2001). Reading chemical fine print: Resolution and identification of 3000 nitrogen-containing aromatic compounds from a single electrospray ionization Fourier transform ion cyclotron resonance mass spectrum of heavy petroleum crude oil. *Energy and Fuels*, 15(2), 492–498.

Qian, Kuangnan, Edwards, K. E., Mennito, A. S., Walters, C. C., & Kushnerick, J. D. (2010). Enrichment, resolution, and identification of nickel porphyrins in petroleum asphaltene by cyclograph separation and atmospheric pressure photoionization fourier transform ion cyclotron resonance mass spectrometry. *Analytical Chemistry*, 82(1), 413–419.

Qian, Kuangnan, Mennito, A. S., Edwards, K. E., & Ferrughelli, D. T. (n.d.). Observation of vanadyl porphyrins and sulfur-containing vanadyl porphyrins in a petroleum asphaltene by atmospheric pressure photonization Fourier transform ion cyclotron resonance mass spectrometry. *Rapid Communications in Mass Spectrometry*, 22(14), 2153–2160.

Raffaelli, A., & Saba, A. (n.d.). Atmospheric pressure photoionization mass spectrometry. *Mass Spectrometry Reviews*, 22(5), 318–331.

Ramírez-Pradilla, J. S., Blanco-Tirado, C., & Combariza, M. Y. (n.d.). Electron Transfer

Ionization of Nanoparticles, Polymers, Porphyrins and Fullerenes Using Synthetically-Tunable  $\alpha$ -Cyano-Phenylenevinylenes as UV MALDI-MS Matrices. *ACS Applied Materials & Interfaces*, 0(ja), null.

Ramírez-Pradilla, J. S., Blanco-Tirado, C., Hubert-Roux, M., Giusti, P., Afonso, C., & Combariza, M. Y. (n.d.). Comprehensive Petroporphyrin Identification in Crude Oils Using Highly Selective Electron Transfer Reactions in MALDI-FTICR MS. *Energy & Fuels*, 0(ja), null.

Rodgers, R. P., Hendrickson, C. L., Emmett, M. R., Marshall, A. G., Greaney, M., & Qian, K. (2001). Molecular characterization of petroporphyrins in crude oil by electrospray ionization Fourier transform ion cyclotron resonance mass spectrometry. *Canadian Journal of Chemistry*, 79(5–6), 546–551.

Rodgers, R. P., & McKenna, A. M. (2011). Petroleum analysis. *Analytical Chemistry*, 83(12), 4665–4687.

Scudiero, L., Barlow, D. E., & Hipps, K. W. (2002). Scanning Tunneling Microscopy, Orbital-Mediated Tunneling Spectroscopy, and Ultraviolet Photoelectron Spectroscopy of Nickel(II) Octaethylporphyrin Deposited from Vapor. *The Journal of Physical Chemistry B*, 106(5), 996–1003.

Scudiero, L., Barlow, D. E., Mazur, U., & Hipps, K. W. (2001). Scanning tunneling microscopy, orbital-mediated tunneling spectroscopy, and ultraviolet photoelectron spectroscopy of metal (II) tetraphenylporphyrins deposited from vapor. *Journal of the American Chemical Society*, 123(17), 4073–4080.

Treibs, A. (n.d.). Chlorophyll- und Hämin-Derivate in bituminösen Gesteinen, Erdölen, Kohlen, Phosphoriten. *Justus Liebigs Annalen Der Chemie*, 517(1), 172–196.

Valencia-Dávila, J. A., Witt, M., Blanco-Tirado, C., & Combariza, M. Y. (2018). Molecular

characterization of naphthenic acids from heavy crude oils using MALDI FT-ICR mass spectrometry. *Fuel*, 231(February), 126–133.

Vorapalawut, N., Martinez Labrador, M., Pohl, P., Caetano, M., Chirinos, J., Arnaudguilhem, C., ... Lobinski, R. (2012). Application of TLC and la ICP SF MS for speciation of S, Ni and v in petroleum samples. *Talanta*, 97, 574–578.

Witt, M., Godejohann, M., Oltmanns, S., Moir, M., & Rogel, E. (2017). Characterization of Asphaltenes Precipitated at Different Solvent Power Conditions Using Atmospheric Pressure Photoionization (APPI) and Laser Desorption Ionization (LDI) Coupled to Fourier Transform Ion Cyclotron Resonance Mass Spectrometry (FT-ICR MS). *Energy & Fuels*, 32(3), 2653–2660.

Zhao, X., Liu, Y., Xu, C., Yan, Y., Zhang, Y., Zhang, Q., ... Shi, Q. (2013). Separation and Characterization of Vanadyl Porphyrins in Venezuela Orinoco Heavy Crude Oil. *Energy & Fuels*, 27(6), 2874–2882.

Zhao, X., Shi, Q., Gray, M. R., & Xu, C. (2014). New Vanadium Compounds in Venezuela Heavy Crude Oil Detected by. *Scientific Reports*, 4, 1–6.

## **5. A comprehensive Petroporphyrin Identification in Crude Oils Using Highly Selective Electron Transfer Reactions in MALDI-FTICR MS**

### **5.1. Abstract**

Petroporphyrins are biomarkers used to extract information about petroleum genesis among other characteristics. Identification of particular types such as Ni, Cu, Mn, vanadyl (VO), oxygenated or sulfur-containing porphyrins, typically involves exhaustive isolation and purification processes followed by high resolution mass spectrometry analysis using atmospheric pressure photoionization (APPI-(+)) or electrospray (ESI-(+)) sources. Simultaneous identification of all porphyrins present in a particular crude oil or organic-matter rich sediment, still remains an analytical challenge. Here, we report a straightforward petroporphyrin isolation and identification methodology based on a single-step liquid-liquid (L-L) extraction (Crude-Oil:Acetonitrile) and high performance thin-layer chromatography fractionation (HPTLC – aminopropyl-bonded silica) followed by selective ionization via electron transfer in matrix assisted laser desorption ionization (ET) MALDI-FTICR. Mass spectrometric analysis of the extracts resulted in detection of 351 individual compounds in the ACN extract and 519 in the HPTLC extract, corresponding to the porphyrin families  $N_4VO$ ,  $N_4VO_2$ ,  $N_4VO_3$ ,  $N_4VOS$  and  $N_4Ni$  as verified by isotopic structure analysis. To the extent of our knowledge, this observation constitutes in the largest simultaneous identification of Ni, VO, oxygenated and sulfur-containing porphyrins in a single crude oil sample. In addition, the use of MALDI significantly reduces the amount of sample required for analysis (pico to femto mole levels) in comparison with continuous infusion methods such as APPI and ESI.

## 5.2. Introduction

Nickel, copper, vanadium, iron and manganese porphyrins, commonly known as petroporphyrins, are tetrapyrrole-based metal complexes directly derived from chlorophylls and other biologically active light- and oxygen-harvesting molecules, commonly found in fossil fuels (crude-oils, bitumens, and oil sands). (Mohammad Farhat Ali & Abbas, 2006) In 1934, Alfred Treibs suggested the biogenic origin of fossil fuels by studying chlorophyll-like compounds present in asphaltenes. (Treibs, n.d.)

Nowadays, petroporphyrins are not only considered geochemical markers that hold valuable information about fossil fuels genesis, (Hodgson & Peake, 1961) (Sundararaman, 1993) but also crucial compounds in catalysts' performance during refining processes; particularly nickel and vanadium porphyrins. (Filby & Berkel, 1987) The actual structures of nickel and vanadyl petroporphyrins are the result of geochemical modifications of the original chlorophyll core caused by the mineral matrix and source conditions of the organic matter during early diagenesis and catagenesis processes. (Filby & Berkel, 1987) Chlorophyll structural changes during fossil fuel formation include phytol loss, demetallation, aromatization by temperature and pressure, peripheral ring attachment, sulfur insertion, Ni/V derivatization, and finally transalkylation, the latter commonly associated with thermal conversion and degradation during catagenesis. (Filby & Berkel, 1987) (Lash, 1993) These transformations yield several structurally diverse porphyrin families of the types  $N_4VO$ ,  $N_4VO_2$ ,  $N_4VO_3$ ,  $N_4VOS$  and  $N_4Ni$ , depending upon the peripheral functional groups as shown in Figure 1.

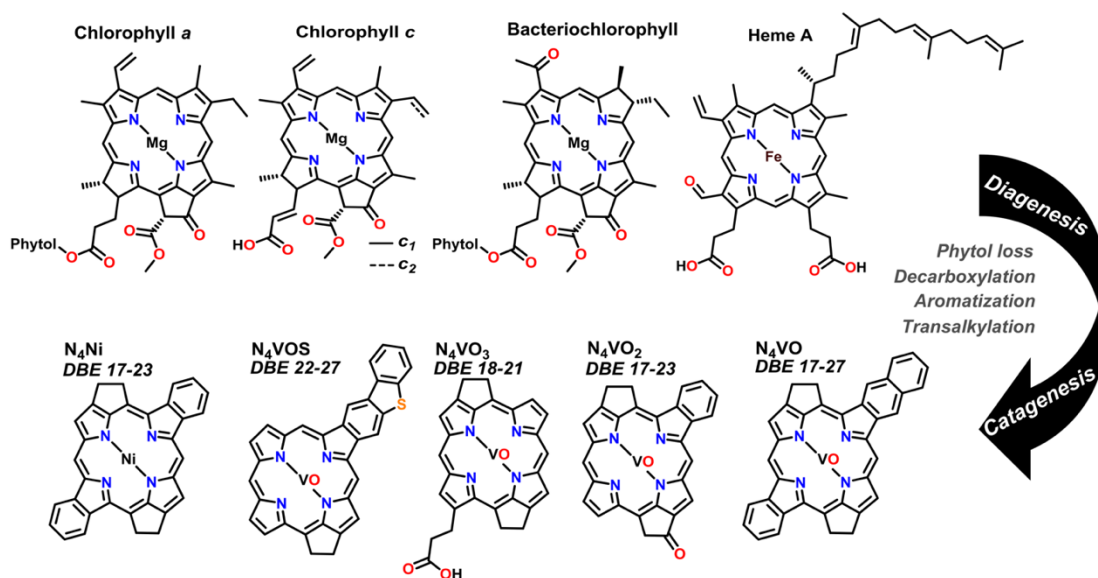


**Figure 26** Geochemical transformations of chlorophylls. Diagenesis involves phytol loss, decarboxylation, aromatization, metalation and heteroatom insertion; catagenesis involves thermal induced transalkylation and degradation.(Filby & Berkel, 1987)

In general, the simplest and most abundant structures resulting from chlorophyll transformation to petroporphyrins are etioporphyrins (Etio: DBE 17) and deoxophylloerythroetioporphyrins (DPEP: DBE 18).(Sundararaman, 1993) The transalkylation process suffered by the DPEP series under thermal conditions give valuable information about crude-oil kerogen conditions;(Bonnett, 1995) hence, the ratio  $\sum DPEP/\sum Etio$  is currently used as a maturity indicator in fossil fuels.(Sundararaman, 1993) In contrast, low abundance petroporphyrin families that originate from peripheral aromatic ring insertion or partial degradation are classified as dicyclic-deoxophylloerythroetioporphyrins (Di-DPEP: DBE = 19), rhodo-etioporphyrins (Rhodo-Etio, DBE = 20), rhodo-deoxophylloerythroetioporphyrins (Rhodo-DPEP, DBE = 21), Rhodo-dicyclicdeoxophylloerythroetioporphyrins (Rhodo-Di-DPEP, DBE = 22) and polycondensed porphyrins with DBE between 23 and 27.(Zhao, Shi, Gray, & Xu, 2014a)(Zhao, Xu, & Shi, 2016)

In refining schemes, compositional and structural information about petroporphyrins could be vital during Ni/V removal and asphaltene destabilization, since porphyrins can interact with aromatic cores via peripheral substituents and cause dramatic problems, such as emulsification and aggregate formation.(Yin, Tan, Müllen, Stryker, & Gray, 2008) Historically, spectroscopic techniques such as UV-Vis,(Freeman & O'Haver, 1990)(Foster, Day, Filby, Alford, & Rogers, 2002) Raman,(Cantu, Stencel, Czernuszewicz, Jaffe, & Lash, 2000) NMR-<sup>1</sup>H,(Ocampo, Callot, Albrecht, & Kintzinger, 1984) and X-Ray diffraction,(Senglet, Williams, Faure, Courières, & Guillard, 1990) have been used to study porphyrins structure. However, during the last two decades high resolution mass spectrometry (particularly FTICR-MS) has become an important tool for the identification, compositional space analysis and molecular level characterization of nickel and vanadyl porphyrins in complex mixtures (crude oils, bitumens, asphalt and asphaltenes). Table 1 shows the most relevant contributions of mass spectrometry, combined mainly to chromatographic separations, to porphyrin identification over the past 20 years. In 2001, Rodgers *et al.* reported the molecular level identification, using ESI-(+) FTICR, of DPEP and Etio porphyrins extracted from crude-oils by column chromatography.(Rodgers et al., 2001) This first work showed the breadth of high resolution mass spectrometry applications, opening a window for vanadyl porphyrin speciation in complex mixtures, and can be considered the starting point of high-level compositional space and structural characterization for these compounds. Later on, Qian *et al.* used APPI-(+) for the ionization of porphyrin-enriched asphaltenes, reporting the identification of sulfur porphyrins (88 molecular formula assignments for N<sub>4</sub>VO and 18 for N<sub>4</sub>VOS).(Qian, Mennito, Edwards, & Ferrughelli, n.d.) Using APPI-(+) McKenna et al. reported the direct analysis of porphyrins from crude-oils and Athabasca bitumen, showing the presence of Etio and DPEP as [M+H]<sup>+</sup> and [M]<sup>2+</sup> ion series.(Mckenna, Purcell, Rodgers, & Marshall, 2009) Typically, in crude-

oils and bitumens the Ni:V ratio is around 1:4,(Mohammad Farhat Ali & Abbas, 2006)(Mohammad F. Ali, Perzanowski, Bukhari, & Al-Haji, 1993)(Mohammad F. Ali, Bukhari, & Saleem, 1983) with nickel concentrations in the range of 50-300 ppm.(López & Mónaco, 2017) In 2010 Qian et al. reported nickel porphyrins in asphaltenes, observed as Etio and DPEP homologous series only after an exhaustive cyclograph purification process. These authors showed that nickel porphyrins have ionization efficiencies three times lower than vanadyl porphyrins in APPI(+), which may explain why they were not observed before.

**Table 2.** Relevant MS contributions to porphyrin identification

Author	Sample	Isolation Method	Ion Source	Number of porphyrins per family					Total identified porphyrins*
				N <sub>4</sub> VO	N <sub>4</sub> Ni	N <sub>4</sub> VO S	N <sub>4</sub> VO <sub>2</sub>	N <sub>4</sub> VO <sub>3</sub>	
Rodgers et al, 2001	<i>Crude-oil</i>	Chromatography	ESI-FTICR (+)	30	-	-	-	-	~30
Xu et al, 2005	<i>Crude-oil</i>	Chromatography	LDI-TOF (+)	36	-	-	-	-	~36
Qian et al, 2008	<i>Asphaltene</i>	Direct analysis	APPI-FTICR (+)	88	-	18	-	-	~106
McKenna et al, 2009	<i>Crude-oil</i>	Direct analysis	APPI-FTICR (+)	34	-	-	-	-	~34
Qian et al, 2010	<i>Asphaltene</i>	Cyclography	APPI-FTICR (+)	-	52	-	-	-	~52
Zhao et al, 2013	<i>Heavy crude-oil</i>	Extrography	ESI-FTICR (+)	152	-	-	52	48	~252
Zhao et al, 2014	<i>Crude-oil</i>	Chromatography	ESI-FTICR (+)	84	-	69	-	-	~153
McKenna et al, 2014	<i>Bitumen</i>	Direct Analysis	APPI-FTICR (+)	>100	33	-	18	16	~180
Cho et al, 2014	<i>Crude-Oil</i>	Direct Analysis	LDI-FTICR (+)	12	7	-	-	-	~19
Putman et al, 2014	<i>Volcano Asphalt</i>	Chromatography	ESI-FTICR (+)	91	101	57	8	11	~268
Liu et al, 2015	<i>Heavy Oil Residue</i>	Chromatography	ESI-FTICR (+)	163	36	79	16	-	~294
Giraldo et al, 2016	<i>Crude-Oil</i>	Extrography	APPI-FTICR (+)	159	-	-	-	-	~159
<b>This work</b>	<b><i>Crude-oil</i></b>	<b>L-L, HPTLC</b>	<b>ET-MALDI(+)-FT-ICR</b>	<b>234</b>	<b>84*</b>	<b>83</b>	<b>95</b>	<b>43</b>	<b>~539*</b>

In petroporphyrin analysis sample isolation and enrichment is of paramount importance, particularly for observation of low-abundance compounds. Zhao et al. reported in 2013 extensive porphyrin identification from a Venezuelan heavy crude-oil (more than 250 molecular formulae) after column chromatography purification and ESI-(+) FTICR analysis. (Zhao et al., 2013b) The observation, for the first time, of the  $N_4VO_2$  and  $N_4VO_3$  homologous series showed that the propyl-carboxylic acid moiety or the cyclopentanone residues in chlorophyll can be preserved during diagenesis. Zhao et al. also reported a new series of vanadyl porphyrins containing an extra nitrogen atom, present in an aminoether functionality. (Zhao et al., 2014a) These findings proved the Hodgson hypothesis about association of protein fragments with porphyrins during the diagenesis, highlighting also the role of polar porphyrins in asphaltene stabilization. (Hodgson & Peake, 1961)

In 2014, McKenna et al. (McKenna et al., 2014) reported the direct observation of nickel and vanadyl porphyrins in a bitumen, with 180 molecular formulae assigned, setting a record in the number of compounds detected without sample enrichment. The species corresponded mostly to the  $N_4VO$  and  $N_4Ni$  compound families. In the same year, Putman et al. reported 230 molecular formulae corresponding to  $N_4VO$ ,  $N_4VO_2$ ,  $N_4VO_3$  and  $N_4Ni$  species in a volcano asphalt. The porphyrinic compounds were isolated via primary/secondary amine (PSA) solid phase extraction (SPE) and examined by ESI(+)-FTICR. (Putman, Rowland, Corilo, & McKenna, 2014) Liu et al. (Liu et al., 2015) studied heavy residues, setting a record in the number of identified porphyrins with about 294 molecular formulae assigned to  $N_4VO$ ,  $N_4Ni$ ,  $N_4VO_2$  and  $N_4VOS$  homologous series. Interestingly, 79 sulfur vanadyl porphyrins were detected with DBE ranging from 21 to 27. Recently, our group reported an extrography methodology applied to enriched acetonitrile

fractions followed by column chromatography and APPI-(+) FTICR experiments for porphyrin analysis, revealing more than 150 vanadyl porphyrins in heavy american crude-oils,(Giraldo-Dávila, Chacón-Patiño, Orrego-Ruiz, Blanco-Tirado, & Combariza, 2016) however, species like  $N_4Ni$ ,  $N_4VO_2$  or sulfur vanadyl porphyrins  $N_4VOS$  were not detected.

When targeting particular compounds - such as porphyrins - in complex mixtures - such as fossil fuels - there are two choices from an analytical perspective: selective isolation or selective ionization. The former is extensively illustrated in Table 1, while the latter has not been applied to porphyrin analysis since the ionization sources used are not very selective towards these compounds (APPI, ESI and LDI). However, porphyrins have particular physicochemical characteristics, such as low ionization potentials, when compared to other compound families in crude oils, that can be used to devise selective ionization strategies for their study. Our group has been working on developing new electron-transfer (ET) MALDI matrices based on optoelectronic compounds, we recently reported a new matrix based on  $\alpha$ -cyanophenylenevinylene moiety ( $\alpha$ -CNPV-CH<sub>3</sub>) with an outstanding analytical performance for the analysis of nanoparticles, polymers, conjugated molecules and biomarkers,(Ramírez-Pradilla, Blanco-Tirado, & Combariza, n.d.) additionally, we have used the  $\alpha$ -CNPV-CH<sub>3</sub> as matrix for the selective ionization of vanadyl porphyrins extracted from heavy crude-oils.(Giraldo-Dávila, Chacón-Patiño, Ramirez-Pradilla, Blanco-Tirado, & Combariza, 2018) In general,  $\alpha$ -CNPV-CH<sub>3</sub> outperformed DCTB (a standard ET matrix) in terms of selectivity, resolution, ion abundance and signal-to-noise ratio for petroporphyrins analysis by MALDI-TOF. According to McCarley and co-workers(McCarley, McCarley, & Limbach, 1998) the formation of analyte ions in gas-phase ET-MALDI reactions is determined by the net difference between analyte and matrix ionization energies, with a threshold

value in  $\Delta IP \leq -0.5$  eV required for a thermodynamically-favorable ET reaction. Porphyrins have IP values between 6.5 and 7.0 eV, while the  $\alpha$ -CNPV-CH<sub>3</sub> matrix has EI of 8.42 eV; this difference ensures efficient ET reactions from the neutral porphyrin to the ionized matrix ions, resulting in formation of secondary ions of the analyte. As we demonstrated previously, the high selectivity of ET reactions in MALDI-(+) combined with the high mass accuracy and resolution of FTICR could provide an additional tool for porphyrin analysis by mass spectrometry, without the need for the complex sample enrichment or purification procedures required when using APPI, ESI or LDI sources. In this contribution, we report the simultaneous identification of N<sub>4</sub>VO, N<sub>4</sub>VO<sub>2</sub>, N<sub>4</sub>VO<sub>3</sub>, N<sub>4</sub>VOS and N<sub>4</sub>Ni porphyrins in a Middle-Eastern crude oil. With a simple L-L extraction step (ACN:Crude-Oil) direct ET-MALDI experiments revealed more than 351 porphyrins, whereas sample enrichment using aminopropyl-bonded HPTLC increased the number of assigned formulas to 525. A total of 539 individual molecular formulas corresponding to N<sub>4</sub>VO, N<sub>4</sub>VO<sub>2</sub>, N<sub>4</sub>VO<sub>3</sub>, N<sub>4</sub>VOS and N<sub>4</sub>Ni were assigned, using isotopic structure analysis to corroborate identification, breaking the record on total number of identified porphyrins set at 294 by Liu and co-workers in 2015.(Liu et al., 2015)

### 5.3. Experimental Section

**5.3.1. Materials.** The  $\alpha$ -cyanophenylenevinylene ( $\alpha$ -CNPV-CH<sub>3</sub>) matrix was synthesized and purified following a previously reported methodology.(Giraldo-Dávila et al., 2018) Coronene, fluoranthene, anthracene, fluorene, cobalt porphyrin, nickel octaethylporphyrin and vanadyl octaethylporphyrin were purchased from Sigma-Aldrich (Darmstadt, Germany) and used as an external calibration mixture. Analytical grade (99.5%) acetonitrile (ACN),

tetrahydrofuran (THF) dichloromethane (DCM), n-hexane and aminopropyl-bonded HPTLC plates were purchased from Merck Millipore (Darmstadt, Germany).

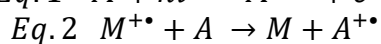
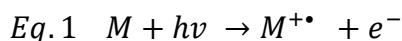
**5.3.2. Mass spectrometry.** A mixture of crude-oil and ACN (1:2 mL) was placed on a vial and heated at 50 °C under magnetic stirring; after 30 min the upper layer was separated. 50  $\mu$ L of the extract were dried at room temperature and reserved for direct ET-MALDI-FTICR experiments; the remaining extract was concentrated to a final volume of 500  $\mu$ L and manually spotted on aminopropyl-bonded HPTLC plate. The plate was eluted using a mixture of  $\text{CH}_2\text{Cl}_2$ :n-hexane 1:1 as mobile phase. Nickel octaethylporphyrin and vanadyl octaethylporphyrin were also spotted on the plate and used as standards to calculate retention factors ( $R_f$ ). The whole ACN extract and the porphyrin pink fraction taken from the HPTLC plate were scanned in a double channel Shimadzu UV-2401PC spectrophotometer (Kyoto, Japan) with a range of 200 to 700 nm using  $\text{CH}_2\text{Cl}_2$  as solvent; for commensurate results, UV-Vis spectra were normalized. For ET-MALDI experiments the dried extracts was redissolved in 10  $\mu$ L of THF, mixed with an equal volume of  $\alpha$ -CNPV- $\text{CH}_3$  (5 mM) matrix solution and vortexed; 2  $\mu$ L of the resulting solution were placed on a polished steel MALDI target. For HPTLC-ET-MALDI-FTICR experiments, 50  $\mu$ L of  $\alpha$ -CNPV- $\text{CH}_3$  5 mM were spotted directly on the HPTLC plate and analyzed directly in the instrument.

ET-MALDI-FTICR experiments were performed on a Bruker solarix XR 12T (ParacellTM) instrument, equipped with a MALDI source with a Nd:YAG solid state laser (355 nm) operated in positive ion mode. LDI and ET-MALDI experiments were performed using 20% of laser power. All spectra were acquired in broadband mode, with accumulation of 300 scans and number of data

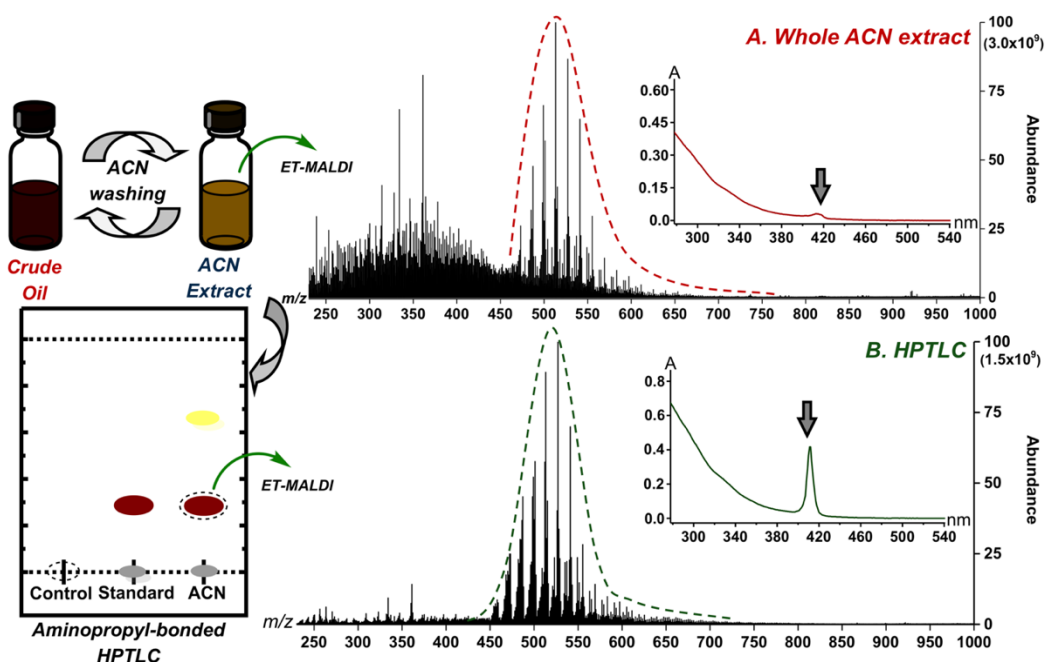
points set to 16M at  $m/z$  500; an active exclusion with minimum threshold intensity of  $7.0 \times 10^8$  and maximum of  $1.0 \times 10^9$  was used. An external calibration was performed using a mixture of PAHs and standard Ni and VO porphyrins. All spectra were internally calibrated following compounds of the N<sub>1</sub>, CH and N<sub>4</sub>VO series with an average RMS of 21 ppb for the whole fraction data and 43 ppb for the HPTLC data. Molecular formula assignments and isotopic fine structure analysis were performed with the DataAnalysis (Bruker Daltonics, Bremen, Germany). DBE vs carbon number diagrams and mass spectra data were plotted using OriginPro Software (North Hampton, MA).

## 5.4. Results and Discussion

**5.4.1. Direct analysis of an ACN extract via ET-MALDI-FTICR.** Figure 25 shows the ET-MALDI FTICR spectra resulting from the direct analysis of the L-L ACN extract and the HPTLC band (corresponding to porphyrins) from a Middle-Eastern crude oil sample. Interestingly, in the ACN extract mass spectrum (Figure 25A) two distributions are observed: one in the low mass region (centered around  $m/z$  349) and another in the medium mass region (centered around  $m/z$  513) corresponding to aromatic compounds with low H/C ratios and porphyrins, respectively. Electron transfer (ET) reactions in MALDI-MS are two-step processes suitable for the ionization of labile, unstable, non-polar and highly conjugated molecules as seen in Equations 1-2, where A refers to analyte and M to matrix. (Calvano et al., 2017) (Castellanos-García et al., 2017)



Porphyryns, are compounds with an enriched  $\pi$ -electron cloud as a consequence of the presence of  $\pi$ -exceeding pyrrole units, exhibiting relatively low IPs (6.5 to 7.5 eV) depending upon the extension of the conjugated system, the presence of functional groups or the nature of the metal center.(Barlow, Scudiero, & Hipps, 2004) Under MALDI conditions, the ET reaction between neutral porphyryns and primary ions of the  $\alpha$ -CNPV-CH<sub>3</sub> matrix (IP: 8.42 eV) is thermodynamically favored ( $\Delta$ IP between -0.92 and -1.92 eV).(McCarley et al., 1998)(Kotsiris et al., 2006) Thus, porphyryns are easily ionized and detected in the ET-MALDI experiment, as seen in the prominent medium mass region distribution in Figure 2A where 351 individual molecular formulae (in the form of [M]<sup>+</sup> molecular ions) corresponding to porphyryns were assigned (See Table S1 of the Supporting Information). In contrast, the  $\Delta$ IP for ET reactions between saturated, polar or less conjugated compounds possibly present in the ACN extract (IP ranging from 7.8 to 11 eV) and the primary ions of the matrix, range from -0.62 to +2.58 eV (See Figure S1 in the Supporting Information). This indicates a least (or not at all) thermodynamically favorable ET process. Thus, the least abundant distribution, in the low mass region of Figure 25A mostly corresponds to CH, N<sub>1</sub>, S<sub>1</sub>, S<sub>2</sub> and N<sub>1</sub>S<sub>1</sub> classes with low contribution of polar species (See supporting material, Figure S2, heteroatom class distribution for whole ACN fraction). The ionization energy of organic compounds decrease, in terms of HOMO energy, as DBE and heteroatom content increases. Hence, some competing secondary electron transfer reactions may occur between low IP aromatic species present in the ACN extract and the matrix. In Figure S3 of the Supporting Information, the DBE vs carbon number plots of species in the low MW distribution of Figure 2A show high DBE values (10 to 25) corresponding to CH, N<sub>1</sub>, S<sub>1</sub>, S<sub>2</sub> and N<sub>1</sub>S<sub>1</sub> compound classes. In addition, van Krevelen plots in Figure S3 show low H/C ratios, particularly for the S<sub>1</sub> class.



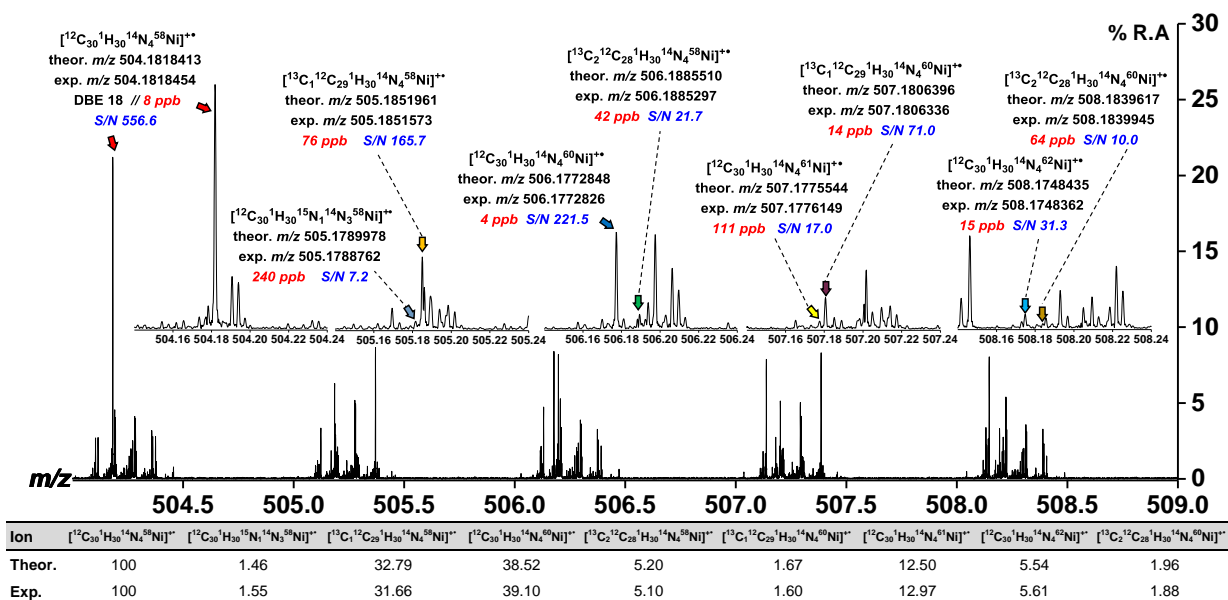
**Figure 27** ET-MALDI FTICR spectra resulting from the direct analysis of the L-L ACN extract (A) and the HPTLC band (corresponding to porphyrins) (B) from a Middle-Eastern crude oil sample.

Figure 25B shows the effect of eliminating compounds that may interfere with porphyrin detection from the raw ACN extract. Evidently, after the HPTLC fractionation and ET-MALDI ionization, directly from the plate, a cleaner spectrum is obtained where 6550 individual molecular formulae (in the form of  $[M]^{+}$  molecular ions) were assigned (See Table S1 of the Supporting Information). The MS data in Figure 25 indicate ET-MALDI ionization affords selective formation of  $[M]^{+}$  for nickel and vanadyl porphyrins, even for the direct analysis of the ACN extract, contrarily to APPI-(+) or ESI-(+) sources where ionization depends on molecular properties different than IP (results not shown). Interestingly, ICP-MS measurements revealed a 1:3.37 Ni:V ratio for the ACN extract; while in ET-MALDI MS the ratio between the sum of relative

abundances for the total number of assigned nickel porphyrins to vanadyl porphyrins in the ACN fraction corresponds to 1:3.17 (see supporting info, Table S1). This observation suggests that ET-MALDI does not appear to discriminate between the low-abundance nickel and the high-abundance vanadium species in the ACN extract, due to the nature of the ionization process, contrarily, in ion sources such as APPI(+) nickel porphyrins exhibit ionization efficiencies three times lower than vanadyl ones, as reported by Qian et al, (Qian, Edwards, Mennito, Walters, & Kushnerick, 2010) using nickel. As mentioned in the experimental section, ICP-MS of whole ACN extract showed a total concentration of ~9.2% and ~5.1% of vanadium and nickel from the parental crude-oil, consequently, the observation window is limited and, speculatively, we observed the nickel and vanadyl porphyrins whose are not occluded in the heavy fractions and can be easily extracted with the L-L approach.

On the other hand, for low abundance  $N_4Ni$  porphyrins, the high mass accuracy of the measurements (< 100 ppb) together with nickel particular isotopic distribution ( $^{58}Ni$ ,  $^{60}Ni$ ,  $^{61}Ni$  and  $^{62}Ni$ ) allowed unambiguous elemental composition assignments. Figure 26 shows signal assignments corresponding to isotopologues of the monoisotopic molecular ion  $C_{30}H_{30}N_4Ni$ , the most abundant nickel porphyrin in the ACN extract. At  $m/z$  505, the species  $^{12}C_{30}^{1}H_{30}^{14}N_3^{15}N^{58}Ni$  and  $^{12}C_{29}^{13}C^1H_{30}^{14}N_4^{58}Ni$  were detected, respectively, with mass accuracy of 240 and 76 ppb and S/N ratios of 7.2 and 165.7. At  $m/z$  506, the contribution of  $^{60}Ni$  isotopologue and  $^{13}C_2$  were assigned in a 4 and 42 ppb of mass accuracy. From nickel isotopologues, the contribution of  $^{61}Ni$  shows the lower abundance, however at  $m/z$  507 it was observed in a mass accuracy of 111 ppb (S/N 17) and differentiated from the contribution of  $^{13}C_1^{60}Ni$  signal. At  $m/z$  508, the signal corresponding to nickel isotopologue  $^{62}Ni$  was detected in a 15 ppb of mass accuracy. The relative

ion abundance for all signals were established in function of monoisotopic ion signal and compared with theoretical isotopic distribution, Figure 26.



**Figure 28** Expanded scale mass spectrum of the ACN extract containing Ni and V porphyrins. Insets correspond to isotopologue assignment for Nickel porphyrin DBE 18  $\text{C}_{30}\text{H}_{30}\text{N}_4\text{Ni}$ .

As mentioned above, we detected 351 unique molecular formulae corresponding to  $\text{N}_4\text{VO}$  (173),  $\text{N}_4\text{VO}_2$  (34),  $\text{N}_4\text{VO}_3$  (16),  $\text{N}_4\text{VOS}$  (43) and  $\text{N}_4\text{Ni}$  (84) porphyrins by direct ET-MALDI analysis of the whole ACN extract isolated from the crude oil sample as illustrated in Figure 27 (See also Supporting Information Table S1 for assignments, mass accuracy and signal-to-noise ratios for all species). The DBE vs carbon number plots show that  $\text{N}_4\text{VO}$ ,  $\text{N}_4\text{VO}_2$ ,  $\text{N}_4\text{VO}_3$  and  $\text{N}_4\text{Ni}$  compound families share the same compositional space, with the most abundant species clustered around DBEs 16 to 20 and carbon numbers 27 to 37. In contrast,  $\text{N}_4\text{VOS}$  species exhibit higher DBE values (22 to 27) and carbon numbers (35 to 50). Figure 24 shows petroporphyrins structural

changes during diagenesis and catagenesis, the attachment of peripheral aromatic rings in particular goes up to of DBE values of 27. When comparing the most abundant  $N_4VO$  and  $N_4Ni$  families, we observed a maximum DBE of 27 for  $N_4VO$  while for nickel porphyrins we had a maximum DBE of 23. The metal insertion on the porphyrin core during early diagenesis can produce both, nickel and vanadyl porphyrins; however, the concentration of each metal during metalation plays a crucial role, resulting in more abundant vanadyl porphyrins which can be transformed by sulfur insertion, partial degradation or ring attachment.

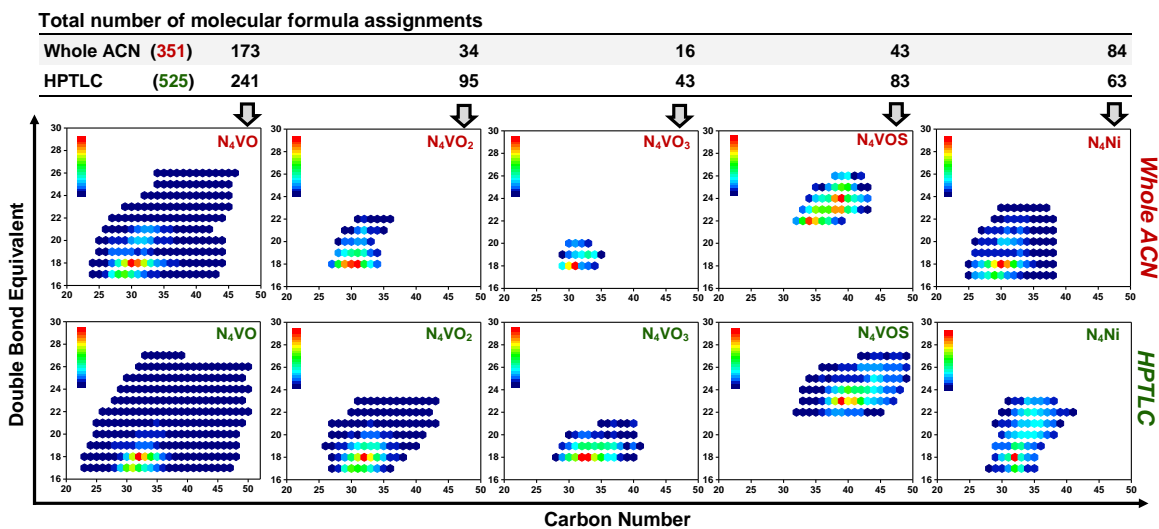


**Figure 29** Isoabundance color-map plots corresponding to all porphyrin families found in the ACN and the HPTLC fractions.

Sulfur vanadyl porphyrins are presumably formed in source kerogens after thermo/bacterial sulfate reduction which inserts thiophene and benzothiophene-like peripheral substituents (Figure 24). (Hodgson & Peake, 1961) (Zhao et al., 2014a) (Orr, 1986) (Jørgensen, 1977) Interestingly, the presence of  $N_4VO_2$  and  $N_4VO_3$  families shows that it is also possible to maintain the oxygen (or the carboxylic moiety as acid or ester groups) on the five-membered fused ring of the chlorophylls in a partial degradation. Unfortunately, the low concentration of nickel porphyrins dramatically

influence these transformations and sulfur-containing or extra oxygen nickel porphyrins are not observed. In summary, up to this point we demonstrated that a simple L-L procedure followed by selective ET-MALDI ionization can afford access to porphyrin targeted analysis in crude-oils.

**5.4.2. HPTLC-ET-MALDI-FTICR.** Historically, several chromatographic approaches (*e.g.* column, TLC, extrography) with a wide range of stationary and mobile phases have been applied to isolate and concentrate petroporphyrins for mass spectrometric analysis.(Putman et al., 2014)(Giraldo-Dávila et al., 2016) However, additional selective enrichment strategies are used to observe low-abundance families such as  $N_4VO_2$ ,  $N_4VO_3$  and nickel porphyrins, particularly when using ESI-(+) or APPI-(+) sources. As discussed above, ET reactions in MALDI might provide a way to selectively detect particular compound classes sharing a common physicochemical characteristic (*i.e.* ionization energy), as occurs with porphyrins. Considering the observation of a bimodal distribution when interrogating directly the ACN extract (Figure 25A), we performed an additional purification step using aminopropyl-bonded HPTLC plates to fraction the original extract. As observed in figure S5 (see supporting material) this process induced separation of the ACN extract into three bands, one of them corresponding to a concentrated porphyrin fraction ( $R_f$  0.27) suitable for direct MALDI analysis on the HPTLC plates. UV-Vis measurements of the TLC bands (DCM extracts after L-S extraction from the solid aminopropyl silica phase scratched from the plate) show a strong Soret band corresponding to petroporphyrins at 420 nm, in the band with  $R_f$  0.27.

The ET-MALDI-FTICR spectrum in Figure 25B shows a unique distribution centered around  $m/z$  527, corresponding exclusively to porphyrins, in contrast with the bimodal spectrum of Figure 25A. Using HPTLC we were able to detect 534 unique molecular formulae corresponding to  $N_4VO$

(241),  $N_4VO_2$  (95),  $N_4VO_3$  (43),  $N_4VOS$  (83) and  $N_4Ni$  (63) porphyrins as illustrated in Figure 28 (See also Supporting Information Table S1 for assignments, mass accuracy and signal-to-noise ratios for all species). The compound families observed in the HPTLC fraction are apparently the same as the ones found in the ACN extract, however, previous reports on solid phase extraction (SPE) using aminopropyl-bonded stationary phase, revealed a high retention of acidic porphyrins whose were extracted with formic acid elution. Because these  $N_4VO_3$  porphyrins were observed in the porphyrin-enriched fraction, the significant oxygen-content can be attributed to other functional groups like ester, ketones, ethers, among others, nevertheless, the comparison against characterized standards and additional experiments like tandem MS need to be examined for a consistent molecular structure attribution. Figure S6 of the Supporting Information show a significant reduction of signals corresponding to heteroatomic compounds, and enhancement of porphyrin ions, after HPTLC fractionation. In addition, an expanded scale spectrum at  $m/z$  587 in Figure 29, shows a significant increase in S/N ratios for the radical cations of  $[C_{32}H_{34}N_4VO]^+$  (DBE 22),  $[C_{33}H_{36}N_4VO_3]^+$  (DBE 18) and  $[C_{34}H_{40}N_4VO_2]^+$  (DBE 17) species when compared with the whole ACN extract. Interestingly, after HPTLC all porphyrins classes showed an increase in number of species with the exception of nickel porphyrins ( $N_4Ni$ ) where the total number of assigned molecular formulae dropped from 84 in the ACN extract to 63 in the HPTLC band with a dramatic decrease on S/N ratios. Previous reports concerning ICP-MS analysis of TLC bands in crude-oils, revealed that after elution nickel compounds spread over the plate exhibiting several  $R_f$  values, while vanadium is efficiently separated and clearly identified at specific  $R_f$ . (Vorapalawut et al., 2012) The reduced number of  $N_4Ni$  in HPTLC suggest a spread over the plate and certainly, a different  $R_f$  when compared with vanadyl porphyrins as previously reported by Xu and Lesage; (Xu, 1992) these effects can either decrease the concentration and dramatically affects the

desorption during the ET-MALDI process. In contrast, the HPTLC separation increased the number of formulae corresponding to vanadyl species, providing enhanced isotopologue assignments, and revealing new porphyrins of the  $N_4VO_2$  or  $N_4VO_3$  types, commonly buried in the noise and present in low concentration. (Xu, 1992) The DBE vs carbon number plots in Figure 28 show significant increase in the number of assignments corresponding to sulfur vanadyl porphyrins  $N_4VOS$ . Efforts on chromatographic sample enrichment, using silica gel open column chromatography, (Liu et al., 2015) (Zhao et al., 2013a) aimed to selective isolation of sulfur-containing porphyrins showed that this particular class is always accompanied by aromatic  $S_1$ ,  $N_1S_1$  and  $N_1$  compounds, very abundant in crude oils, having similar polarities than porphyrins. Additionally,  $S_1$ ,  $N_1S_1$  and  $N_1$  classes exhibit relatively good ionization efficiencies in APPI, (Putman et al., 2014) while in ESI formation of  $[M+H]^+$  is highly favored. (Zhao, Shi, Gray, & Xu, 2014b) These effects combined hinder detection of sulfur-containing porphyrins by current chromatographic-MS strategies. The use of ET-MALDI allows significant increment on S/N ratios for the sulfur vanadyl porphyrin  $[C_{38}H_{36}N_4VOS]^+$  (3.7 times increase) and the high DBE  $[C_{40}H_{44}N_4VO]^+$  (6.7 times increase) for the HPTLC fraction when compared with the ACN extract, as seen in Figure 30. The same observation is true for most species in the  $N_4VOS$  compound family.

Figures 29 and 30, show increased S/N ratios for high carbon number porphyrins after HPTLC fractionation, particularly for V-containing families such as:  $N_4VO$ ,  $N_4VO_2$  and  $N_4VO_3$ ; while Table S1 of the Supporting Information show that we duplicate the number of assigned formulas for these compounds, reaching a total of 221. For  $N_4VOS$  we observed a 1.45 increase in the number of assignments (83). When compared with previous reports, as shown in Table 1, the

HPTLC-ET-MALDI-FTICR experiments shown here (525 assigned formulae) represent a net increase of 1.8 times the number of porphyrins previously reported by Liu et al. (294 assigned formulae)(Liu et al., 2015) and Putman et al. (231 assigned formulae)(Putman et al., 2014). From our perspective, we believe that comprehensive identification of porphyrins in complex mixtures not only depends on isolation strategies, but on the use of selective ionization methods such as ET-MALDI.

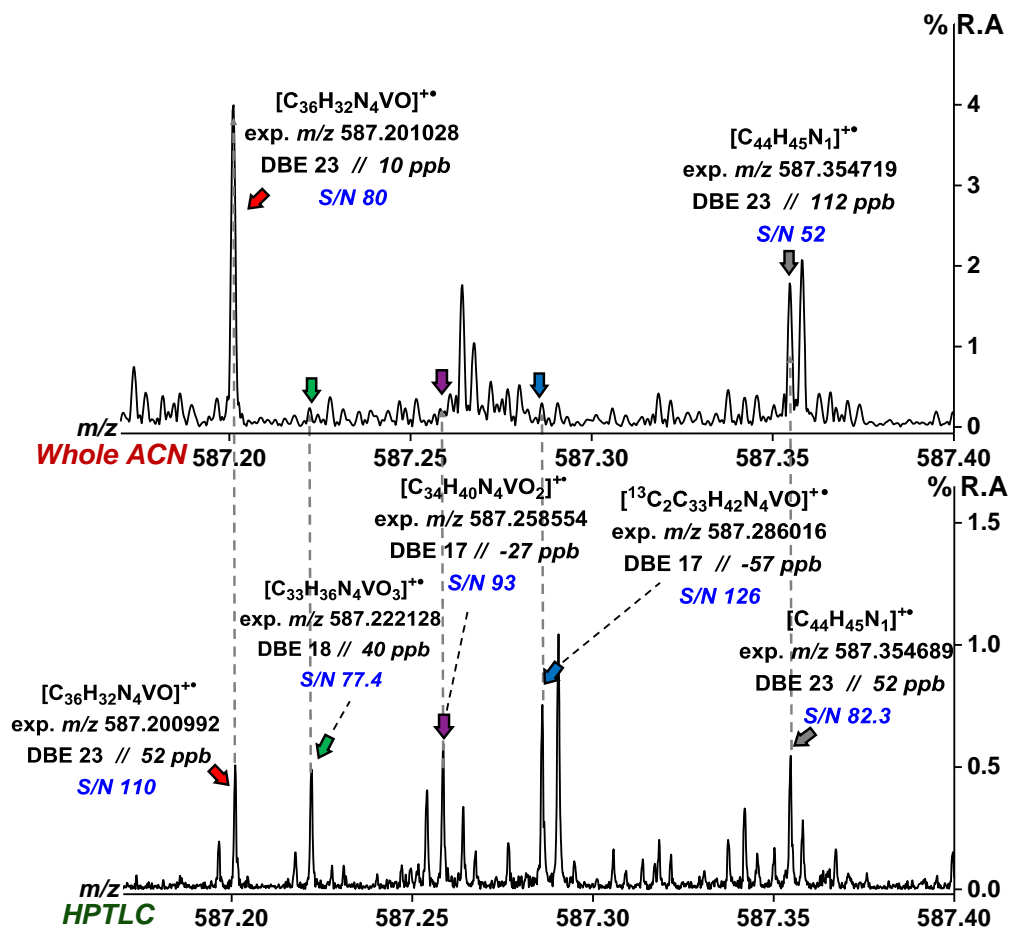


**Figure 30** Expanded scale ET-MALDI mass spectra for the ACN extract and the HPTLC fraction.

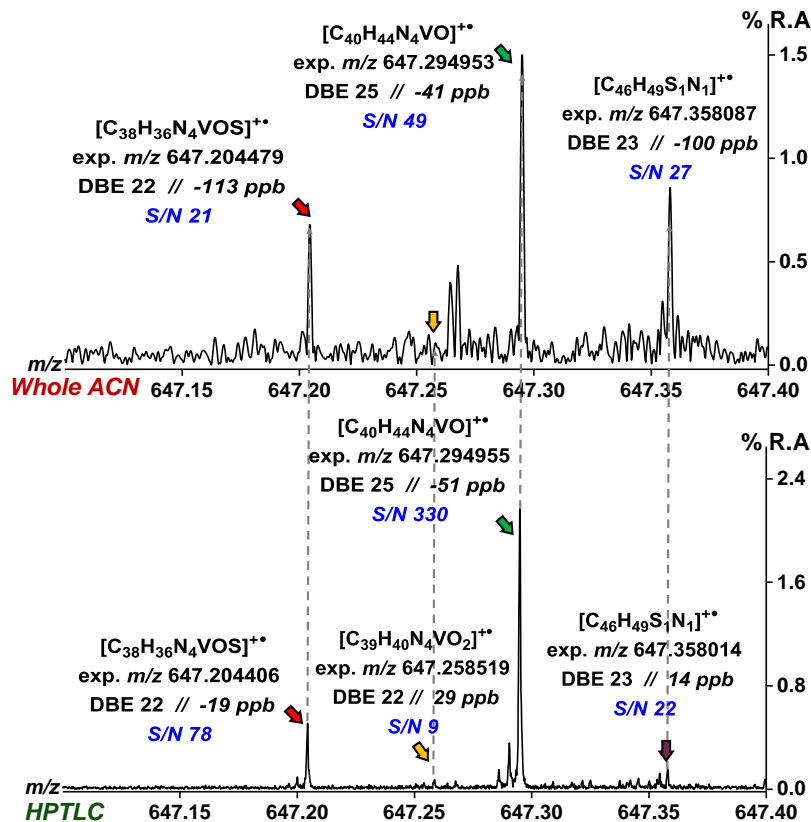


**Figure 31** Significant increase in S/N ratios in the simultaneous identification of N<sub>4</sub>OV, N<sub>4</sub>VOS and N<sub>4</sub>VO<sub>2</sub> porphyrins by ET-MALDI experiments.

**5.4.3. Observation of new oxygenated vanadyl porphyrins.** Figure 31 shows the expanded mass scale spectra at m/z 531, revealing the presence of the monoisotopic signal for porphyrin [C<sub>30</sub>H<sub>32</sub>N<sub>4</sub>VO<sub>2</sub>]<sup>++</sup> (DBE 17, 16 ppb, S/N 280) in the HPTLC fraction and its isotopic distribution. In 2013, Zhao, et al. (Zhao et al., 2013a) reported for the first time the identification of vanadyl porphyrins containing an extra oxygen atom, believed to originate from partially modified chlorophylls still maintaining the carbonyl group attached to the five membered saturated ring, as seen in Figure 1. The DBE value for the N<sub>4</sub>VO<sub>2</sub> family starts at 18 because of the C=O double bond; however, we observe thirteen new porphyrins at DBE 17 with mass accuracy under 100 ppb (See Table S1 of the Supporting Information) suggesting that N<sub>4</sub>VO<sub>2</sub> porphyrins with

DBE 17 can exist. Interestingly, in 2014, Zhao, et al.,(Zhao et al., 2014a) identified a new series of amino-containing porphyrins with ether-like structures, as shown by CID experiments, consequently, a “DBE 17” oxygenated vanadyl porphyrin can incorporate an unsaturated oxygen-carbon bond like an alcohol or ether moiety, however, this consist in a speculative statement and tandem MS experiments need to be considered for a truly elucidation.

Chlorophylls are carboxylic acid-containing compounds, as shown in Figure 1, transforming into reduced species (with peripheral alkyl chains) during diagenesis geochemical processes. However, Hodgson observations,(Hodgson & Peake, 1961) suggested that chlorophylls can be partially derived and remaining functional groups such carboxylate or carbonyl unit are preserved. Figure 28, revealed an important contribution of acidic porphyrins ranging from DBE 18 to 21, going up to a total of 47 assigned formulas with a major contribution of Etio acidic vanadyl porphyrins DBE 18, see Figure 24.

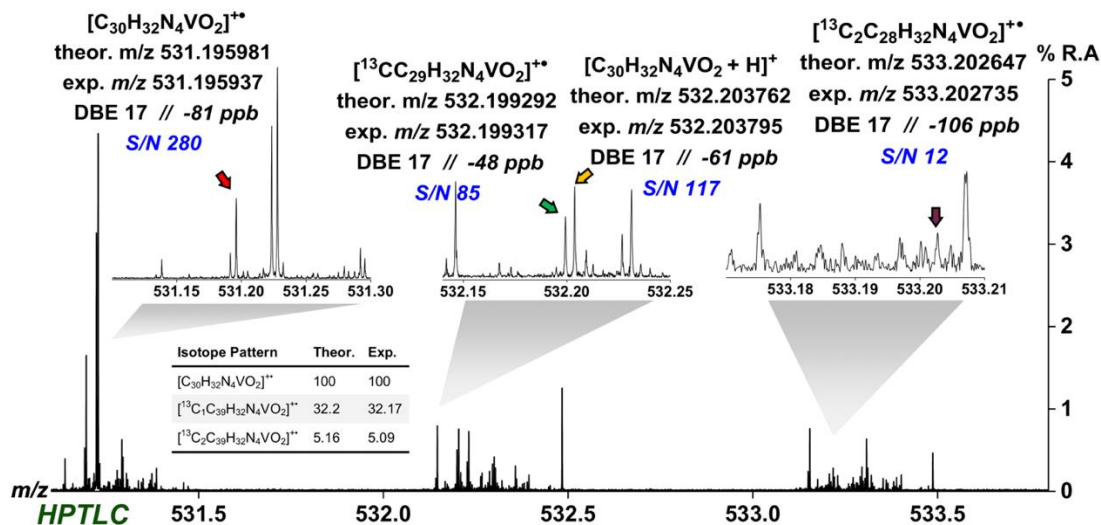


**Figure 32** HPTLC purification combined with high sensitivity ET-MALDI experiments, provided a significant increasing on signal-to-noise ratio corresponding to novel  $N_4VO_2$  at DBE 17 porphyrins.

## 5.5. Conclusion

The use of similar physical properties of a group of molecules present in a complex mixture, *e.g.* IP values, can be advantageously used to devise MS-based analytical strategies for their selective detection. The electron-transfer (ET) process in MALDI MS is one of such strategies, providing that there is a suitable organic matrix able to efficiently produce primary and secondary ions in the gas-phase. We demonstrate that the compound  $\alpha$ -CNPV-CH<sub>3</sub> can be effectively used as ET MALDI matrix for the selective ionization and detection of nickel and vanadyl porphyrins present in ACN extracts and HPTLC purified fractions from a middle east crude-oil. Selective ionization by ET is warranted by an  $\Delta$ IP > 0.5 eV between matrix primary ions ( $\alpha$ -CNPV-CH<sub>3</sub>, IP= 8.42 eV) and petroporphyrins neutral molecules (IP= 6.5-7.0 eV). The high selectivity of ET reactions in MALDI-(+) combined with the high mass accuracy and resolution of FTICR provide an additional tool for porphyrin analysis by mass spectrometry, without the need for the complex sample enrichment or purification procedures required when using APPI, ESI or LDI sources. This approach allowed us to detect more than 500 molecular formulae, at mass accuracy within parts per billion, corresponding to N<sub>4</sub>Ni, high DBE N<sub>4</sub>VO, N<sub>4</sub>VO<sub>2</sub>, N<sub>4</sub>VO<sub>3</sub> and sulfur vanadyl porphyrins N<sub>4</sub>VOS. In addition, we report the observation of N<sub>4</sub>VO<sub>2</sub> porphyrins at DBE 17, presumably corresponding to ether or alcohol-like structures as previously reported by Zhao, et al. (Zhao et al., 2014b) The experiments of tandem MS using the ET-MALDI approach will be considered for further publications.

## References

- Ali, Mohammad F., Bukhari, A., & Saleem, M. (1983). Trace metals in crude oils from Saudi Arabia. *Industrial & Engineering Chemistry Product Research and Development*, 22(4), 691–694.
- Ali, Mohammad F., Perzanowski, H., Bukhari, A., & Al-Haji, A. A. (1993). Nickel and Vanadyl Porphyrins in Saudi Arabian Crude Oils. *Energy and Fuels*, 7(2), 179–184.
- Ali, Mohammad Farhat, & Abbas, S. (2006). A review of methods for the demetallization of residual fuel oils. *Fuel Processing Technology*, 87(7), 573–584.
- Barlow, D. E., Scudiero, L., & Hipps, K. W. (2004). Scanning Tunneling Microscopy Study of the Structure and Orbital-Mediated Tunneling Spectra of Cobalt(II) Phthalocyanine and Cobalt(II) Tetraphenylporphyrin on Au(111): Mixed Composition Films. *Langmuir*, 20(11), 4413–4421.
- Bonnett, R. (1995). Photosensitizers of the porphyrin and phthalocyanine series for photodynamic therapy. *Chem. Soc. Rev.*, 24(1), 19–33.
- Calvano, C. D., Ventura, G., Trotta, M., Bianco, G., Cataldi, T. R. I., & Palmisano, F. (2017). Electron-Transfer Secondary Reaction Matrices for MALDI MS Analysis of Bacteriochlorophyll a in Rhodobacter sphaeroides and Its Zinc and Copper Analogue Pigments. *Journal of the American Society for Mass Spectrometry*, 28(1), 125–135.
- Cantu, R., Stencel, J. R., Czernuszewicz, R. S., Jaffe, P. R., & Lash, T. D. (2000). Surfactant-enhanced partitioning of nickel and vanadyl deoxophylloerythroetioporphyrins from crude oil into water and their analysis using surface-enhanced resonance Raman spectroscopy. *Environmental Science & Technology*, 34(1), 192–198.

- Castellanos-García, L. J., Agudelo, B. C., Rosales, H. F., Cely, M., Ochoa-Puentes, C., Blanco-Tirado, C., ... Combariza, M. Y. (2017). Oligo p-Phenylenevinylene Derivatives as Electron Transfer Matrices for UV-MALDI. *Journal of The American Society for Mass Spectrometry*.
- Filby, R. H., & Berkel, G. J. Van. (1987). Chapter 1 Geochemistry of Source Metal and Complexes in Petroleum, Coals: An Overview Rocks, Department of Chemistry and Nuclear Radiation Center, Washington State University, Pullman, WA 99164-1300 The geochemistry of metal complexes.
- Foster, N. S., Day, J. W., Filby, R. H., Alford, A., & Rogers, D. (2002). The role of Namontmorillonite in the evolution of copper, nickel, and vanadyl geoporphyryns during diagenesis. *Organic Geochemistry*, 33(8), 907–919.
- Freeman, D. H., & O'Haver, T. C. (1990). Derivative Spectrophotometry of Petroporphyrins. *Energy and Fuels*, 4(6), 688–694.
- Giraldo-Dávila, D., Chacón-Patiño, M. L., Orrego-Ruiz, J. A., Blanco-Tirado, C., & Combariza, M. Y. (2016). Improving compositional space accessibility in (+) APPI FT-ICR mass spectrometric analysis of crude oils by extrography and column chromatography fractionation. *Fuel*, 185, 45–58.
- Giraldo-Dávila, D., Chacón-Patiño, M. L., Ramirez-Pradilla, J. S., Blanco-Tirado, C., & Combariza, M. Y. (2018). Selective ionization by electron-transfer MALDI-MS of vanadyl porphyrins from crude oils. *Fuel*, 226(March), 103–111.
- Hodgson, G. W., & Peake, E. (1961). Metal Chlorin Complexes in Recent Sediments as Initial Precursors to Petroleum Porphyrin Pigments. *Nature*, 191, 766.
- Jørgensen, B. B. (1977). Bacterial sulfate reduction within reduced microniches of oxidized marine sediments. *Marine Biology*, 41(1), 7–17.

- Kotsiris, S. G., Vasil'ev, Y. V., Streletskii, A. V., Han, M., Mark, L. P., Boltalina, O. V, ... Drewello, T. (2006). Application and evaluation of solvent-free matrix-assisted laser desorption/ionization mass spectrometry for the analysis of derivatized fullerenes. *European Journal of Mass Spectrometry*, 12(6), 397–408.
- Lash, T. D. (1993). Geochemical Origins of Sedimentary Benzoporphyrins and Tetrahydrobenzoporphyrins. *Energy and Fuels*, 7(2), 166–171.
- Liu, H., Mu, J., Wang, Z., Ji, S., Shi, Q., Guo, A., ... Lu, J. (2015). Characterization of Vanadyl and Nickel Porphyrins Enriched from Heavy Residues by Positive-Ion Electrospray Ionization FT-ICR Mass Spectrometry. *Energy and Fuels*, 29(8), 4803–4813.
- López, L., & Mónaco, S. Lo. (2017). Vanadium, nickel and sulfur in crude oils and source rocks and their relationship with biomarkers: Implications for the origin of crude oils in Venezuelan basins. *Organic Geochemistry*, 104, 53–68.
- McCarley, T. D., McCarley, R. L., & Limbach, P. A. (1998). Electron-transfer ionization in matrix-assisted laser desorption/ionization mass spectrometry. *Analytical Chemistry*, 70(20), 4376–4379.
- Mckenna, A. M., Purcell, J. M., Rodgers, R. P., & Marshall, A. G. (2009). Identification of Vanadyl porphyrins in a heavy crude oil and raw asphaltene by Atmospheric pressure photoionization Fourier transform ion cyclotron resonance (ft-icr) mass spectrometry. *Energy & Fuels*, 23(4), 2122–2128.
- McKenna, A. M., Williams, J. T., Putman, J. C., Aeppli, C., Reddy, C. M., Valentine, D. L., ... Rodgers, R. P. (2014). Unprecedented ultrahigh resolution FT-ICR mass spectrometry and parts-per-billion mass accuracy enable direct characterization of nickel and vanadyl porphyrins in petroleum from natural seeps. *Energy and Fuels*, 28(4), 2454–2464.

- Ocampo, R., Callot, H. J., Albrecht, P., & Kintzinger, J. P. (1984). A novel chlorophyll c related petroporphyrin in oil shale. *Tetrahedron Letters*, 25(24), 2589–2592.
- Orr, W. L. (1986). Kerogen/asphaltene/sulfur relationships in sulfur-rich Monterey oils. *Organic Geochemistry*, 10(1), 499–516.
- Putman, J. C., Rowland, S. M., Corilo, Y. E., & McKenna, A. M. (2014). Chromatographic enrichment and subsequent separation of nickel and vanadyl porphyrins from natural seeps and molecular characterization by positive electrospray ionization FT-ICR mass spectrometry. *Analytical Chemistry*, 86(21), 10708–10715.
- Qian, K., Edwards, K. E., Mennito, A. S., Walters, C. C., & Kushnerick, J. D. (2010). Enrichment, resolution, and identification of nickel porphyrins in petroleum asphaltene by cyclograph separation and atmospheric pressure photoionization fourier transform ion cyclotron resonance mass spectrometry. *Analytical Chemistry*, 82(1), 413–419.
- Qian, K., Mennito, A. S., Edwards, K. E., & Ferrughelli, D. T. (n.d.). Observation of vanadyl porphyrins and sulfur-containing vanadyl porphyrins in a petroleum asphaltene by atmospheric pressure photonionization Fourier transform ion cyclotron resonance mass spectrometry. *Rapid Communications in Mass Spectrometry*, 22(14), 2153–2160.
- Ramírez-Pradilla, J. S., Blanco-Tirado, C., & Combariza, M. Y. (n.d.). Electron Transfer Ionization of Nanoparticles, Polymers, Porphyrins and Fullerenes Using Synthetically-Tunable  $\alpha$ -Cyano-Phenylenevinylenes as UV MALDI-MS Matrices. *ACS Applied Materials & Interfaces*, 0(ja), null.
- Rodgers, R. P., Hendrickson, C. L., Emmett, M. R., Marshall, A. G., Greaney, M., & Qian, K. (2001). Molecular characterization of petroporphyrins in crude oil by electrospray ionization Fourier transform ion cyclotron resonance mass spectrometry. *Canadian Journal of*

*Chemistry*, 79(5–6), 546–551.

Senglet, N., Williams, C., Faure, D., Courières, T. Des, & Guillard, R. (1990). Microheterogeneity study of heavy crude petroleum by u.v.-visible spectroscopy and small angle X-ray scattering.

*Fuel*, 69(1), 72–77.

Sundararaman, P. (1993). On the mechanism of change in DPEP / ETIO ratio with maturity.

*Geochimica et Cosmochimica Acta*, 57, 4517–4520.

Treibs, A. (n.d.). Chlorophyll- und Hämin-Derivate in bituminösen Gesteinen, Erdölen, Kohlen, Phosphoriten. *Justus Liebigs Annalen Der Chemie*, 517(1), 172–196.

Vorapalawut, N., Martinez Labrador, M., Pohl, P., Caetano, M., Chirinos, J., Arnaudguilhem, C., ... Lobinski, R. (2012). Application of TLC and la ICP SF MS for speciation of S, Ni and v in petroleum samples. *Talanta*, 97, 574–578.

Xu, H. (1992). Short Communication Separation of vanadyl and nickel petroporphyrins aminopropyl column by high-performance liquid chromatography. *Journal of Chromatography*, 607, 139–144.

Yin, C. X., Tan, X., Müllen, K., Stryker, J. M., & Gray, M. R. (2008). Associative  $\pi$ - $\pi$  interactions of condensed aromatic compounds with vanadyl or nickel porphyrin complexes are not observed in the organic phase. *Energy and Fuels*, 22(4), 2465–2469.

Zhao, X., Liu, Y., Xu, C., Yan, Y., Zhang, Y., Zhang, Q., ... Shi, Q. (2013a). Separation and characterization of vanadyl porphyrins in Venezuela Orinoco heavy crude oil. *Energy and Fuels*, 27(6), 2874–2882.

Zhao, X., Liu, Y., Xu, C., Yan, Y., Zhang, Y., Zhang, Q., ... Shi, Q. (2013b). Separation and Characterization of Vanadyl Porphyrins in Venezuela Orinoco Heavy Crude Oil. *Energy & Fuels*, 27(6), 2874–2882.

Zhao, X., Shi, Q., Gray, M. R., & Xu, C. (2014a). New Vanadium Compounds in Venezuela Heavy Crude Oil Detected by. *Scientific Reports*, 4, 1–6.

Zhao, X., Shi, Q., Gray, M. R., & Xu, C. (2014b). New vanadium compounds in Venezuela heavy crude oil detected by positive-ion electrospray ionization fourier transform ion cyclotron resonance mass spectrometry. *Scientific Reports*, 4, 1–6.

Zhao, X., Xu, C., & Shi, Q. (2016). Porphyrins in Heavy Petroleums: A Review. In C. Xu & Q. Shi (Eds.), *Structure and Modeling of Complex Petroleum Mixtures* (pp. 39–70). Cham: Springer International Publishing.